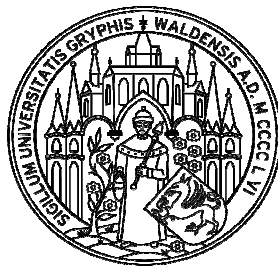


**Atmospheric-Pressure Dielectric Barrier Discharge:
Synthesis and Deposition of Organic Plasma Polymers
and their Characterizations**

**Inauguraldissertation
zur
Erlangung des akademischen Grades
doktorerum naturalium (Dr. rer. nat)
an der Mathematisch-Naturwissenschaftlichen Fakultät
der
Ernst-Moritz-Arndt-Universität Greifswald**



vorgelegt von

H C Thejaswini

**geboren 21 September 1982
in Bangalore, India**

**Greifswald, 2012
Germany**

Dekan:	Prof. Dr. Klaus Fesser
1. Gutachter::	Prof. Dr. Rainer Hippler
2. Gutachter::	Prof. Dr. Franz Faupel
Tag der Promotion:	16. 11. 2012

Dedicated To My Father

Acknowledgement

First and foremost I express my deep and sincere gratitude to Prof. Rainer Hippler for his constant encouragement and patience through out this thesis, without his support and knowledge this thesis would not have been completed. And I am very grateful to him for providing me an opportunity to work at Ernst-Moritz-Arndt University, Greifswald.

I would like to thank Prof. Jürgen Meichsner, University of Greifswald, Greifswald and Prof. Eckart Ruehl, Free University of Berlin, Berlin, for working collaboration and several scientific discussions.

I thank Dr. Robert Bogdanowicz and Dr. Jan Schäfer for collaborative works in several experimental techniques, and scientific discussions.

It is my great pleasure to thank all my group colleagues. Especially I'd like to thank our lab technicians Mr. Axel Knuth, Mr. Micheal Beck and Mr. Robert Mrotzek for their timely help during my experiments. I thank Dr. Vasile Vartolomei and Dr. Abhijit Majumdar for their kind help during my initial days of stay in Greifswald. My kind regards to Heidelore Boldt and Elfi Werner. And I thank Mr. Vladimir Danilov and Mr. Vladimir Sushkov for collaborative works and several scientific discussions.

I also thank all colleagues at physics institute, International Max-Planck Research School (IMPRS) Program, and Helmholtz Graduate School for Plasma Physics (HEPP). I thank IMPRS and HEPP committee for organizing seminars, those seminars gave a benefit to me. I thank all summer school organizers here in Greifswald at the institute for physics; I learnt and had fun during the courses, few excursions were great and useful.

It gives me a great pleasure in acknowledging the financial support provided for my study, from International Max-Planck Research School for “Bounded plasmas” through a Landesgraduierstipendium from the university of Greifswald, and Deutsche Forschungsgemeinschaft (DFG) through SFB/TR 24 “Fundamentals of Complex Plasma”.

It is my great pleasure to thank everyone at Indian community here in Greifswald.

My sincere thanks to Prof. Srinivasan Sampath, Inorganic and Physical Chemistry department, Indian Institute of Science (IISc), Bangalore, India, for providing me a great research opportunity to work in such a reputed institution.

I also thank my well-wishers/seniors Dr. G. R. Vasanth Kumar and Dr. Tharamani for their kind help/suggestion during my stay at IISc.

I would like to thank my family members, especially my husband, Basavaraju A B for his unlimited support and love. Million thanks to my mother, my brothers, H C Shiva Kumar and H C Harish Kumar and all my in-laws for their support and encouragement to pursue this degree. Without my mother's and husband's encouragement, I would not have finished this degree. I owe my deepest gratitude to my grandfathers H. N. Somashekaraiah and Prof. H. V. Veerabhadraiah for their invaluable advice and support.

Last but not the least, one above all of us, the omnipresent God, for answering my prayers, thank you so much Dear Lord.

Abstract

Atmospheric Pressure Discharges have attracted much interest in recent years. The development of a new processes based on this discharge needs a clear understanding of plasma and discharge physics and chemistry. At the present time much attention is paid to the chemical processes in barrier discharge plasma in various gas mixtures, since the understanding of these processes is necessary for the development of industrial reactors. Besides these, hydrocarbons are being used for the formation of diamond like or amorphous carbon (DLC) films. Specially, hydrogenated amorphous carbon (a-C: H) and plasma polymerization. In this work we have used Dielectric Barrier Discharge (DBD) a plasma device used to investigate simple hydrocarbon reactions in a plasma phase. Our aim of plasma phase chemical reaction studies is to form molecular hydrogen, higher order hydrocarbons C_nH_m up to $n \geq 12$ series and nitrogen - containing organic complexes using simple hydrocarbons. Deposition of thin organic films or DLC films were carried out using the DBD. In this study we have chosen certain combination of gases such as C_2H_m/N_2 ($m = 2, 4, 6$) and C_2H_m/Ar ($m = 2, 4, 6$); the purpose of using N_2 and Ar gases are to dilute and stabilize the hydrocarbon plasma and to investigate plasma chemical reactions with nitrogen gas. All reactions were carried out under an atmospheric pressure (300 mbar) with gas ratio 1:2; Experiments were performed by applying high voltage with a frequency 5.5 kHz. The plasma phase diagnostics have been investigated using mass spectrometry and FTIR spectroscopy. Formation of molecular hydrogen, N-containing organic complexes and higher order hydrocarbons with $C \geq 12$, have been investigated with mass spectrometry. FTIR spectroscopy reveals the formation of substituted alkanes (sp^3), alkenes (sp^2) and alkynes (sp) and nitrogen containing functional groups from the individual gases which are used in this work. Abundant formation of acetylene occurs with C_2H_6 and C_2H_4 as precursor gases.

Amorphous hydrogenated carbon nitride (a-CN_x:H) films have been deposited on Si (100) and glass substrates using gas mixtures C_2H_m/N_2 ($m = 2, 4, 6$). Surface chemical compositions have been derived from Fourier Transform Infrared Reflection Absorption Spectroscopy (FT-IRRAS) and X-ray Photo electron Spectroscopy (XPS). FT-IRRAS and

XPS show the presence of sp , sp^2 and sp^3 bonds of carbon and nitrogen for C_2H_m/N_2 thin films. Various functional groups such as amines, saturated and unsaturated alkyl groups have been identified. Thin films obtained from C_2H_2/N_2 and C_2H_4/N_2 gas mixture had a larger N/C ratio when compared to the film obtained from C_2H_6/N_2 . Thickness, refractive index and extinction co-efficient were investigated by ellipsometry. Rate of deposition have been investigated. Different surface morphology has been derived using Scanning Electron Microscopy.

Amorphous hydrogenated carbon (a-C:H) films or diamond like carbon (DLC) films have been deposited on Si (100) and glass substrates using gas mixtures C_2H_m/Ar ($m = 2, 4, 6$). Diagnostics for the deposited films have been done using different spectroscopic techniques. Surface chemical compositions have been derived from Fourier Transform Infrared Reflection Absorption Spectroscopy (FT-IRRAS) and X-ray Photo electron Spectroscopy (XPS). FT-IRRAS show the presence of sp , sp^2 and sp^3 bonds of carbon and hydrogen for C_2H_m/Ar ($m = 2, 4, 6$) thin films. The characteristic peak for C1s has been observed from XPS. Thickness, refractive index and extinction co-efficient were investigated by ellipsometry. Rate of deposition have been investigated.

Contents

Acknowledgement.....	vii
Abstract.....	ix
Contents.....	xi

1 General Introduction.....1 - 9

- 1.1 Plasma: Definition and Examples
- 1.2 Dielectric Barrier Discharges (DBD)
 - 1.2.1 Applications of DBD
- 1.3 Objective of this work

2 Experimental techniques.....10 - 24

- 2.1 Mass Spectrometry
 - 2.1.1 Working principle
 - 2.1.2 General applications of mass spectrometry
- 2.2 Quadrupole mass spectrometry
 - 2.2.1 Working principle
 - 2.2.2 Applications
- 2.3 Fourier transform infrared spectroscopy
 - 2.3.1 Fundamentals of vibration
 - 2.3.2 Working principle
 - 2.3.3 Applications
- 2.4 X-ray photoelectron spectroscopy
 - 2.4.1 Working principle
 - 2.4.2 Applications
- 2.5 Ellipsometry
 - 2.5.1 Working principle

2.5.2 Data acquisition	
2.6 Scanning electron microscopy	
2.6.1 Working principle	
2.6.2 Applications	
3 Experimental part.....	25 - 28
3.1 Experimental setup	
3.2 Electrode configuration for the preparation of thin films	
4 Plasma chemical reactions in C_2H_2/N_2, C_2H_4/N_2, and C_2H_6/N_2 gas mixtures.....	29 - 37
4.1 Results and discussion	
4.1.1 C_2H_2/N_2	
4.1.2 C_2H_4/N_2	
4.1.3 C_2H_6/N_2	
4.2 Comparison of C_2H_2/N_2 , C_2H_4/N_2 , and C_2H_6/N_2 mass spectra	
4.2.1 C_2H_2/N_2 and C_2H_4/N_2	
4.2.2 C_2H_4/N_2 and C_2H_6/N_2	
4.2.3 Time dependency	
4.2.4 Properties of deposited films	
5 FTIR spectroscopy for CH_4/N_2, C_2H_2/N_2, C_2H_4/N_2, and C_2H_6/N_2 gas mixtures.....	38 - 48
5.1 Results and Discussion	
5.1.1 CH_4/N_2 Plasma	
5.1.2 C_2H_2/N_2 Plasma	
5.1.3 C_2H_4/N_2 Plasma	
5.1.4 C_2H_6/N_2 Plasma	
5.2 Discussion	
6 Comparative Plasma Chemical Reaction Studies of CH_4/Ar and C_2H_m/Ar ($m = 2, 4, 6$) gas mixtures in an atmospheric Pressure Dielectric Barrier Discharge.....	49 - 68

6.1 Results and discussion

6.1.1 CH₄/Ar

6.1.2 C₂H₂/Ar

6.1.3 C₂H₄/Ar

6.1.4 C₂H₆/Ar

6.1.5 Time Dependency

6.2 Comparison of C₂H₂/Ar, C₂H₄/Ar and C₂H₆/Ar plasma with mass spectra and FTIR spectra

6.2.1 C₂H₂/C₂H₄ Plasma

6.2.2 C₂H₄/C₂H₆ Plasma

7 Deposition and Characterization of Organic Polymer thin films using

C₂H_m/N₂ (m = 2, 4, 6) gas mixtures by Dielectric Barrier Discharge.....69 - 84

7.1 Preparation of Thin films

7.2 Results and Discussion

7.2.1 Fourier Transform Infrared Reflection Absorption Spectroscopy

7.2.1.1 C₂H₂/N₂

7.2.1.2 C₂H₄/N₂

7.2.1.3 C₂H₆/N₂

7.2.1.4 Comparison between C₂H_m/N₂ (m = 2, 4, 6) gas mixtures

7.2.2 X-ray Photoelectron Spectroscopy (XPS)

7.2.3 Spectroscopic Ellipsometry (SE)

7.2.4 Scanning Electron Microscopy

7.2.5 Deposition Rate

7.3 Summary

8 Deposition and Characterization of Diamond like carbon (DLC) films using

C₂H_m/Ar (m = 2, 4, 6) gas mixtures by Dielectric Barrier Discharge.....85 - 96

8.1 Preparation of Thin films

8.2 Results and Discussion

8.2.1 Fourier Transform Infrared Reflection Absorption Spectroscopy

8.2.1.1 C₂H₂/Ar

8.2.1.2 C ₂ H ₄ /Ar	
8.2.1.3 C ₂ H ₆ /Ar	
8.2.1.4 Comparison between C ₂ H _m /Ar (m = 2, 4, 6) gas mixtures	
8.2.2 X-ray Photoelectron Spectroscopy (XPS)	
8.2.3 Spectroscopic Ellipsometry (SE)	
8.2.4 Deposition Rate	
9 Conclusions.....	97 - 99
Bibliography.....	100 - 113
List of figures.....	114 - 119
List of Tables.....	120
Abbreviations.....	121
Declaration.....	122
List of Publications.....	123
Curriculum Vitae.....	126

Chapter 1

1 General Introduction

1.1 Plasma: Definition and examples

Plasma is a partially-ionized gas, which is considered as a ‘fourth state’ of matter, and was invented by a Nobel Laureate Irving Langmuir in 1929; he named this state as, ‘plasma’. The word plasma is derived from the Greek, meaning, something molded.

“Plasma is a partially-ionized gas which is composed of ions, neutrals and charged particles.”

Further, plasmas carry electrical currents and generate magnetic fields. Plasmas are the most common form of matter, comprising more than 99% of the visible universe. Some examples for naturally existing plasmas are lightning, the Sun-from core to corona, fluorescent lights and neon signs, nebulae-luminous clouds in space, the solar wind, primordial fusion during the evolution of the universe, magnetic confinement fusion plasmas, inertially confined fusion plasmas, flames as plasmas, auroras, interstellar space, quasars, radiogalaxies and galaxies ^{[1] [2]}.

Examples of industrial or commercial plasma are, plasma displays, fluorescent lamps, plasma torch, fusion energy, ozone generator etc., Plasmas find applications in many fields of research, technology and industry, because of their temperature and density ranges. For example, in industrial and extractive metallurgy ^[3], surface treatments such as thermal spraying (coating), etching in microelectronics ^[4], metal cutting ^[5] and welding; as well as in everyday vehicle exhaust cleanup and fluorescent/luminescent lamps ^[6], while even playing a part in supersonic combustion engines for aerospace engineering ^[7].

Artificially, plasmas can be generated by applying thermal or electrical energy. As a common principle to generate plasma, there must be energy input to produce and sustain it. For this

case, plasma is generated when an electric current is applied across a gas or fluid (an electrically non-conducting material) as can be seen in the Figure 1.1a below, which shows a discharge tube as a simple example. Figure 1.1b shows the plasma generated by, a barrier discharge according to the Wikipedia ^[2].

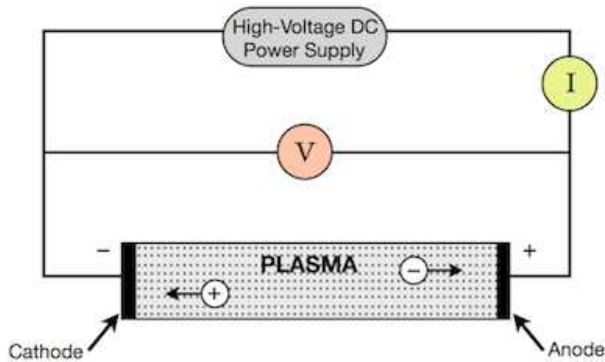


Figure 1.1a Simple circuit showing plasma generation ^[2]

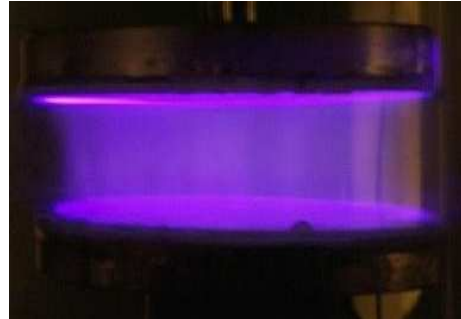


Figure 1.1b Plasma generated under, barrier discharge ^[8]

“The potential difference and subsequent electric field pull the bound electrons toward the anode (positive electrode) while the cathode (negative electrode) pulls the ion. As the voltage increases, the current stresses the material by electric polarization beyond its dielectric limit into a stage of electrical breakdown, marked by an electric spark, where the material transforms from being an insulator into a conductor. This is a stage of avalanching ionization, where collisions between electrons and neutral gas atoms create more ions and electrons. The first impact of an electron on an atom results in one ion and two electrons formation. Therefore, the number of charged particles increases rapidly only after about 20 successive sets of collisions, mainly due to a small mean free path (average distance travelled between collisions). With ample current density and ionization, this forms a luminous electric arc (essentially lightning) between the electrodes. Electrical resistance along the continuous electric arc creates heat, which ionizes more gas molecules (where the degree of ionization is determined by temperature), and as per the sequence: solid-liquid-gas-plasma, the gas is gradually turned into a thermal plasma” ^[2].

Artificially discharges can be divided into two types, low-pressure discharges and atmospheric-pressure discharges.

Glow discharge plasmas: “These are the non-thermal plasmas generated by DC or low frequency RF (<100 kHz) electric field, in the gap between two metal electrodes. This type of plasmas can be mostly generated within fluorescent light tubes” ^{[8][9]}.

Capacitively coupled plasma (CCP): “Capacitively coupled plasmas are generated with high-frequency RF electric fields, typically 13.56 MHz. These differ from glow discharges in that the sheaths are much less intense. These are widely used in the microfabrication and integrated circuit manufacturing industries for plasma etching, and plasma enhanced chemical vapor deposition” ^{[2][10]}.

Inductively coupled plasma (ICP): Inductively coupled plasmas are similar to CCP but the electrode consists of a coil wrapped around the discharge volume that inductively excites the plasma ^[2].

Wave heated plasma: Wave heated plasmas are similar to capacitively coupled and inductively coupled plasmas. Wave heated plasmas are heated by both electrostatic and electromagnetic field ^[2].

Arc discharge: Arc discharge is a high power thermal discharge of very high temperature (~10,000 K). It can be generated using various power supplies. It is commonly used in metallurgical processes. For example, it is used in the processes such as for melting rocks containing Al_2O_3 to produce aluminium.

Corona discharge: Corona discharge is a non-thermal discharge generated by the application of high voltage to sharp electrode tips. It is commonly used in ozone generators and particle precipitators.

Capacitive discharge: Capacitive discharge is a non-thermal plasma generated by the application of RF power (e.g., 13.56 MHz) to a powered electrode, with a grounded electrode held at a small separation distance in the order of 1 cm. Such discharges are commonly stabilized using a noble gas such as helium or argon ^{[2][11]}.

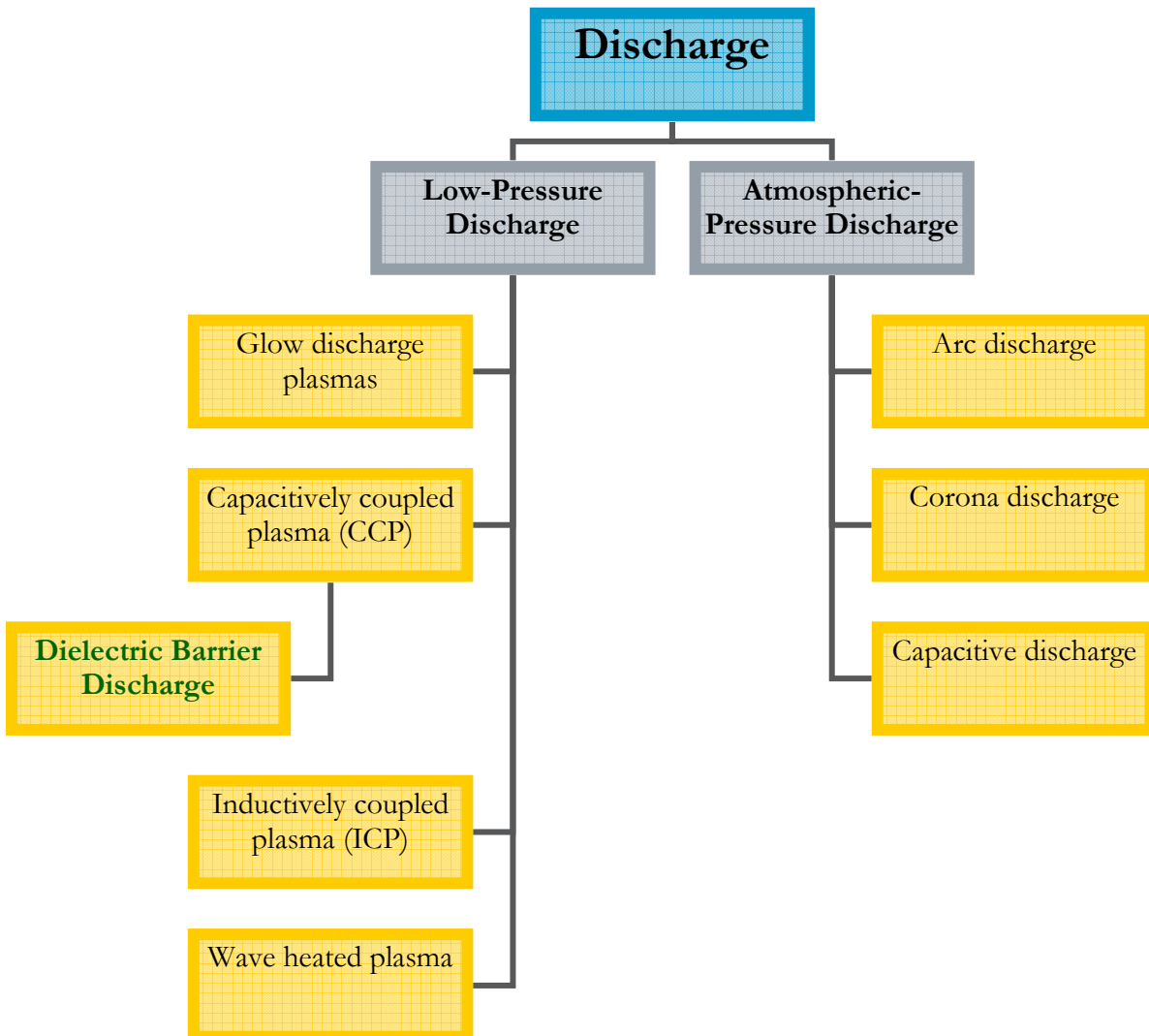


Figure 1.2 Flow chart shows the classification of discharge

1.2 Dielectric Barrier Discharge (DBD)

Dielectric barrier discharges can be characterized by the presence of one or more dielectric material in the current path between metal electrodes in addition to a discharge air gap. These were originally developed in 1857 by Ernst Werner von Siemens as a method of ozone production. These processes require high alternating current, ranging from lower to microwave frequencies. DBD is a non-thermal discharge wherein a non-conducting coating prevents the transition of the plasma discharge into an arc. In DBD, different configurations^[12] exist, planar and cylindrical configurations are quite commonly used see Figure 1.3(a) and 1.3(b). Out of these, again DBD can be classified into surface discharge (SD) (SD can be arranged in such a way that the electrode on one side of the dielectric, and a metallic one was covered on the other side), and volume discharge (VD) (VD can be arranged in such a way that two parallel dielectric plates with electrodes outside fitted or two electrodes on the same side of the dielectric material). Closely related are surface discharge configurations in which discharges are initiated at a dielectric surface due to strong electric fields generated by imbedded metal electrodes. The presence of the dielectrics precludes dc operation (common dielectric materials include glass, quartz, ceramics and polymers). Although, the DBD configuration can be operated between line and microwave frequencies, the typical operating range for most technical DBD applications lies between 500 Hz and 500kHz. The gas spaces bounded by one or two dielectrics have practically the same breakdown voltage as if they were between metal electrodes. Typically, the clearances vary from less than 100 μm to several cm. For atmospheric pressure discharges, the gap spacings of a few mm are common, thus requiring alternating driving voltages with amplitudes of typically 10 kV^[12]. Typical conditions for barrier discharges are given in the Table 1.1^[13].

1.2.1 Applications of DBD

DBDs are being used in various fields. DBDs are extensively used in the industrial wastewater treatment.^[14] In an early 19th century, DBDs were used for the commercial production of nitric acid and ammonia^[15]. Recent applications include gas chemistry^[16]^[17], Sterilization

^[18] ^[19] ^[20], Surface activation ^[21] ^[22], Modification or thin film deposition ^[23] ^[24], biomedical applications such as plasma medicine and decontamination or waste-water treatment ^[25].

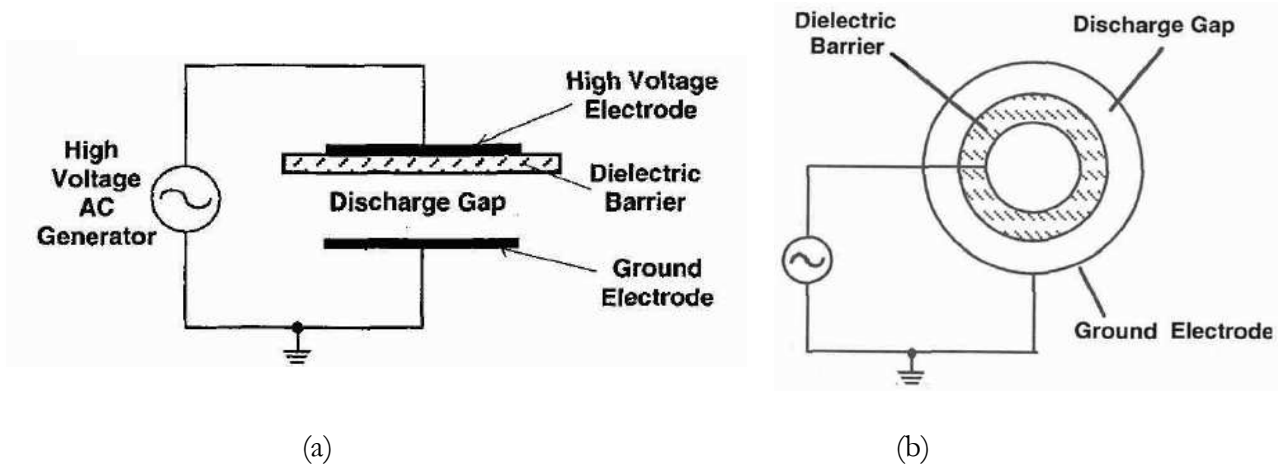


Figure 1.3(a) and 1.3(b) Schematic of the different configurations of DBD ^[12]

Table 1.1 Typical conditions for barrier discharges ^[13]

Electrical field strength E of first breakdown	$\approx 150 \text{ Td}$ ($p = 1 \text{ bar}$, $T = 300 \text{ K}$)
Voltage V	3 – 20 kV
Pressure P	1 – 3 bar
Repetition Frequency f	50 Hz – 10 kHz
Gap distance g	0.2 – 5 mm
Dielectric material thickness d	0.5 – 2 mm
Relative dielectric permittivity ϵ_r	5 – 10 (glass)

1.3 Objective of this work

This work has two objectives, (i) to understand the plasma chemical reactions which are taking place in the Titan's atmosphere, and (ii) deposition of thin films, of carbon nitride (CN_x) and diamond like carbon (DLC).

Titan is the largest moon of the planet Saturn, discovered in 1655 by the Dutch astronomer Christiaan Huygens. Titan atmosphere is composed of 98.4% of N_2 , 1.6% mostly of CH_4 , C_2H_6 , C_2H_4 and C_2H_2 , other gases like H_2 , Ar, CO_2 , HCN, He, CO, etc., Cassini-Huygens a spacecraft which has been launched into space on October 15, 1997, by National Aeronautics and Space Administration (NASA) in collaboration with European Space Agency (ESA) for space studies. Sixteen European countries and the United States make up the team responsible for designing, building, flying and collecting data from the spacecraft Cassini-Huygens. The mission is managed by NASA's Jet Propulsion Laboratory in the United States. The spacecraft consists of two main elements: Cassini orbiter and Huygens probe. Cassini orbiter was developed in United States, which was named after an Italian-French astronomer Giovanni Domenico Cassini and the ESA developed Huygens probe; which was named after the Dutch astronomer, mathematician and physicist Christiaan Huygens. Cassini-Huygens provided significant new information about surface topography, composition and atmospheric characteristics of Titan. It revealed that the organic compounds, which are present on the Titan's atmosphere, formed as a result of the recombination of molecular fragments produced by smaller hydrocarbons and N_2 by photolysis. In 1979, two famous scientists Carl Sagan and B N Khare, reported the mechanism of how higher ordered organic compounds, formed on Titan's atmosphere. According to them when UV-radiations from Sun and the energetic particles from, Saturn's magnetosphere falls on molecular N_2 and CH_4 , dissociation takes place. As a result of dissociation ions, neutrals are formed, these ions and neutrals combine to form a higher order organic compounds which are having molecular weight more than 8000 daltons. These higher organic compounds are also called "Tholins". Tholins are nitrogen-rich organic compounds produced by the irradiation of N_2 and CH_4 . The term Tholin was coined by Carl Sagan. It is derived from a Greek word meaning, "muddy". Again, Carl Sagan and B N Khare showed that the hydrolysis of tholins yields amino acids. Amino acids, are the

building blocks of proteins and play a vital role in life formation. The investigation of chemistry of higher-order organic compounds becomes significantly important, in order to understand the probability of life formation and sustainability under extreme conditions. In this thesis, we have used C_2H_2 , C_2H_4 , C_2H_6 and CH_4 hydrocarbons in combination with N_2 and Ar gases, to produce H_2 , higher-order hydrocarbons and nitrogen containing organic compounds (Tholins). Here we have chosen a set of gas mixtures, C_2H_2/N_2 , C_2H_2/Ar , C_2H_4/N_2 , C_2H_4/Ar , C_2H_6/N_2 and C_2H_6/Ar . The plasma chemical diagnostics was carried out with mass spectrometry and Fourier transform infrared (FTIR) spectroscopy ^{[26] [27] [28][29][30]}.

In recent years organic polymer films are playing a pivotal role in the development of chemical and biochemical sensors, electronic devices, passivation coatings and packaging. Considerable interest in growing diamond layers and thin films for a wide range of applications. Such as wear-protective and antireflective coating for tri-biological tools, engine parts, razor blades and sunglasses, biomedical coatings and micro-electromechanical system. Carbon exists in two allotropic forms: crystalline and amorphous. Pure diamond (sp^3) and graphite (sp^2) are examples of carbon state. An amorphous carbon with high fraction of diamond-like (sp^3) bond is known as diamond like carbon (DLC). The term DLC was first used by Aisenberg and Chabot. Because of their properties resembles with diamond they have gained much interest in the preparation of DLC films. In 1989, Liu and Cohen suggested that crystalline $\beta-C_3N_4$ would have a bulk modulus comparable to or even higher than diamond due to its small bond length and low ionicity. The $\beta-C_3N_4$, which so far has resulted just a hypothetical phase since no experimental result has demonstrated definitely the existence of such a phase. However, hydrogenated amorphous CN films are of great importance, both from a scientific and technological point of view because of their applications ^{[31][32][33][34][35]}.

There are several techniques to prepare thin films such as Chemical Vapor Deposition (CVD) ^{[36][37]}, sputtering ^{[38][39]}, Plasma Enhanced Chemical Vapor Deposition (PECVD) ^{[40][41]}, Pulsed Laser Deposition (PLD) ^{[42][43]}, pyrolysis ^{[44][45]}, spin coating ^{[46][47]}, etc., It is known that CN_x films which were deposited with lower N/C ratios, exhibit a more graphitic structure, increased hardness and much-improved room temperature, electrical conductivity. Enhanced surface atom mobility, and an increased tendency for rupture of weak $\sigma(C-N)$ bonds have all

been advanced as potential explanations for these observations ^{[48][49]}. Here we present results for films deposited by DBD using C_2H_m/N_2 ($m = 2, 4, 6$) and C_2H_m/Ar ($m = 2, 4, 6$) gas mixtures with 1:2 ratio, at atmospheric pressure of 300 mbar.

Chapter 2

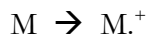
2. Experimental Techniques

2.1 Mass Spectrometry (MS)

Mass spectrometry is an analytical technique that measures the mass-to-charge ratio of charged particles. It is used for determining masses of particles, for determining the elemental composition of a sample. And for elucidating the chemical structures of chemical and bio-chemical compounds.

2.1.1 Working Principle

Basic principle of mass spectrometry is when a sample is loaded into to MS instrument, it undergoes vaporization. The vaporized sample is bombarded with an electron beam, As a result of bombardment of the sample with electrons the sample converts into highly energetic positively charged ions called molecular ions or parent ions, which can break up into smaller ions called fragment ions or daughter ions. The loss of electron from a molecule leads to a radical cation, and we can represent this process as,



The molecular ion $M.^{+}$ commonly decomposes to a pair of fragments, which may be either a radical plus an ion, or a small molecule plus a radical cation.



The molecular ions, the fragment ions and the fragment radical ions are separated by deflection in a variable magnetic field according to their mass and charge, and generate a current called the ion current, at the collector in proportion to their relative abundances. A

mass spectrum is a plot of relative abundance or ion current versus the mass/charge (m/z) ratio.

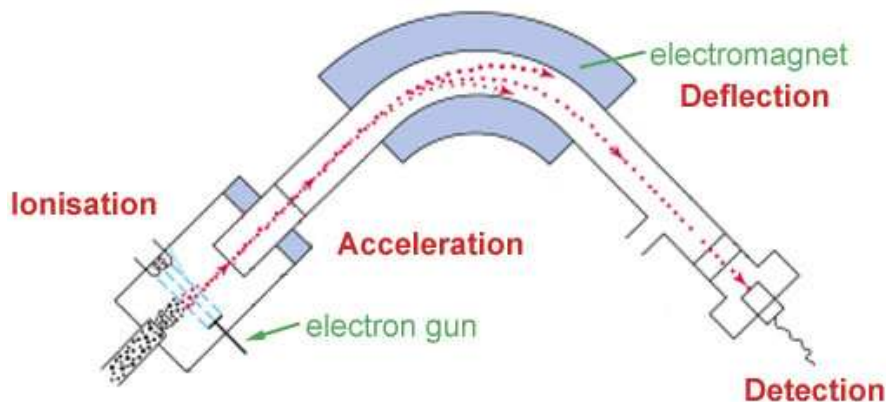


Figure 2.1 Schematic of the typical mass spectrometer ^[51]

Mass spectrometers consist of three basic parts.

- **Ion Source:** Ion source is a device to convert sample into ions by electron bombardment. In this stage, the sample undergoes ionization and forms molecular ions and fragment ions.

- **Mass Analyzer:** Mass analyzer is a filter that separates ions by their m/z values. The behavior of the ions in a magnetic field can be explained.

The kinetic energy E , of an ion of mass m traveling with velocity v is given by,

$$E = \frac{1}{2} mv^2 \quad 2.1$$

The potential energy of an ion of charge z being repelled by an electrostatic field of voltage V is zV . When the ion is repelled, the potential energy, zV , is converted into the kinetic energy, mv^2 , so that

$$zV = \frac{1}{2} mv^2 \quad 2.2$$

Therefore,

$$v^2 = \frac{2zV}{m} \quad 2.3$$

When ions are shot into the magnetic field of the analyzer, they are drawn into a circular motion by the field, and at equilibrium the centrifugal force of the ion (mv^2/r) is equaled by the centripetal force exerted on it by the magnet (zBv), where r is the radius of the circular motion and B is the field strength. Thus,

$$\frac{mv^2}{r} = zBv$$

Therefore,

$$v = \frac{zBr}{m} \tag{2.4}$$

Combining equations 2.3 and 2.4,

$$\frac{2zV}{m} = \left(\frac{zBr}{m}\right)^2$$

Therefore,

$$\frac{m}{z} = \frac{B^2 r^2}{2V} \tag{2.5}$$

From the above equation 2.5, we can see the inability of a mass spectrometer to distinguish between an ion m^+ and an ion $2m^{2+}$ since the ratio, m/z , between them has the same value of $(B^2 r^2 / 2V)$, and these three parameters B , r and V dictate the path of the ions.

To change the path of the ions so that they will focus on the collector and be recorded, we can vary either V (the accelerating voltage) or B (the strength of the focusing magnet). Voltage scans (the former) can be affected much more rapidly than magnetic scans and are used where fast scan speed is desirable.

- **Detector:** Detector is the final basic component of the mass spectrometer. The focused ion beam passes through the collector slit to the detector, which must convert the impact of a stream of positively charged ions into an electrical current. This must be amplified and recorded, either graphically or digitally ^{[50] [51] [52]}.

2.1.2 General Applications of Mass Spectrometry

MS has been used in various fields of study such as,

Environmental analysis, Forensic analysis, Clinical research, Proteomics and genomics

Generation of physico-chemical data ^[51].

2.2 Quadrupole Mass Spectrometry (QMS)

There are several types of mass analyzers or filters exists such as quadrupoles, ion traps, magnetic sector, time-of-flight, radio frequency and cyclotron resonance etc., Out of all ion traps and quadrupole filters are most commonly used filters. The quadrupole mass analyzer is one type of mass analyzer used in mass spectrometry. As the name implies, it consists of four circular rods, set parallel to each other.

2.2.1 Working Principle

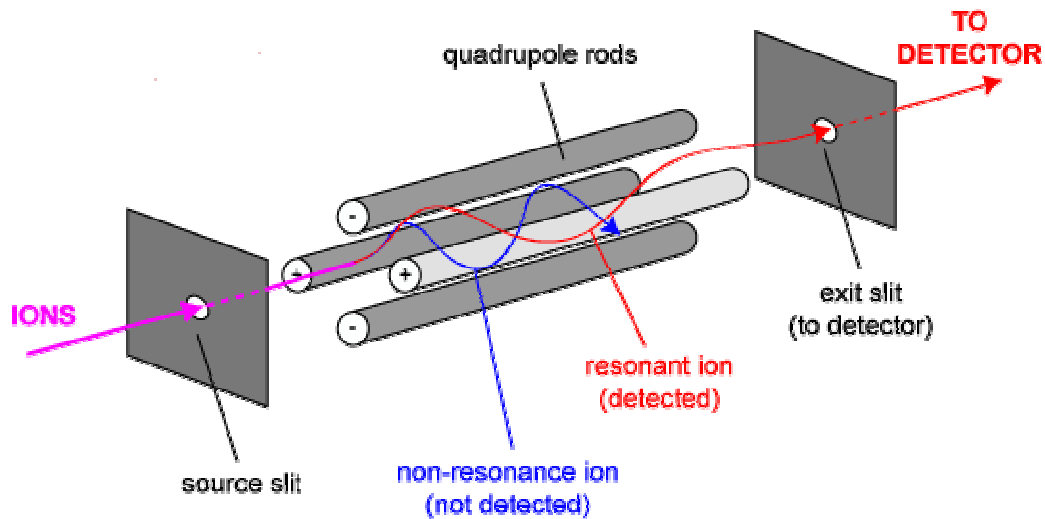


Figure 2.2 Schematic of the quadrupole mass filter ^[54]

A quadrupole mass filter consists of four parallel metal rods arranged as shown in the figure. 2.2. Two opposite rods have an applied potential of $(U + V \cos(\omega t))$ and the other two rods have a potential of $-(U + V \cos(\omega t))$, where U is a dc voltage and $V \cos(\omega t)$ is an ac voltage with radial frequency ω . The applied voltages affect the trajectory of ions traveling down the flight path centered between the four rods. For given dc and ac voltages, only ions of a certain mass-to-charge ratio pass through the quadrupole filter and all other ions are thrown out of their original path. A mass spectrum is obtained by monitoring the ions passing through the quadrupole filter as the voltages on the rods are varied. There are two methods varying ω and holding U and V constant, or varying U and V (U/V) fixed for a constant ω .

2.2.2 Applications

Since QMS can withstand the extreme temperature and the harsh vibrations. Because of these reasons scientists are using QMS for space studies. One place where this QMS is useful is in liquid chromatography-mass spectrometry or gas chromatography-mass spectrometry where they serve as exceptionally high specificity detectors ^{[50] [53] [54]}.

2.3 Fourier Transform Infrared Spectroscopy

Fourier transform infrared (FTIR) spectroscopy is an important technique in organic chemistry, to identify the presence of certain functional groups in a solid, liquid or gas. Also, one can use the unique collection of absorption bands to confirm the identity of a pure compound or to detect the presence of specific impurities. FTIR spectroscopy is a method of obtaining infrared spectra by first collecting an interferogram of a sample signal using an interferometer, and then performing a Fourier Transform (FT) on the interferogram to obtain the spectrum. An FT-IR Spectrometer collects and digitizes the interferogram, performs the FT function, and displays the spectrum ^[50].

Most of the molecules absorb infrared light at their particular frequency of molecular vibration. Only the monatomic (He, Ne, Ar, etc.,) and homopolar diatomic (H_2 , N_2 , O_2 , etc.,) molecules do not absorb infrared light. Molecules only absorb infrared light at those frequencies where the infrared light affects the dipolar moment of the molecule.

2.3.1 Fundamentals of Vibration

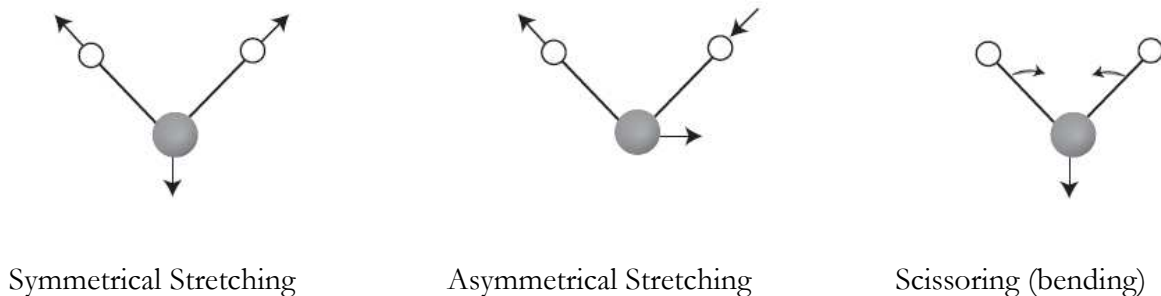


Figure 2.3 Stretching and bending vibrational modes for H_2O ^[56]

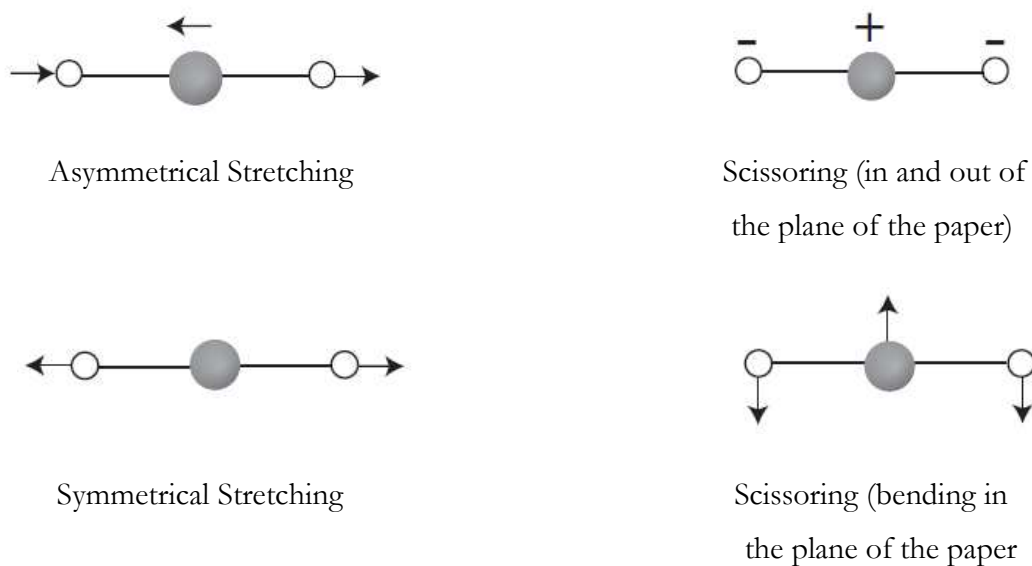


Figure 2.4 Stretching and bending vibrational modes for CO_2 ^[56]

In a molecule, the differences of charges in the electronic fields of its atoms produce the dipolar moment of the molecule. Molecules with a dipolar moment allow infrared photons to interact with the molecule causing excitation to higher vibrational states. The homopolar diatomic molecules do not have a dipolar moment since the electronic fields of its atoms are equal. Monatomic molecules do not have a dipolar moment since they only have one atom. Therefore, homopolar diatomic molecules and monatomic do not absorb infrared light ^[55].

A molecular vibration occurs when atoms in a molecule are in periodic motion while the molecule as a whole has constant translational and rotational motion. The frequency of the periodic motion is known as a vibrational frequency. In general, a molecule with N atoms has $3N - 6$ normal modes of vibration, but a linear molecule has $3N - 5$ modes, as rotation about its molecular axis cannot be observed. A diatomic molecule has one normal mode of vibration. The normal modes of vibration of polyatomic molecules are independent of each other but each normal mode will involve simultaneous vibrations of different parts of the molecule such as different chemical bonds ^[50]. Some examples for fundamental vibrations for linear (CO_2) and non-linear (H_2O) molecules are given in the figure 2.3 and figure 2.4.

2.3.2 Working Principle

An FTIR is typically based on the Michelson Interferometer. In 1887 Albert Michelson perfected this instrument and used it for several measurements in his study of light and relativity ^[50]. The schematic representation of Michelson Interferometer is shown in the figure. The interferometer consists of a beam splitter, a fixed mirror with distance d , and a mirror that translates back and forth, with a distance $d+x$, very precisely. The beam splitter is made of a special material that transmits half of the radiation striking it and reflects the other half. Radiation from the source strikes the beam splitter and separates into the two beams.

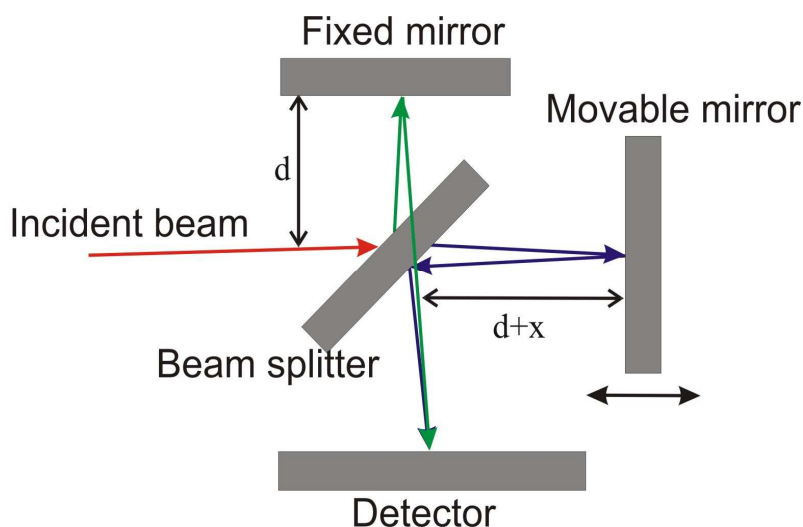


Figure 2.5 Schematic representation of the Michelson interferometry set-up ^[57]

One beam is transmitted through the beam splitter to the fixed mirror and the second is reflected off the beam splitter to the moving mirror. The fixed and moving mirrors reflect the radiation back to the beam splitter. Again, half of this reflected radiation is transmitted and half is reflected at the beam splitter, resulting in one beam passing to the detector and the second back to the source. The interferogram can be collected from the detector. Once an interferogram is collected, it needs to be translated into a spectrum (emission, absorption, transmission, etc.). The process of conversion can be done by Fourier Transform algorithm [58].

2.4 X-Ray Photoelectron Spectroscopy (XPS)

X-ray Photoelectron spectroscopy (XPS), also known as Electron Spectroscopy for Chemical Analysis (ESCA), is widely used to quantitative spectroscopic technique that investigates the chemical composition of surfaces. XPS was developed in the mid-1960s by Kai Siegbahn. In 1981, Siegbahn was awarded the Nobel Prize for physics for his work with XPS. Surface analysis by XPS involves irradiating a solid in vacuum with monoenergetic soft x-rays and analyzing the emitted electrons by energy. The spectrum is obtained as a plot of the number of detected electrons per energy interval versus their kinetic energy.

2.4.1 Working Principle

X-ray photoelectron spectroscopy (XPS) works based on the photoelectric effect. Each atom in the surface has core electron with the characteristic binding energy that is conceptually, not strictly, equal to the ionization energy of that electron. When a beam from X-ray source directs to the sample surface, the energy of the X-ray photon is adsorbed completely by the core electron of an atom. If the photon energy, $h\nu$, is large enough, the core electron will then escape from the atom and emit out of the surface. The emitted electron with the kinetic energy of KE is referred to as the photoelectron. The binding energy of the core electron is given by the Einstein relationship:

$$h\nu = BE + KE + \varphi$$

$$BE = h\nu - KE - \varphi$$

Where, ' $h\nu$ ' is the X-ray photon energy, ' KE ' is the kinetic energy of photoelectron, which can be measured by the energy analyzer; and φ is the spectrometer work function induced by the analyzer. Since the work function, φ , can be compensated artificially, it is eliminated, giving the binding energy ' BE ' as follows:

$$BE = h\nu - KE$$

As seen in Figure 2.6, XPS system uses a switchable Mg or Al K_{α} line at 1253.6 eV or 1486.6 eV, respectively. At these energies, it is primarily core electron energy levels that are probed. Valence level spectra can be collected, but at relatively low resolution the ejected photoelectrons are collected and analyzed as a function of their kinetic energy using a photoelectron spectrometer. This consists of a series of electrostatic lenses and steering voltages to selectively separate electrons of varying kinetic energies and bring them to an electron multiplier where they are detected. All this takes place under ultra high vacuum (UHV) conditions of $<10^{-9}$ mbar pressure. Any non-volatile solid sample can be analyzed, although non-conducting materials may require some special techniques to properly analyze.

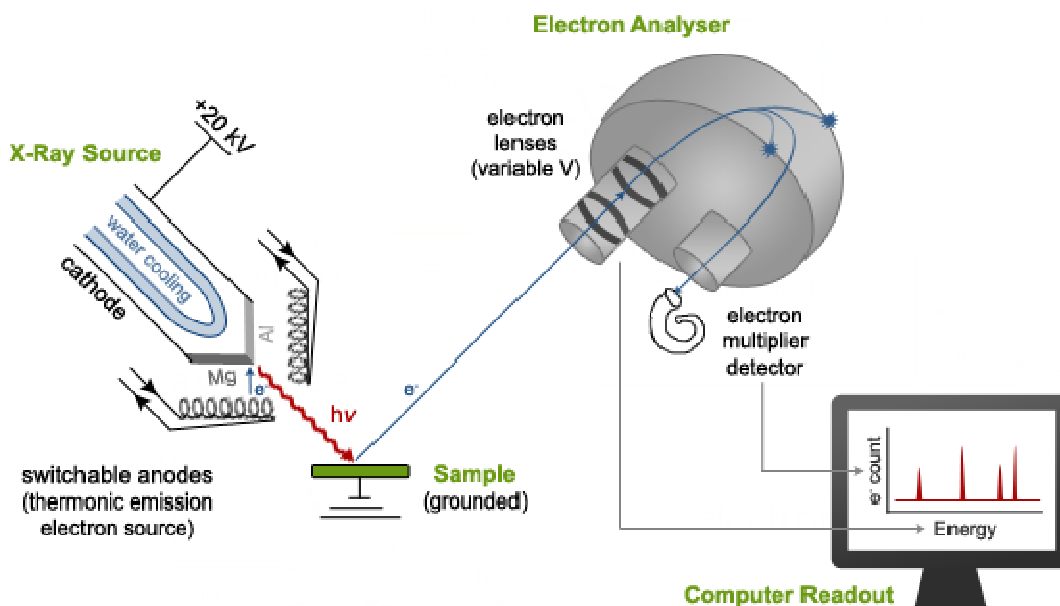


Figure 2.6 Schematic diagram of X-ray Photoelectron Spectroscopy ^[61]

A XPS spectrum is a plot of the number of photoelectron intensity as a function of binding energy. The binding energy is the energy difference between the initial and final states after the photoelectron has left the atom. Because each element has a unique set of binding energies, XPS can be used to identify and determine the concentration of the elements in the surface. Variations in the elemental binding energies called the chemical shifts arise from differences in the chemical potential and polarizability of compounds. These chemical shifts can be used to identify the chemical state of the materials being analyzed. The number of peaks produced by a single element varies from 1 to more than 20. Tables of binding energies that identify the shell and spin-orbit of each peak produced by a given element are included with modern XPS instruments, and can be found in various handbooks and websites. Because these experimentally determined BEs are characteristic of specific elements, they can be directly used to identify experimentally measured peaks of a material with unknown elemental composition ^{[60] [61] [62]}.

2.4.2 Applications

X-ray Photoelectron Spectroscopy can be used to determine ^[62],

The elements and the quantity of those elements those are present within the top 1- 12 nm of the sample surface. Contamination, if any, exists in the surface or the bulk of the sample.

Empirical formula of a material that is free of excessive surface contamination.

The chemical state identification of one or more of the elements in the sample.

The binding energy of one or more electronic states. The thickness of one or more thin layers (1–8 nm) of different materials within the top 12 nm of the surface. The density of electronic states.

2.5 Ellipsometry

Ellipsometry is an optical technique which allows one to measure very accurately and with high reproducibility the complex dielectric function $\epsilon = \epsilon_1 + i \epsilon_2$ of a given material. The technique of ellipsometry was invented by Paul Drude in 1887 who used it to determine the dielectric function of various metals and dielectrics. It has become one of the most

important and powerful tools for the characterization of layer thickness, composition, surface roughness, optical anisotropy and optical properties such as complex refractive index or dielectric function, of thin-film and multi-layered materials. It has applications in many different fields, from semiconductors physics to microelectronics and biology, from basic research to industrial applications.

2.5.1 Working Principle

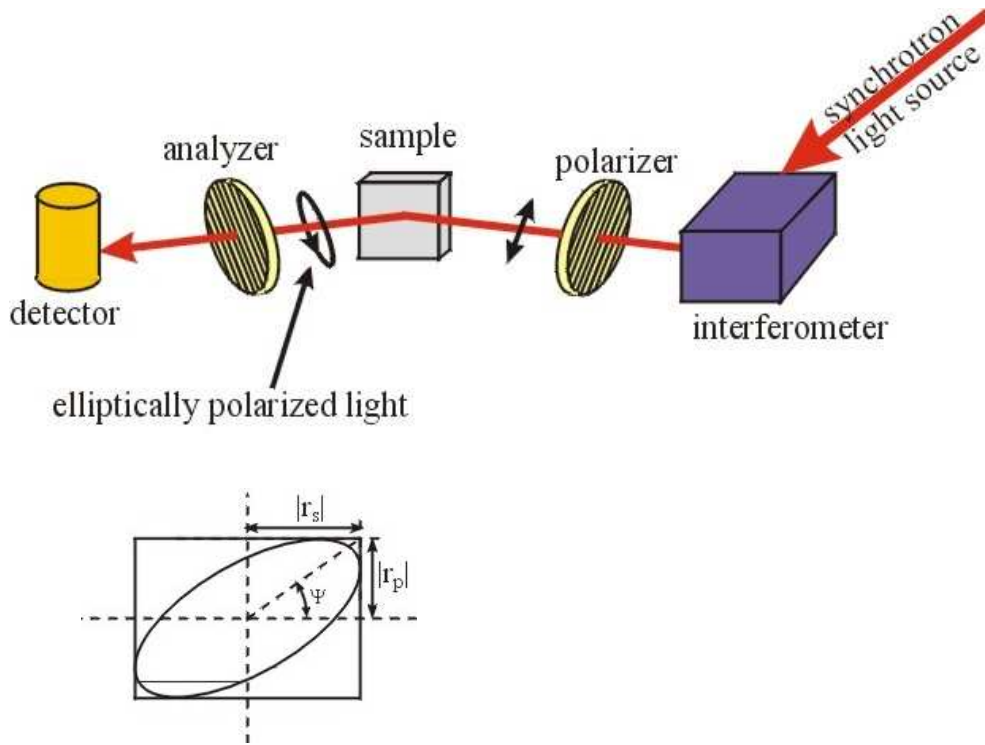


Figure 2.7 A typical experimental setup of an ellipsometry ^[64]

A typical setup of an ellipsometry experiment is shown in Figure 2.7. Electromagnetic radiation is emitted by a light source and linearly polarized by a polarizer. It can pass through an optional compensator and falls onto the sample. After reflection the radiation passes a compensator (optional) and a second polarizer, which is called an analyzer, and falls into the detector. Instead of the compensators some ellipsometers use a phase-modulator in the path of the incident light beam. Ellipsometry is a specular optical technique. The angle of

incidence equals the angle of reflection. The incident and the reflected beam span the plane of incidence. Light which is polarized parallel to this plane is named p-polarized. A polarization direction perpendicular is called s-polarised. As a result of reflection, the s- and p-components experience a different attenuation and phase shift according to the Fresnel equations (which are easily derived from Maxwell's equations of electrodynamics). The reflected light therefore is elliptically polarized giving the technique its name. The ellipse of polarization of the reflected light is then measured with a second polarizer (the so-called analyzer). The complex dielectric function epsilon can be obtained directly from the ellipticity of the reflected light simply by an inversion of the Fresnel-equations. Unlike conventional reflections techniques, ellipsometry requires no reference measurement and no extrapolation of the reflectivity towards zero and infinite energy. This makes the ellipsometry measurements more accurate and more reproducible than the conventional reflection measurements.

2.5.2 Data Acquisition

Ellipsometry measures the complex reflectance ratio ρ of a system, which may be parameterized by the amplitude component Ψ and the phase difference Δ . The polarization state of the light incident upon the sample may be decomposed into an s and a p component. The amplitudes of the s and p components, after reflection and normalized to their initial value, are denoted by r_s and r_p , respectively. Ellipsometry measures the complex reflectance ratio ρ (a complex quantity), which is the ratio of r_p over r_s :

$$\rho = r_p / r_s = \tan\Psi e^{i\Delta}$$

Thus, $\tan\Psi$ is the amplitude ratio upon reflection, and Δ is the phase shift (phase difference). Since ellipsometry is measuring the ratio (or difference) of two values (rather than the absolute value of either), it is very robust, accurate, and reproducible. For instance, it is relatively insensitive to scatter and fluctuations, and requires no standard sample or reference beam ^{[63] [64] [65]}.

2.6 Scanning Electron Microscopy (SEM)

Scanning electron microscopy is one of the microscopic techniques to study the surface morphology of the thin films. Electron microscopy was invented by Ruska (Noble prize in physics 1986). Scanning electron microscope (SEM) uses a focused beam of high-energy electrons to generate a variety of signals at the surface of solid samples. The signals that derive from electron-sample interactions reveal information about their surface external morphology, chemical composition, and crystalline structure and orientation of materials. The type of signals produced by a SEM include secondary electrons, back-scattered electrons (BSE), characteristic X-rays, light (cathodoluminescence), specimen current and transmitted electrons.

2.6.1 Working Principle

Figure 2.8 shows the schematic experimental set-up for SEM. An electron beam is thermionically emitted from an electron gun fitted with a tungsten filament cathode. Tungsten is normally used in thermionic electron gun because it has the highest melting point and lowest vapour pressure of all metals, thereby allowing it to be heated for electron emission, and because of its low cost. The electron beam which is emitted from tungsten filament carries an energy ranging from 0.2 keV to 40 keV, is focused by one or two condenser lenses to a spot about 0.4 nm to 5 nm in diameter. The beam passes through pairs of scanning coils or pairs of deflector plates in the electron column, typically in the final lens, which deflect the beam in the x and y axes so that it scans in a raster fashion over rectangular area of the sample surface. When the primary electron beam interacts with the sample, the electrons lose energy by repeated random scattering and absorption within a teardrop-shaped volume of the specimen known as the interaction volume, which extends from less than 100 nm to around 5 μm into the surface. The size of the interaction volume depends on the electron's landing energy, the atomic number of the specimen and the reflection of high-energy electrons by inelastic scattering and the emission of electromagnetic radiation, each of which can be detected by specialized detectors.

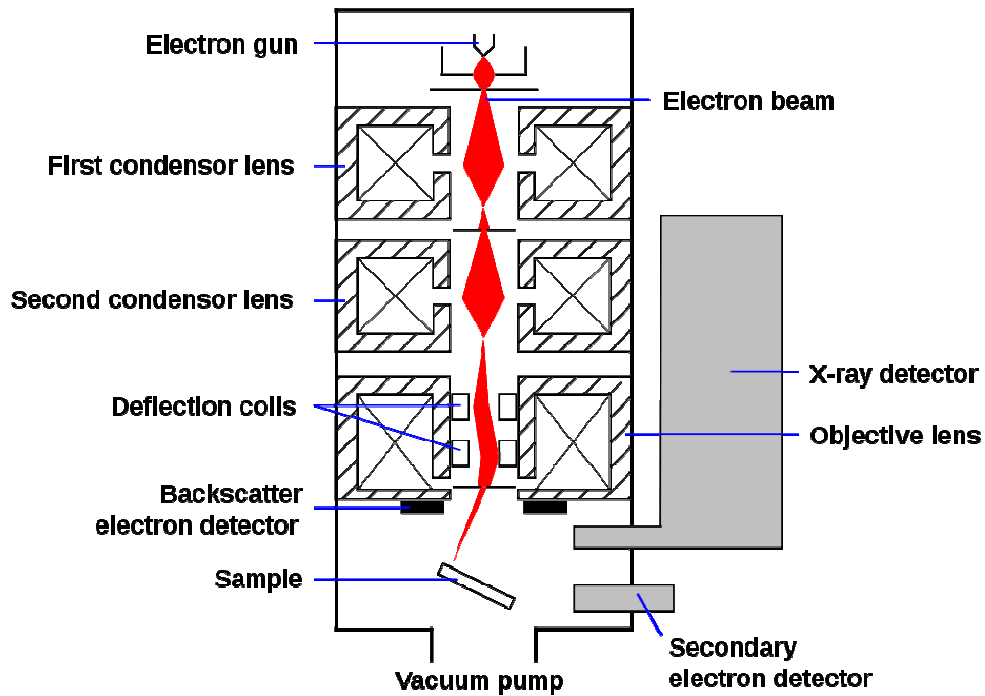


Figure 2.8 Schematic diagram of the SEM experimental set-up ^[69]

The beam current absorbed by the specimen can also be detected and used to create images of the distribution of specimen current. Electronic amplifiers of various types are used to amplify the signals, which are displayed as variations in brightness on a computer monitor. Each pixel of computer video memory is synchronized with the position of the beam on the specimen in the microscope, and the resulting image is therefore a distribution map of the intensity of the signal being emitted from the scanned area of the specimen. In older microscopes image may be captured by photography from a high-resolution cathode ray tube, but in modern machines image is saved to computer data storage ^{[66] [67] [68] [69]}.

2.6.2 Applications

1. SEM is routinely used to generate high-resolution images of shapes of objects and to show spatial variations in chemical compositions.

2. SEM is widely used to identify phases based on qualitative chemical analysis and crystalline structure.
3. Precise measurement of very small features and objects down to 50 nm in size can be accomplished.
4. SEMs equipped with diffracted backscattered electron detectors (EBSD) can be used to examine microfabric and crystallographic orientation in many materials ^[68].

Chapter 3

3 Experimental Part

3.1 Experimental setup

The experimental setup is shown in the figure 3.1. The plasma chamber is made of stainless steel. The inner dimensions of the chamber are of height 12.3 cm, length 18.0 cm, and width 15.0 cm, yielding a chamber volume of 3.32 dm³. The two electrodes are made from copper plates (or stainless steel plates) with a length of 8.3 cm, width 3.3 cm, and thickness 0.15 cm. Both copper electrodes are covered by dielectrics: the upper (powered) electrode is covered by Al₂O₃ and the lower (grounded) one is covered by glass. Both electrodes are separated by 0.15 cm from each other. The upper electrode is connected to a home-built high-voltage power supply, while the lower electrode is grounded. The chamber is pumped by a membrane pump down to about 10 mbar. The experiments were performed at a pressure of 300 mbar. Pressure inside the plasma chamber was controlled by two gas flow controllers for C₂H_m and N₂/Ar and by an adjustable needle valve between the chamber and the membrane pump. The high-voltage power supply consists of a frequency generator delivering a sinusoidal output that is fed into an audio amplifier. The amplifier can be operated at up to 500 W; its output is fed into a spark plug transformer. Experiments were performed at 5.7 kV and at 5.5 kHz. In order to measure the discharge power a small capacitor (C= 10 nF) is placed in series between the lower electrode and ground. The voltage applied to the powered electrode is measured with a high-voltage probe and together with the voltage at the lower electrode serve as x and y inputs of a digital oscilloscope. The discharge power (about 2-5 W) is calculated from the resulting Lissajous figure using the standard method based on the area enclosed by the curve^[70] and was kept constant during the experiments.

Gas composition of stable reaction products only was detected by a mass spectrometer (Balzers QMS 200). It is pumped by a turbo molecular pump (Pfeiffer TSU 062H) to a base pressure of about 1×10^{-8} mbar increasing to about 10^{-6} mbar during the experiment. A

capillary tube of length 103 cm and inner diameter 0.01 cm connects the mass spectrometer with the plasma chamber. The capillary tube is connected to the chamber's wall in a distance of about 5 cm from the electrodes. The tube is necessary to maintain the pressure difference of up to one atmosphere between the plasma chamber and the mass spectrometer. A pressure of 10^{-2} mbar at the entrance to the mass spectrometer is maintained during the experiments with the help of a second turbo molecular pump (Balzers 071P).

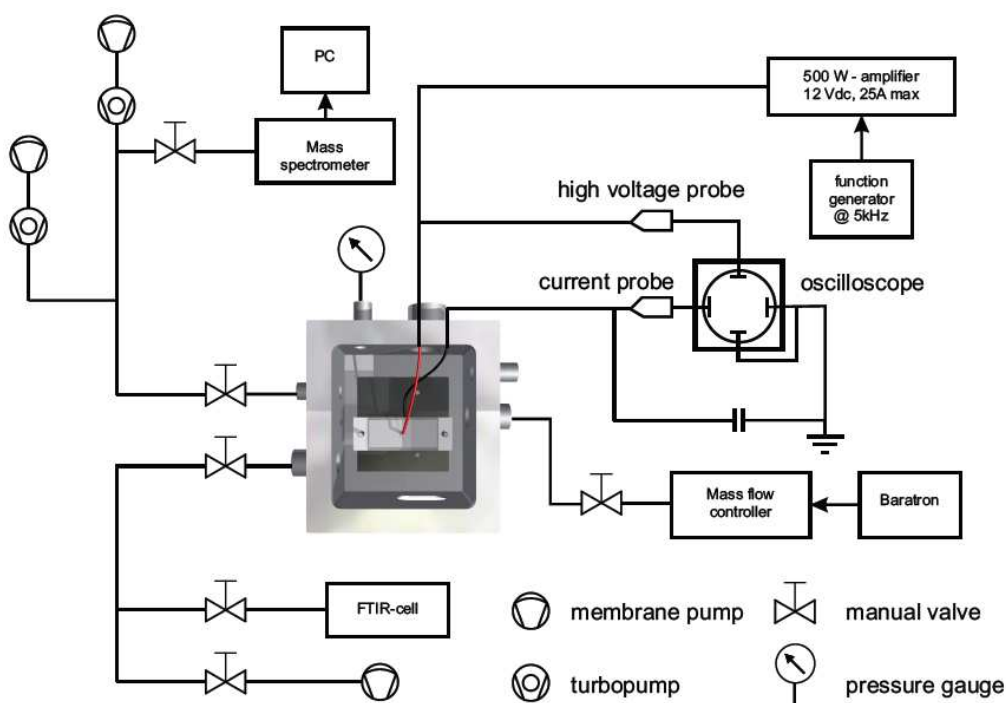


Figure 3.1 Schematic of the DBD experimental setup

Gas composition was continuously monitored. Mass spectra were taken every hour at typical sampling rates of 0.5-1 mass numbers per second. The experiments were performed until 6 hours for all the gas mixtures. And in order to check the stability at larger mass numbers, for a C_2H_4/Ar (300 mbar) gas mixture with a varying SF_6 admixture (up to 100 mbar). A linear relationship between SF_6 count rate and SF_6 partial gas pressure was observed. As a further test, mass spectra were recorded over several hours and no signal distortions of relevance were noted.

In order to measure Fourier Transform Infrared (FTIR) Spectroscopy a gas cell is connected to the discharge chamber. The connection is made in the path between chamber and membrane pump, and in such a way that the FTIR gas cell can be evacuated separately. The FTIR gas cell is made up of Pyrex glass and, equipped with two 5 mm thick KBr windows with closable PTFE (Poly Tetra Fluoro Ethylene) taps on the Pyrex cell. Length and volume of the cell 10 cm and 132 cm³, respectively. Before starting the experiments the cell was cleaned by the continuous flow of N₂ for about 10-15 mins to remove all impurities. Then the cell is connected to the discharge chamber, after the connection the cell is cleaned again by the continuous flow of N₂/Ar gas. The cell is pumped by the membrane pump down to about 10 mbar and then filled with the gas from the discharge chamber. FTIR analysis is performed with the help of a FTIR spectrometer (Perkin Elmer). FTIR spectra are recorded in the range of 400-4000 cm⁻¹ with a resolution of 4 cm⁻¹. The spectra presented here are after subtracting the absorbance of background and empty cell.

3.2 Electrode Configuration for the Preparation of thin films

From figure 3.2, we can see that the three-dimensional picture of the two electrodes as placed in the DBD chamber. The electrodes were made of Cu (copper) or stainless steel plates. Both the electrodes were placed in a rectangular shaped Plexiglas. Both the electrodes were covered with different dielectric materials. The upper electrode was covered with aluminium oxide, which has a dielectric constant of $\epsilon \approx 10$ and the lower electrode was covered with glass plate of dielectric constant $\epsilon \approx 3.8$, which are already mentioned in the above experimental schematics. To separate the dielectric material and the Cu (or stainless steel) electrode, we have placed a mesh which is made from stainless steel. The two electrodes in the chamber were separated by a 1.5 or 2mm TEFLON spacer which has symmetrical holes throughout its edge as shown in the figure 3.2. Silicon or glass substrates can be cut according to the experimental characterizations. Substrates can be placed in between the electrodes. The upper electrode is connected to the high-voltage power supply,

and the lower one is grounded. The chamber is pumped by a membrane pump down to about 10 mbar. The experiments were performed at a pressure of 300 mbar.

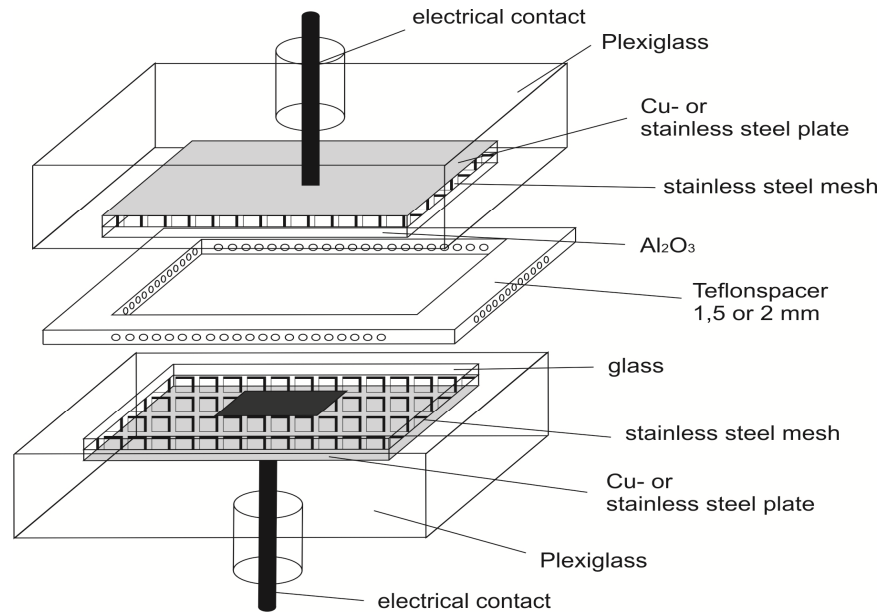


Figure 3.2 Three dimensional picture of the electrodes.

Chapter 4

Plasma Chemical Reactions in C_2H_2/N_2 , C_2H_4/N_2 , and C_2H_6/N_2 Gas Mixtures

In this chapter we present the experimental results obtained from mass spectrometry for C_2H_m/N_2 ($m = 2, 4, 6$) gas mixtures. Mass spectra were taken every hour at typical sampling rates of 0.5-1 mass numbers per second. The long term stability was investigated for CH_4/Ar gas mixture with a varying hydrogen admixture (Majumdar et al., 2005) ^[85] and in order to check the stability at larger mass numbers, for a C_2H_4/Ar (300mbar) gas mixture with a varying SF_6 admixture (up to 100 mbar). A linear relationship between SF_6 count rate and SF_6 partial pressure was observed. As a further test, mass spectra were recorded over several hours and no signal distortions of relevance were noted.

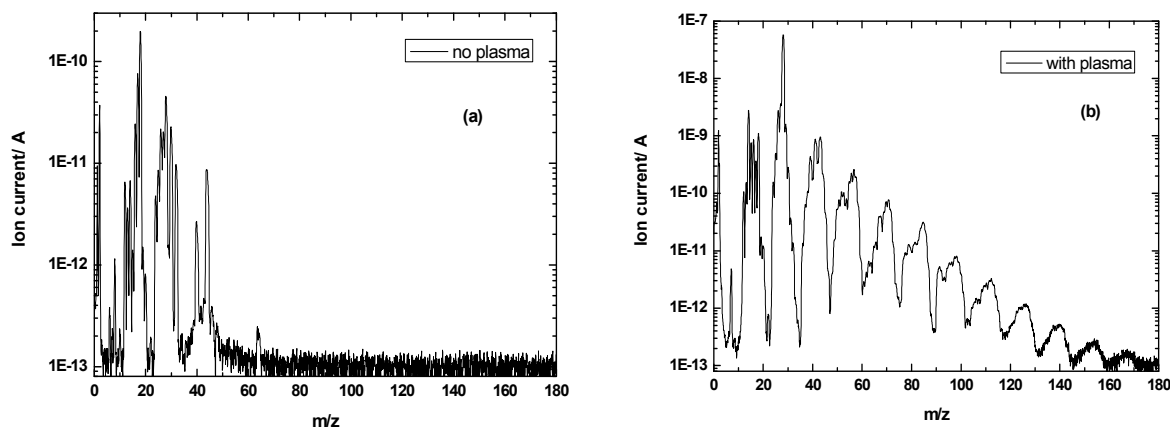


Figure 4.1 Mass spectra obtained from a C_2H_4/N_2 gas mixture without plasma (a) and after 360 min with the plasma on (b)

Figure 4.1 displays two typical mass spectra up to mass numbers $m/z = 180$ that were obtained after the chamber has been filled with 300 mbar of a C_2H_4/N_2 gas mixture (mixing

ratio 1: 2). Figure 4.1(a) represents the initial gas composition consisting of nitrogen and ethylene (C_2H_4) gas. Impurities that are present consist, e. g., of water (H_2O , $m/z = 18$), oxygen (O_2 , $m/z = 32$) and small amounts of higher hydrocarbons and of other gas impurities around mass numbers $m/z = 39-41$ (e.g., C_3H_4 , Ar), 44 (CO_2), and 50-58 (e.g., C_4H_6 , C_4H_8). It should be noted that stable molecules dissociate inside the ion source of the mass spectrometer, giving rise to the formation of unstable radical ions that complicate the data analysis ^{[71], [72]}. For example, ethane shows up in the mass spectra with masses $m/z = 12$ (C^+), 13-15 ($CH_n^+ = 1-3$), 24 (C_2^+), and 25-30 ($C_2H_n^+$, $n = 1-6$). Hexane ($M=86$), on the other hand, prominently shows up at mass number $m/z = 27, 29, 41-43, 56, 57$, and only weakly (with about 4%) at 86. Information about fragmentation pattern have been derived from the NIST Chemistry WebBook (Linstrom and Mallard, 2010).

Figure 4.1(b) displays the mass spectrum obtained from the same gas after the discharge has been operated for 360 minutes. The long operation times had to be chosen because of the small discharge power consumed by the plasma. Several differences compared to figure 4.1(a) are noted: (i) a reduction of ethylene peaks, (ii) an increase of the hydrogen peak, and (iii) the appearance of the higher hydrocarbon peaks with up to 12 carbon atoms. The experimental results presented below are obtained by subtracting the mass spectra obtained without plasma from those obtained with plasma, e. g., by subtracting the data of figure 4.1(a) from those of figure 4.1(b).

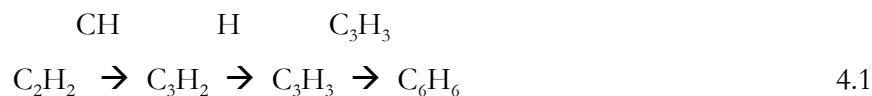
4. 1 Results and discussion

In the following we separately present our results for the three C_2H_2/N_2 , C_2H_4/N_2 , and C_2H_6/N_2 gas mixtures.

4.1.1 C_2H_2/N_2

The difference mass spectrum from the C_2H_2/N_2 gas mixture in the mass number range $m/z = 35-180$ is displayed in Figure 4.2. A certain amount of the consumed C_2H_2 is used for the production of higher chain hydrocarbons which show up at mass numbers $m/z = 49-50$ (butadiyne, C_4H_2) and 74 (hexatriyne, C_6H_2). Formation of cyclic hydrocarbons with mass numbers $m/z = 78$ (benzene, C_6H_6), 92 (toluene C_7H_8), and eventually 106 (e.g., dimethyl-

benzene or ethyl-benzene, C_8H_{10}) also occurs. Benzene and other ring components play a role in e.g., Jupiter's atmosphere and the following reaction pathway for benzene formation has been proposed recently by Wong et al.^[73],



The peak appearing at mass number $m/z = 52$ (cyanogen, C_2N_2) is associated with formation of a nitrogen-containing molecule ^[74], as was inferred from our own measurements without nitrogen where this peak is absent.

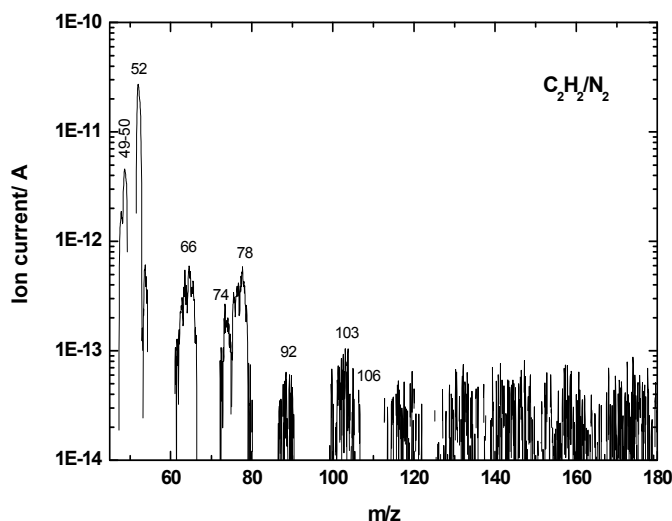


Figure 4.2 Difference mass spectrum with and without plasma in the mass range $m/z = 35$ -180 for a C_2H_2/N_2 gas mixture.

While about 50% of the C_2H_2 gas was consumed during the experiment, a crude estimate shows that only about 1% is converted into larger hydrocarbons and less than 0.3% into molecules. It is well known that the prominent plasma chemical reactions in acetylene



lead to the formation of hydrogen-poor molecules which quickly grow to form nanometer- and micrometer-size (so-called dust) particles ^{[75][76][77][78]}. Dust formation was not observed in the present experiment, however, presumably due to the low plasma density and the small plasma dimensions which prevent particle growth. Further, a significant fraction of the consumed acetylene condenses on the electrodes forming a soft film with a brownish color.

4.1.2 C₂H₄/N₂

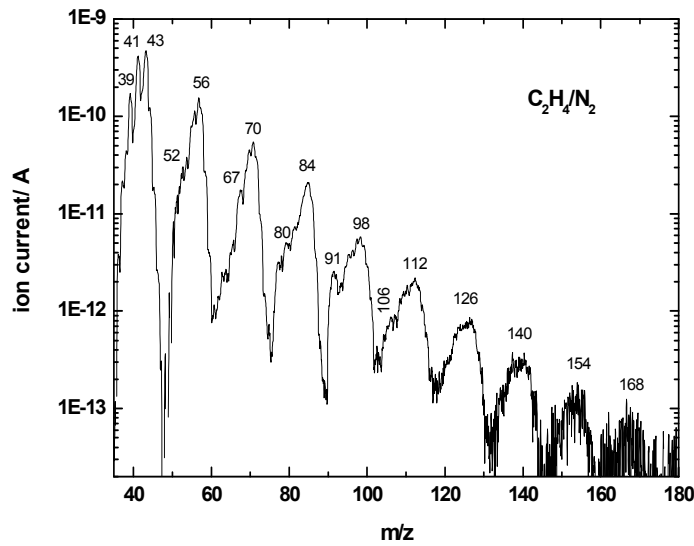


Figure 4.3 Difference mass spectrum with and without plasma in the mass range $m/z = 35$ -180 for a C₂H₄/N₂ gas mixture.

The difference mass spectrum from the C₂H₄/N₂ gas mixture at mass numbers $m/z = 30$ -180 is displayed in Figure 4.3. A significant amount of the consumed C₂H₄ is used for the production of higher hydrocarbons which show up as prominent peaks at mass numbers $m/z = 40$ -180 corresponding to hydrocarbon molecules with up to 12 carbon atoms. The prominent groups appearing at $m \approx 2n$ ($n = 3$ -12) are roughly equally spaced by $\Delta m = 14$ corresponding to one CH₂ group. Evidently, one CH₂ radical is adding up in consecutive reactions, thereby obeying the (gross) reaction scheme,



and in consequence the spectrum becomes periodic. The actual reaction pathways are more complicated, however. For example, chemical reactions of the most prominent C_2H_3 radical with C_2H_4 will contribute to the formation of e.g., C_3H_3 , C_4H_5 , C_4H_6 and C_6H_8 including aromatic molecules like benzene and styrene^[79]. Peaks appearing at mass numbers $m/z = 39$, 41, and 43 presumably originate from fragmentation of higher order hydrocarbons yielding among others $C_3H_m^+$ ($m = 3, 5, 7$) fragment ions. As before, the peak at mass number $m/z = 52$ (cyanogen, C_2N_2) is associated with the formation of a nitrogen-containing molecule. We estimate that about 15% of the consumed C_2H_4 is converted into higher hydrocarbons. Further, a significant fraction of the consumed ethylene condenses on the electrodes forming films/deposits with a brown-orange color.

4.1.3 C_2H_6/N_2

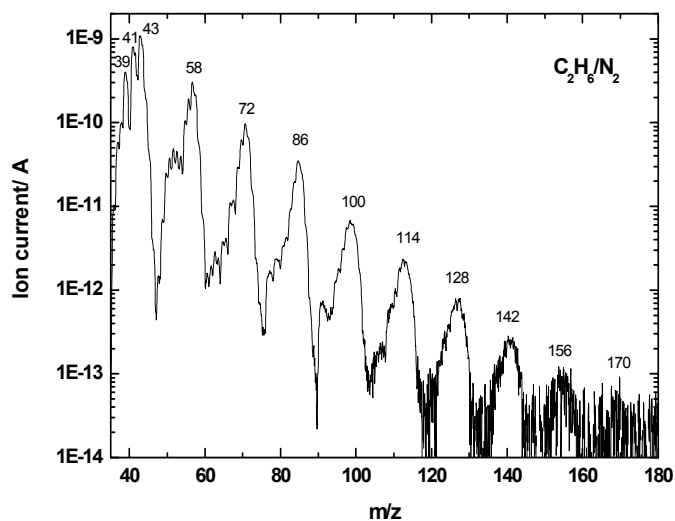


Figure 4.4 Difference mass spectrum with and without plasma in the mass range $m/z = 35$ -180 for a C_2H_6/N_2 gas mixture

Figure 4.4 displays the measured difference spectrum for mass numbers $m/z = 30$ -180. The broad prominent peaks, each composed of several individual peaks, are attributed to C_nH_m molecules with n up to 12 and $m \approx 2n + 2$. The most prominent peaks, hence, approximately differ by $\Delta M \approx 14$ from each other. Evidently, as in the case of C_2H_4/N_2 , one CH_2 radical is

adding up in consecutive reactions and in consequence the spectrum becomes periodic. Prominent peaks in the spectrum occurring at $m/z = 58, 72, 86, 100, 114, 128, 142, 156,$ and 170 are attributed to alkane molecules $C_4H_{10}, C_5H_{12}, C_6H_{14}, C_7H_{16}, C_8H_{18}, C_9H_{20}, C_{10}H_{22}, C_{11}H_{24},$ and $C_{12}H_{26},$ respectively. Formation of cyclic molecules apparently also occurs, as is inferred from the peaks at $m/z = 67/68, 78, 91/92,$ and $105/106$ which are attributed to C_5H_8 (cyclo-pentene), C_6H_6 (benzene), C_7H_8 (toluene or methyl-benzene), and C_4H_{10} (dimethyl-benzene), respectively.

4.2 Comparison of C_2H_2/N_2 , C_2H_4/N_2 , and C_2H_6/N_2 mass spectra

4.2.1 C_2H_2 and C_2H_4

A comparison of C_2H_2/N_2 and C_2H_4/N_2 mass spectra is made in Figure 4.5. The following differences are noted:

- the peak positions are shifted to larger mass number for C_2H_4 compared to C_2H_2 , e.g., $m/z = 56$ vs. $52, 70$ vs. $66, 84$ vs. $78, 98$ vs. 103 and
- the observed peaks are broader in C_2H_4 compared to C_2H_2

Larger molecules produced from C_2H_4 thus contain a larger number of hydrogen atoms compared to molecules produced from C_2H_2 which are known to be hydrogen poor.

4.2.2 C_2H_4 and C_2H_6

A comparison of C_2H_4/N_2 and C_2H_6/N_2 mass spectra is made in Figure 4.6. The following differences are noted:

- A small shift in the peak positions for mass numbers $m/z > 90$ between C_2H_4 and C_2H_6 .
- Peaks in the C_2H_4 spectrum are broader than compared to the C_2H_6 spectrum, except for mass numbers $m/z = 39 - 43$. The latter difference is attributed to the formation of cyclic (aromatic) hydrocarbons which are thus more efficiently produced by C_2H_4 compared to C_2H_6 .

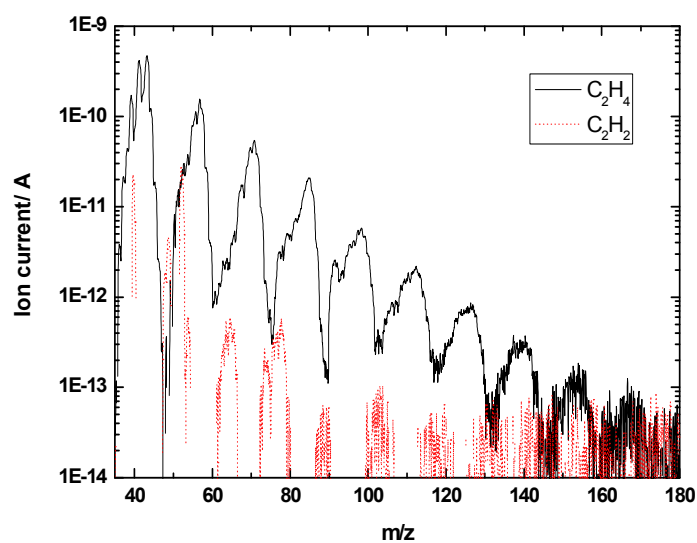


Figure 4.5 Comparison of C_2H_2/N_2 and C_2H_4/N_2 mass spectra with plasma in the mass range M/Z up to 35-180

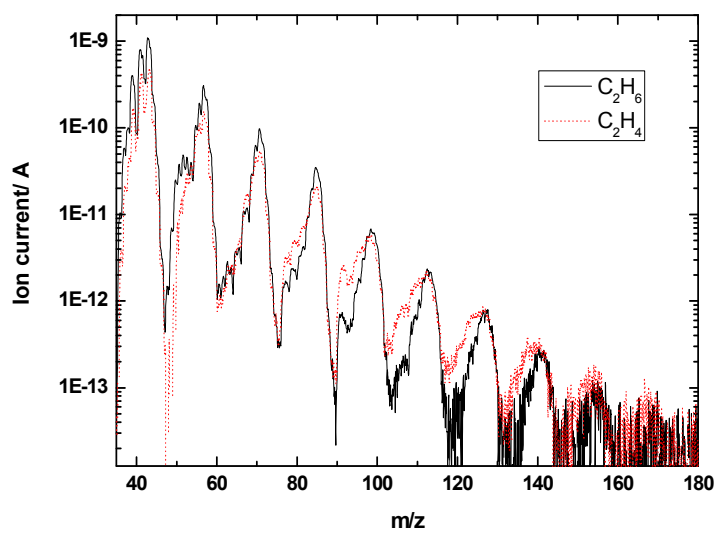


Figure 4.6 Comparison of C_2H_4/N_2 and C_2H_6/N_2 mass spectra with plasma in the mass range M/Z up to 180.

4.2.3 Time dependency

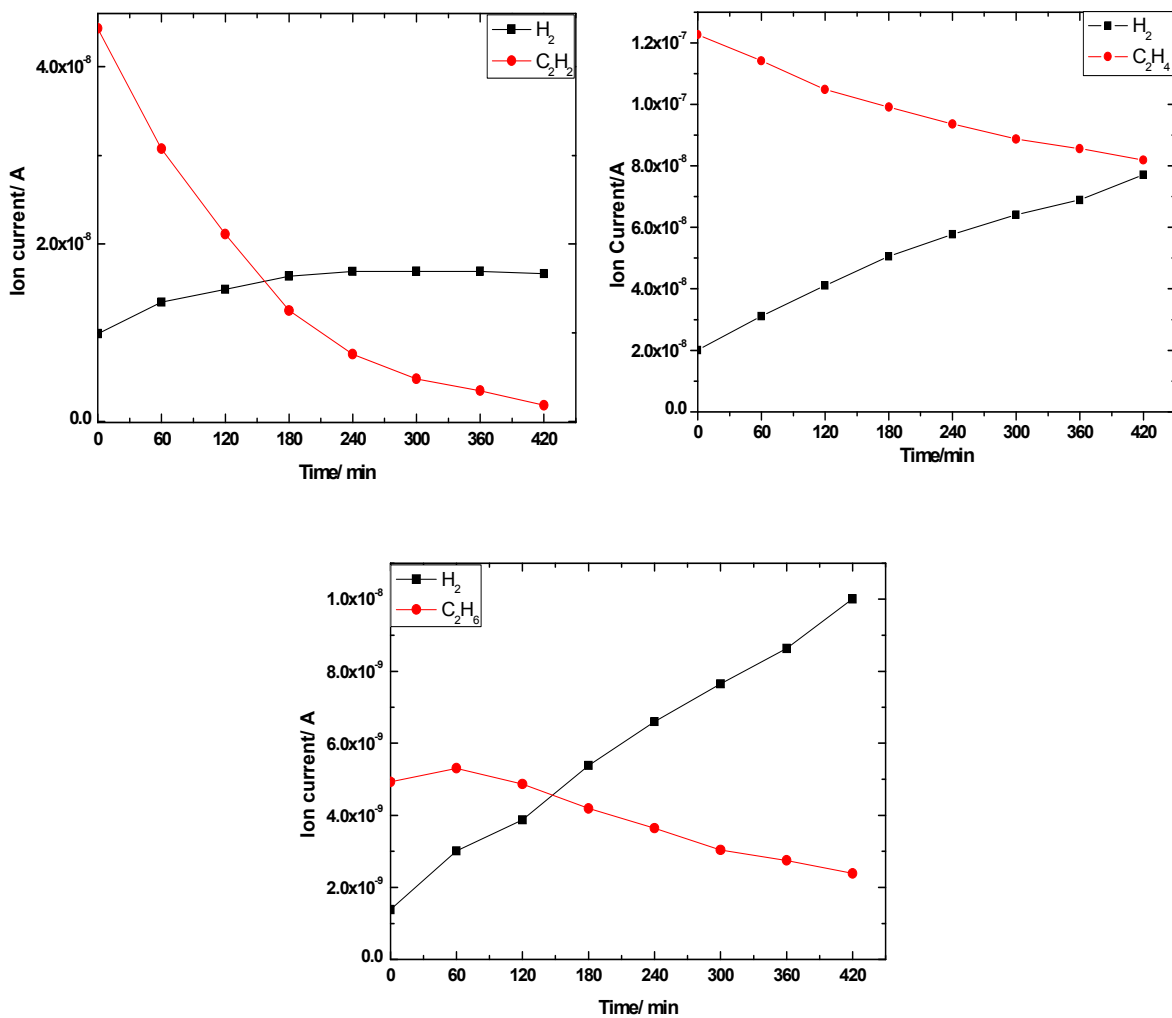


Figure 4.7 Time dependent production of H_2 and time dependent consumption of C_2H_m/N_2 ($m = 2, 4, 6$) gas mixtures with pressure 300 mbar and gas ratio 1:2.

Figure 4.7 shows the time dependent production of H_2 and consumption of C_2H_m/N_2 ($m = 2, 4, 6$) gas mixtures at chamber pressure 300 mbar and the gas ratio 1:2. From above all graphs we can see that the production of H_2 is inversely proportional to the precursor gas used. In addition to this from the mass spectrum we have noticed that there is certain

amount of reduction in the nitrogen peak with the time decay. The reduced amount of nitrogen and C_2H_m ($m = 2, 4, 6$) have been used up in the formation of H_2 and the higher order hydrocarbons and nitrogen containing complexes. That's why in all the plots we can see the decay of precursor gases and the formation of H_2 gas. As the time decays the formation of higher order hydrocarbons and nitrogen containing complexes are also increases. Higher order hydrocarbons and nitrogen containing complexes were formed in a smaller extent. The amount of individual precursor hydrocarbons consumed are in different amount and which lies in the order $C_2H_2 > C_2H_4 > C_2H_6$. In C_2H_2/N_2 plasma the consumption of C_2H_2 gas is noticed to be larger when compared to C_2H_4/N_2 and C_2H_6/N_2 gas mixtures.

4.2.4 Properties of deposited films

Film deposited on the electrodes during the dielectric barrier discharge in a C_2H_6/N_2 gas mixture display a yellow-brown color. The composition of these films was investigated in some details with the help of X-ray photoelectron spectroscopy (XPS). Accordingly, the film is composed of carbon (C) and nitrogen (N) with N/C ratios of ≈ 0.2 and ≈ 0.55 for C_2H_6/N_2 mixing ratios of 1:2 and 1:5, respectively ^[23]. The present results compare favorable with previous investigations of the chemical composition of carbon-nitride films deposited in a CH_4/N_2 dielectric barrier discharge ^{[24] [80]}, where N/C ratios of ≈ 0.25 and ≈ 0.6 for a mixing ratios of 1:2 and 1:20, respectively, had been obtained. Similar ratios had been observed for films deposited in a C_2H_4/N_2 dielectric barrier discharge plasma ^[81].

Chapter 5

FTIR Spectroscopy for CH_4/N_2 and $\text{C}_2\text{H}_m/\text{N}_2$ ($m = 2, 4, 6$) Gas Mixtures in a Dielectric Barrier Discharge

This chapter explains the FTIR spectroscopic results obtained for CH_4/N_2 and $\text{C}_2\text{H}_m/\text{N}_2$ ($m = 2, 4, 6$) gas mixtures and interpretation of results.

5.1 Results and Discussion

5.1.1 CH_4/N_2 Plasma

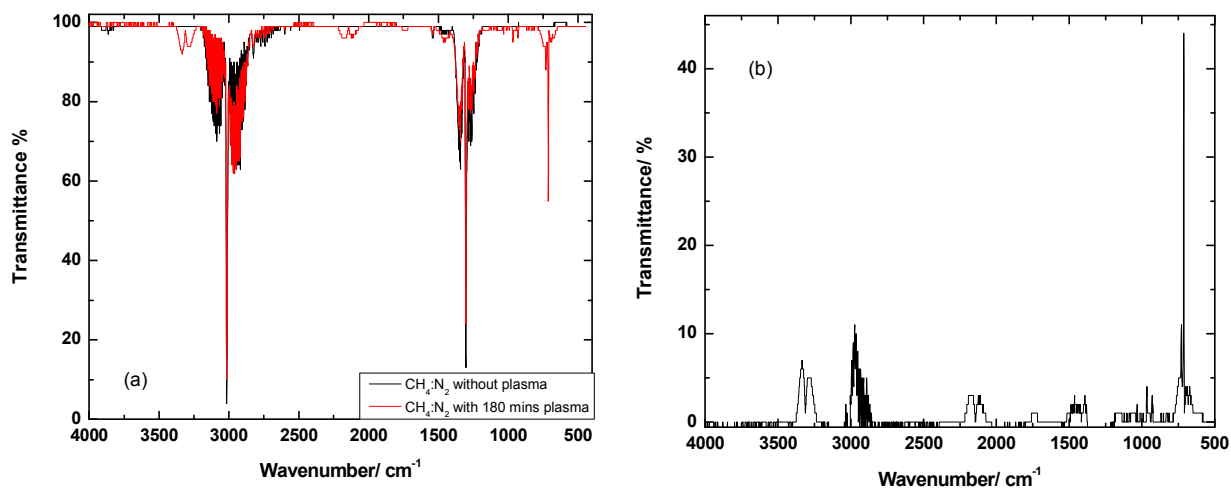


Figure 5.1 FTIR spectrum of CH_4/N_2 gas mixture, with gas ratio 1:2, 300 mbar pressure (a) without and with plasma (b) Difference spectra obtained after the subtraction with 180 mins plasma and without plasma.

Figure 5.1(a) FTIR spectrum of CH₄/N₂ gas mixture with and without plasma. After ignition of the plasma, concentration of methane decreases due to consumption by discharge and several new peaks have been appeared. The bands formed in the region 1306 cm⁻¹ (1215 cm⁻¹ – 1380 cm⁻¹) and 3019 cm⁻¹ (2900 cm⁻¹ – 3150 cm⁻¹) corresponds to C-H bending and C-H stretching vibrations^[86], respectively for methane.

In order to see clearly what is formed and what is consumed we have subtracted the FTIR spectrum obtained with plasma and without plasma. The spectrum obtained after the subtraction are difference FTIR spectra. Such a difference FTIR spectrum for CH₄/N₂ is displayed in Figure 5.1(b). The plots presented here are in transmittance mode. In the difference spectrum we have found the formation of several molecules. Formation of C₂H₂ can be noticed at the wavenumbers 3300 cm⁻¹ and 730 cm⁻¹ which are related to C-H stretching and C-H bending vibrations,^[84] respectively. Nitrogen containing molecule, HCN can be noticed at the wavenumbers 3300 cm⁻¹, 1450 cm⁻¹, and 712 cm⁻¹, which are related to C-H stretching, bending and out-of-plane deformations,^[82] respectively. Another nitrogen containing molecule NH₃ can be noticed at 968/930 cm⁻¹. Formation of aromatic compound benzene can be noticed from the wavenumbers 3035 cm⁻¹, 1504 cm⁻¹, 1033 cm⁻¹, and 673 cm⁻¹. Which are related to C-H stretching, C=C stretching, C-H bending and C-H out-of-plane deformations, respectively for benzene. Formation of C₂H₄ (3000 cm⁻¹, 1443 cm⁻¹ and 950 cm⁻¹) and C₂H₆ (2960 cm⁻¹ and 1462 cm⁻¹) molecules can be confirmed^[83]. Further, the formation of C₂H₂, C₂H₄ and C₂H₆ hydrocarbons from CH₄ were already reported from mass spectrometry by Majumdar et al^[85]. The bands appeared in the region 2215 cm⁻¹ – 2090 cm⁻¹ corresponds to CO and wavenumber 1738 cm⁻¹ corresponds to the formation of CH₂O or C₂H₄O, which are considered as an impurities. We believe that the oxygen comes from the electrode surface. The percentage formation and consumption of each molecules in CH₄/N₂ and C₂H_m/N₂ (m = 2, 4, 6) gas mixtures have been calculated from Beer-Lambertz Law.

5.1.2 C₂H₂/N₂ Plasma

The FTIR spectrum of C₂H₂ is displayed in figure 5.2(a). It shows strong peaks at wavenumbers 3180 cm⁻¹ - 3370 cm⁻¹, 1184 cm⁻¹ - 1488 cm⁻¹, and 851 cm⁻¹ - 1067 cm⁻¹ which are related to C-H stretching and C-H deformation vibrations of C₂H₂^[86]. After ignition of

the plasma several new peaks appear in the spectrum as shown in figure 5.2(b). The pronounced peak at wavenumber 630 cm^{-1} is due to formation of biacetylene (butadiyne, C_4H_2)^[135]. There is evidence for the formation of CH_4 observed at wavenumber 3019 cm^{-1} . Other bands at wavenumbers $2800\text{ cm}^{-1} - 3070\text{ cm}^{-1}$ corresponds to C-H stretching vibrations of saturated alkanes like CH_4 and C_2H_6 ^[83] and unsaturated alkenes like C_2H_4 . Traces of C_2H_4 are detected at 950 cm^{-1} . CO formation by plasma wall interaction is observed at 2150 cm^{-1} ($2063\text{ cm}^{-1} - 2220\text{ cm}^{-1}$).

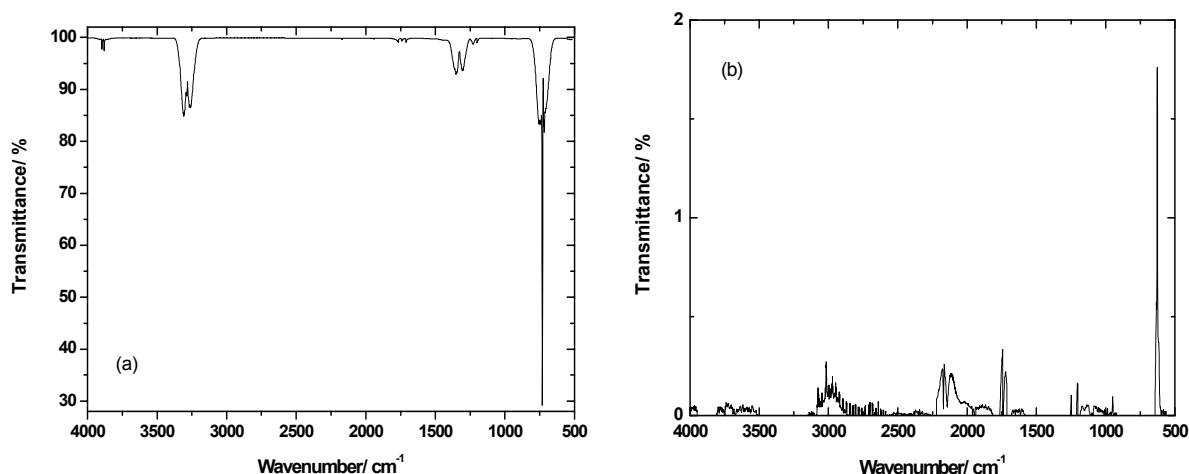


Figure 5.2 FTIR spectrum of $\text{C}_2\text{H}_2/\text{N}_2$ gas mixture, with gas ratio 1:2, 300 mbar chamber pressure (a) without plasma, (b) Difference spectra obtained after subtraction of the FTIR spectrum obtained after 180 mins with plasma from the spectrum obtained without plasma.

5.1.3 $\text{C}_2\text{H}_4/\text{N}_2$ Plasma

Figure 5.3(a) shows the FTIR spectrum of $\text{C}_2\text{H}_4/\text{N}_2$ gas mixture, with gas ratio 1:2, 300 mbar pressure without plasma. The pronounced absorptions appearing at the wavenumber regions $3050\text{ cm}^{-1} - 3000\text{ cm}^{-1}$, $1740\text{ cm}^{-1} - 1730\text{ cm}^{-1}$, $1494\text{ cm}^{-1} - 1398\text{ cm}^{-1}$ and $1081\text{ cm}^{-1} - 827\text{ cm}^{-1}$ corresponds to C-H stretching vibration, $\text{C}=\text{C}$ stretching vibration, CH_2 scissoring and CH_2 wagging for C_2H_4 hydrocarbon^[86], respectively. Figure 5.3(b) is the difference spectra obtained from the same gas mixture after 180 min plasma. The difference spectrum revealed the formation of C_2H_2 from the wavenumbers 3300 cm^{-1} and 730 cm^{-1} , which corresponds to

C-H stretching and C-H bending vibrations, respectively. Formation of HCN molecules can be found at the wavenumbers 3300 cm^{-1} , 1450 cm^{-1} , and 712 cm^{-1} ^[86].

Formation of C_2H_6 can be confirmed from the wavenumbers 2960 cm^{-1} and 1508 cm^{-1} and formation of CH_4 can be found from the wavenumbers 3015 cm^{-1} and 1301 cm^{-1} , which are related to C-H stretching and C-H bending vibrations^{[83] [87] [88]}. Higher order hydrocarbons like C_4H_{10} (2950 cm^{-1} and 1372 cm^{-1}), C_3H_8 (2950 cm^{-1} and 1158 cm^{-1}) are also identified. Formation of C_2H_6 can be confirmed from the wavenumbers 2960 cm^{-1} and 1508 cm^{-1} . A weak band at 630 cm^{-1} is due to the formation of biacetylene (butadiyne, C_4H_2)^[135]. The impurities bands which are appeared in the wavenumber region $2202\text{ cm}^{-1} - 2090\text{ cm}^{-1}$ corresponds to CO formation and 1738 cm^{-1} is related to C=O stretching vibrations^[86] for CH_2O or $\text{C}_2\text{H}_4\text{O}$ molecules, which form by plasma-wall interaction with oxygen-containing surfaces for example, electrodes.

The relative absorbance according to the infrared spectra provided by ANSYCO GmbH (Karlsruhe, Germany) <http://www.ansyco.de/CMS/frontend/index.php> for spectra taken at 7.7 cm^{-1} NH_3 : 0.27/0.22, HCN: 0.205, C_2H_2 : 0.32

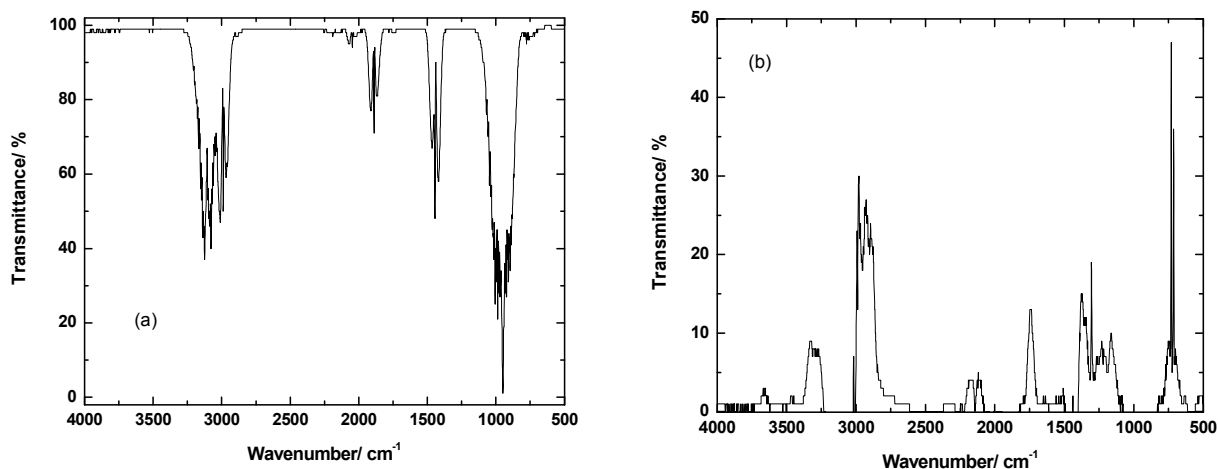


Figure 5.3 FTIR spectrum of $\text{C}_2\text{H}_4/\text{N}_2$ gas mixture, with gas ratio 1:2, 300 mbar pressure (a) without plasma (b) Difference spectra obtained after the subtraction with 180 mins plasma and without plasma

5.1.4 C₂H₆/N₂ Plasma

Figure 5.4(a) shows the FTIR spectrum of C₂H₆/N₂ gas mixture, with gas ratio 1:2, 300 mbar pressure without plasma. The well pronounced bands which have been appeared at wavenumbers 2900 cm⁻¹, 1470 cm⁻¹ and 822 cm⁻¹ are related to C-H stretching vibrations, C-H deformations and out-of-plane C-H deformations for C₂H₆ hydrocarbon^[86], respectively. Figure 5.4(b) is the difference spectrum obtained after the subtraction with 180 mins plasma. Formation of C₂H₂ can be found at the wavenumbers 3300 cm⁻¹ and 730 cm⁻¹. Nitrogen containing molecules such as HCN (3300 cm⁻¹, 1450 cm⁻¹, and 712 cm⁻¹) and NH₃ (968 cm⁻¹ and 932 cm⁻¹) are identified. Smaller hydrocarbon like CH₄ can be found at the wavenumbers 3015 cm⁻¹ and 1303 cm⁻¹ which are related to C-H stretching and C-H bending vibrations, respectively. Formation of C₂H₄ (3000 cm⁻¹ and 949 cm⁻¹) and C₄H₂ (630 cm⁻¹) can be confirmed. The impurities bands can be found in the wavenumber region 2207 cm⁻¹ – 2082 cm⁻¹ for CO formation and 1742 cm⁻¹ corresponds to C=O stretching vibrations for CH₂O or C₂H₄O molecules.

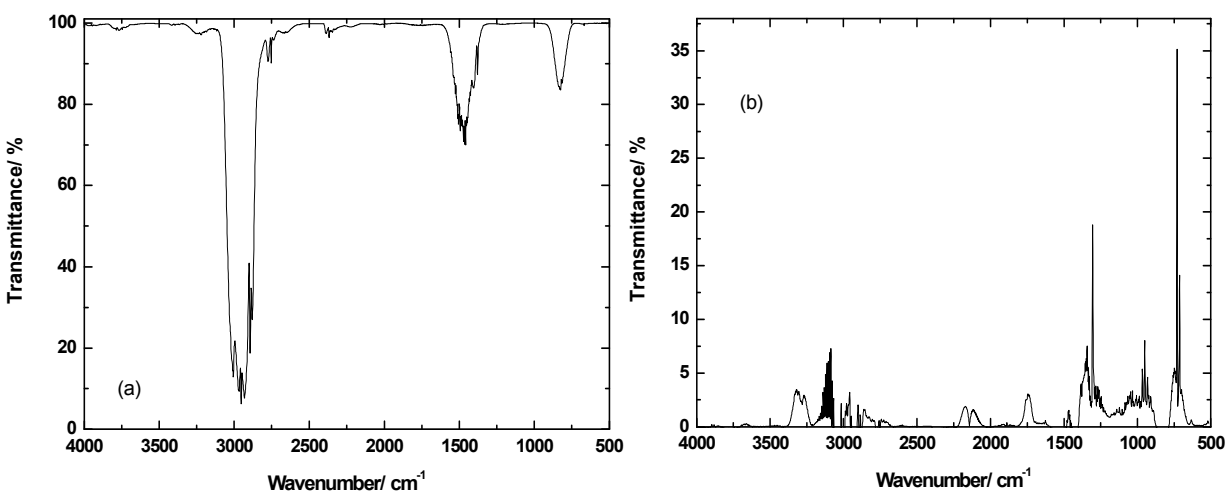


Figure 5.4 FTIR spectrum of C₂H₆/N₂ gas mixture, with gas ratio 1:2, 300 mbar pressure (a) without plasma (b) Difference spectra obtained after the subtraction with 180 mins plasma and without plasma.

5.2 Discussion

Our results are summarized in table 5.1 and in figure 5.5. Evidently, in all gas mixtures about 40% (30 – 49 %) of the initial hydrocarbon gas is consumed during 180 mins of plasma operation. The major net reaction pathways among the investigated hydrocarbons are summarized in figure 5.5. Accordingly, C₂H₄ contributes to the formation of CH₄, C₂H₂, and C₂H₆. C₂H₂ is also produced from CH₄ and C₂H₆. In addition, significant amounts of HCN and comparatively small amounts of NH₃ are formed.

The preference of C₂H₂ formation in the investigated gas mixture is easily understood. Dissociation of molecules by impact energetic electrons is a dominant process in hydrocarbon plasmas. C₂H₂ is directly formed from C₂H₄ by hydrogen abstraction ^[128],



Fragmentation of CH₄ and C₂H₄ yields to the formation of, e.g., CH, CH₂, and CH₃ radicals ^[128]. The radicals further react to either form C₂H₂ via, e.g., ^[128]



or to form larger hydrocarbons via polymerization reactions ^[16], e. g.,



The simple scheme thus suggests that the investigated hydrocarbons largely end up as C₂H₂ and to a smaller amount as nitrogen-containing molecules. Remains the question what happens with C₂H₂. It is known from mass spectrometry that C₂H₂ quickly forms larger hydrogen-poor molecules and radicals which eventually grow to carbonaceous nano-size particles ^{[75][76][77][78]}. Possible pathways are via C₄H₂, C₆H₂, and C₈H₂. Of these, C₄H₂ and C₆H₂ are chain molecules formed by polymerization of C₂H₂, e.g., through chemical reactions involving C₂H radicals ^{[117][118]}.

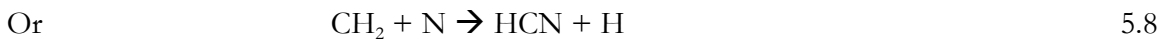


Indeed, biacetylene (C_4H_2)^[135] is the dominant molecule detected in the difference FTIR spectrum from acetylene figure 5.2 (b). Chemical reactions studies during the pyrolysis of C_2H_2 indicate that the corresponding reaction rates are rather large^[79].

Formation of nitrogen-containing molecules begins with the dissociation of N_2 by electron impact,



followed by chemical reactions with CH_2 and CH_3 radicals, e.g.,^{[128] [133][134]}.



Resulting in the formation of the dominant nitrogen-containing molecule HCN. Ammonia production requires reactions of N radicals with hydrogen, e.g.,

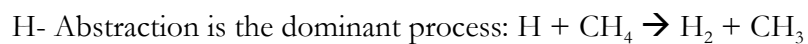
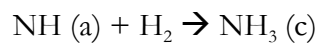
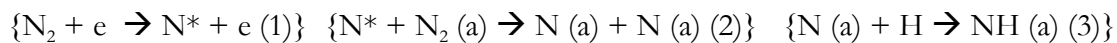


where H_2 is formed in hydrogen abstraction reactions of energetic electrons with hydrocarbon molecules. Subsequent reactions with H_2 may eventually lead to the formation of NH_3 , e.g., via

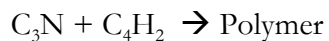
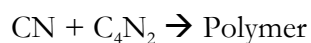


Nitrogen: reactions of metastable N (4S) and N (2D) nitrogen radicals with CH_3 and CH_4 ^[136]





From the scheme proposed by Hiroshi et al.,^[127] formation of heterogeneous polymer (tholins) takes place via heterogeneous nitrogen incorporation mechanism via short lived intermediate species, such as HCCN radical for the formation of nitrogen containing compounds. The possible reaction pathways for the formation of heterogeneous polymer (tholins) is,



Finally, the formation of tholins takes place by the reaction between the polymers.

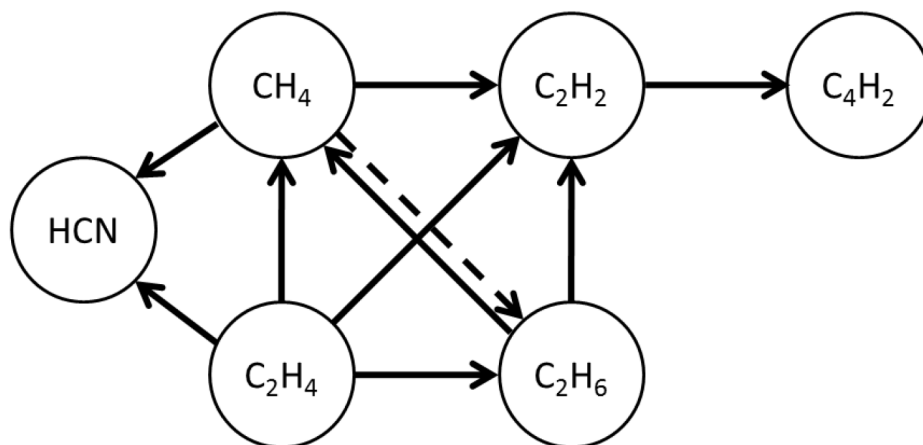


Figure 5.5 Reaction pathways among the hydrocarbons and HCN. Arrows indicate the net balance of forward (e.g., $\text{CH}_4 \rightarrow \text{C}_2\text{H}_6$) and backward (e.g., $\text{CH}_4 \leftarrow \text{C}_2\text{H}_6$) pathways. Strong (solid lines) and medium (dashed lines) pathways are indicated.

Table 5.1 Percentage production and percentage consumption in CH_4/N_2 and $\text{C}_2\text{H}_m/\text{N}_2$ ($m = 2, 4, 6$) plasma

Initial Gas	Gas consumption/Production (%)					
	CH_4	C_2H_2	C_2H_4	C_2H_6	HCN	NH_3
CH_4	-30	3.2	-	4.1	23	1.1
C_2H_2	-	-49	0.02	0.1	-	-
C_2H_4	10	16	-40	13	18	-
C_2H_6	10	11	1.8	-37	6	1.5

Table 5.2 Major Plasma content assignments for plasma FTIR spectra absorption bands

Species	From NIST	From Expt.	Type of mode
CH ₄	3019	3019	Deg str
	1533	1538	Deg deform
	1306	1306	Deg deform
C ₂ H ₂	3295	3304	CH str
	3281	3268	CH str
	730	730	CH bend
C ₂ H ₄	3105	3105	CH ₂ a-str
	2988	2988	CH ₂ s-str
	1443	1448	CH ₂ scis
	949	949	CH ₂ wag
	826	ia	CH ₂ rock
C ₂ H ₆	2985	2988	CH ₃ d-str
	2895	2895	CH ₃ s-str
	1469	1464	CH ₃ d-deform
	1379	1373	CH ₃ s-deform
	821	825	CH ₃ rock
C ₆ H ₆	1486	1492	Ring str +deform
	1038	1033	CH bend
	673	673	CH bend

C ₄ H ₂	3329	3329	CH str
	2020	2020	C≡C str
	630	630	C-H bend
NH ₃	3337	3337	Sym str
	3443	3443	Deg str
	1627	1608	Deg deform
	968	968	Sym deform
	932	932	Sym deform
HCN	3311	3312	CH str
	2097	2097	CN str
	712	712	Bend

Chapter 6

Comparative Plasma Chemical Reaction Studies of CH_4/Ar and $\text{C}_2\text{H}_m/\text{Ar}$ ($m = 2, 4, 6$) gas mixtures in an Atmospheric Pressure Dielectric Barrier Discharge

In this chapter we discuss the mass spectrometry and FTIR spectroscopy results obtained for CH_4/Ar and $\text{C}_2\text{H}_m/\text{Ar}$ ($m = 2, 4, 6$) gas mixtures.

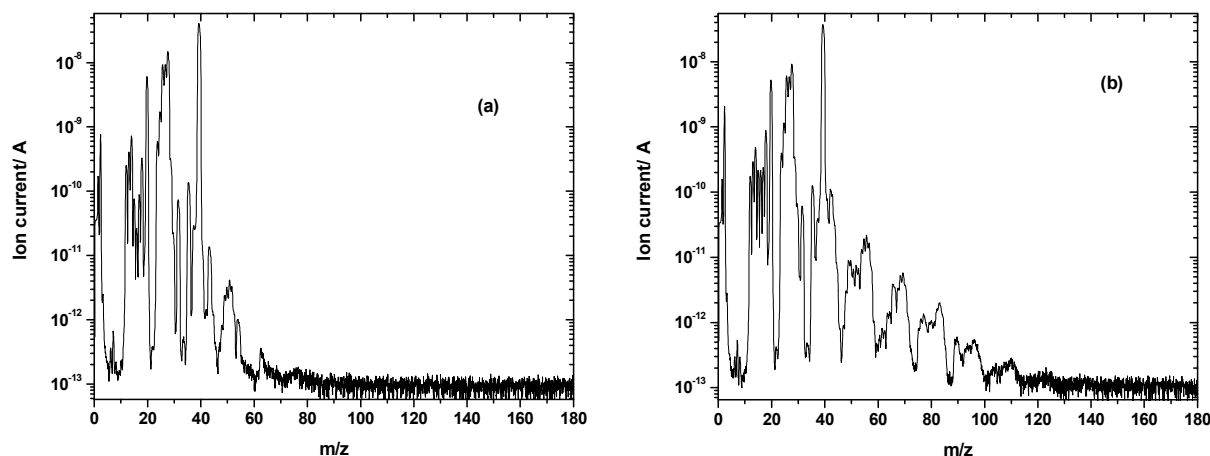


Figure 6.1 Mass spectra obtained from $\text{C}_2\text{H}_4/\text{Ar}$ gas mixture (a) without plasma and (b) after 420min with plasma on

Figure 6.1 show two typical mass spectra in the range of mass number up to $m/z = 180$ which were obtained after the chamber has been filled with 300 mbar of a $\text{C}_2\text{H}_4/\text{Ar}$ gas mixture (mixing ratio 1: 2). Figure 6.1(a) represents the initial gas composition consisting of argon and ethylene (C_2H_4) gas. Impurities that are present consists, e. g., of water (H_2O , $m/z = 18$), oxygen (O_2 , $m/z = 32$) and small amounts of higher hydrocarbons around mass

numbers $m/z = 50-57$ and 78 . Stable molecules dissociate inside the ion source of the mass spectrometer, giving rise to the formation of radical ions that complicate the data analysis ^[71] ^[72]. For example, ethane ($M=30$) shows up in the mass spectra with masses $m/z = 12$ (C^+), $13-15$ ($CH_n^+ = 1-3$), 24 (C_2^+), and $25-30$ ($C_2H_n^+$, $n= 1-6$). Hexane ($M = 86$), on the other hand, prominently shows up at mass number $m/z = 27, 29, 41-43, 56, 57$, and only weakly (with about 4%) at 86 . Information about fragmentation patterns have been derived from the NIST Chemistry WebBook ^[90].

Figure 6.1(b) displays the mass spectrum obtained from the same gas after the discharge has been operated for 420 mins. The long operation times had to be chosen because of the small discharge power consumed by the plasma. Several differences compared to figure 6.1(a) are noted: (i) a reduction of ethylene peaks, (ii) an increase of the hydrogen peak, and (iii) the appearance of the higher hydrocarbon peaks. The experimental results presented below are obtained by subtracting the mass spectra obtained without plasma from those obtained with plasma, e. g., by subtracting the data of figure 6.1(a) from those of figure 6.1(b).

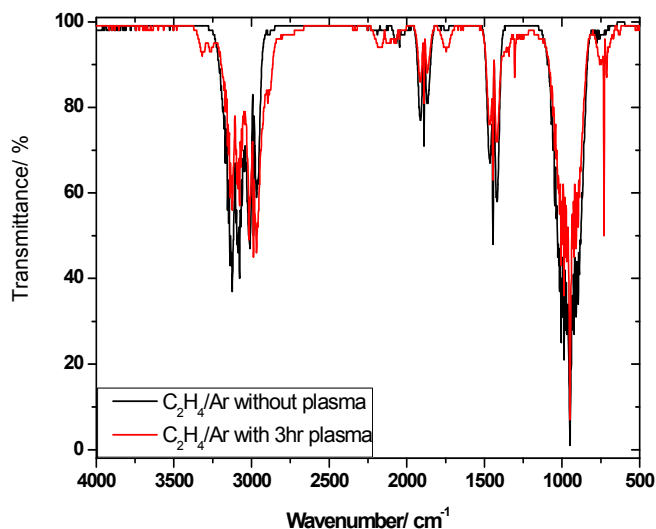


Figure 6.2 FTIR spectrum of C_2H_4/Ar without plasma & with 180 mins plasma on under the 300 mbar pressure and ratio is 1:2

Figure 6.2 shows the FTIR spectrum obtained for C_2H_4/Ar plasma. The black line represents the C_2H_4/Ar without plasma while the red line represents the same gas mixture

after the plasma has been operated for 180 mins. Without plasma we observe pronounced absorptions at wavenumbers 3106 cm^{-1} - 2989 cm^{-1} , 1887 cm^{-1} , 1444 cm^{-1} , and 949 cm^{-1} which are related to C-H asymmetric and symmetric stretching, C=C stretching, CH_2 scissoring, and CH_2 wagging vibrations of C_2H_4 ^[90]. After plasma ignition we observe several additional bands at other wavenumbers. The appearance of these peaks will be discussed in the next section.

6.1 Results and discussion

In the following we separately present our results obtained from mass spectrometry and FTIR spectroscopy for CH_4/Ar , $\text{C}_2\text{H}_2/\text{Ar}$, $\text{C}_2\text{H}_4/\text{Ar}$, and $\text{C}_2\text{H}_6/\text{Ar}$ gas mixtures.

6.1.1 CH_4/Ar

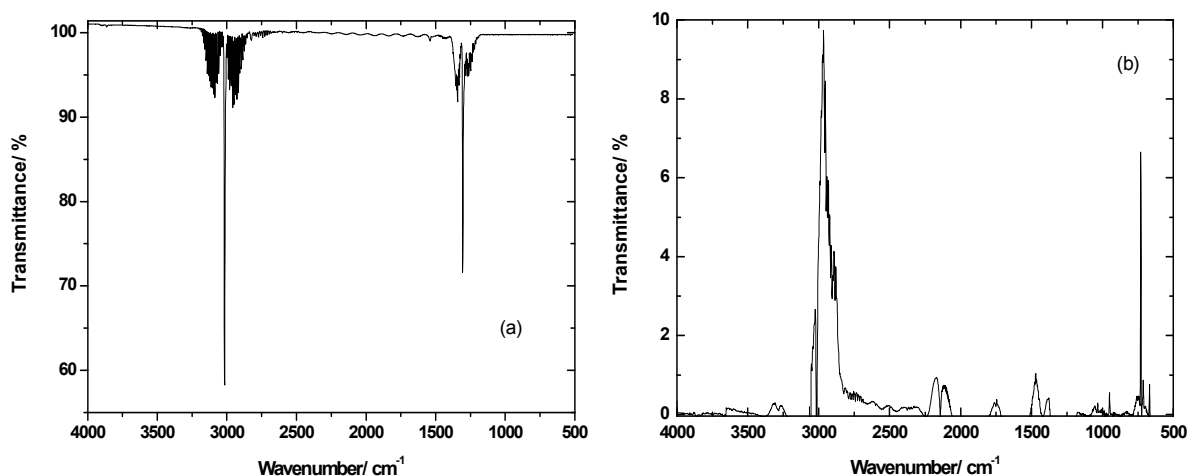


Figure 6.3 FTIR spectrum of CH_4/Ar gas mixture. (a) Without plasma, (b) Difference spectrum obtained by subtracting the spectrum after 180 mins with plasma and without plasma. Gas pressure 300 mbar, gas mixing ratio 1:2, cell pressure reduced to 50 mbar.

Mass spectra of CH_4/Ar have been presented by Majumdar et al ^[85], which show the formation of C_2H_m ($m = 2, 4, 6$) hydrocarbons and higher hydrocarbons is been already published else where ^[85].

FTIR spectra of CH₄/Ar without plasma (a) and the difference spectra (b) of the same gas mixture are displayed in the Figure 6.3. Difference FTIR plots can be obtained by the subtraction of the data obtained with plasma and the data obtained without plasma. The FTIR spectra displayed here are in transmittance mode. After ignition of the plasma for 180 mins, the CH₄ concentration decreases due to consumption by the discharge and several new peaks have been appeared. Mass spectra of CH₄/Ar were already presented by Majumdar et al.^[85]; they show the formation of C₂H_m (m = 2, 4, 6) and of higher order hydrocarbons. FTIR spectra of CH₄/Ar gas mixture are displayed in the figure 6.3(a) shows the bands at 1306 cm⁻¹ (1215 cm⁻¹ – 1380 cm⁻¹) and 3019 cm⁻¹ (2900 cm⁻¹ – 3150 cm⁻¹) which correspond to C-H bending and C-H stretching vibrations, respectively, of CH₄^[82]. After ignition of the plasma for 180 mins, Formation of C₂H₂ is inferred from the bands at wavenumbers 730 cm⁻¹ and 3240 cm⁻¹ – 3295 cm⁻¹, which corresponds to C-H bending and stretching vibrations, respectively, of that molecule, see figure 6.3(b). The bands at wavenumbers 2900 cm⁻¹ – 3008 cm⁻¹, 1390 cm⁻¹ – 1518 cm⁻¹ and 945 cm⁻¹ are related to C-H stretching vibrations, CH₂ scissoring, and CH₂ wagging, respectively, for C₂H₄. Formation of C₂H₆ can be confirmed from the wavenumbers 2900 cm⁻¹ – 3008 cm⁻¹, and 1510 cm⁻¹. Small peaks at 1746 cm⁻¹ (1680 cm⁻¹ – 1840 cm⁻¹) and 2150 cm⁻¹ (2045 cm⁻¹ – 2240 cm⁻¹) are attributed to the formation of acetaldehyde (CH₃-CHO) and carbon monoxide (CO), respectively. We believe that the molecules result from the plasma interaction with oxygen-containing surfaces, e.g., electrodes.

6.1.2 C₂H₂/Ar

Difference mass spectra of the C₂H₂/Ar gas mixture in the mass number range m/z up to 35 and 45 – 180 are displayed in figure 6.4. Figure 6.4(a) shows the expected consumption of acetylene (C₂H₂) of about 60% of the initial supply during 180 min and the production of a small amount of hydrogen of about 5% of the consumed C₂H₂. A rather small amount of the consumed C₂H₂ is used for the formation of higher order hydrocarbons which show up at mass numbers m/z = 48-50 (butadiyne, C₄H₂), 52 (C₄H₄), 54 (C₄H₆), 56 (C₄H₈), 64 (C₅H₄), 74 (hexatriyne, C₆H₂^[93]), 78 (benzene and/or hexadiyne, C₆H₆), 92 (toluene, C₇H₈)^[92]. The broad peak at m/z = 64 – 68 indicates formation of chain molecules like pentadiyne (C₅H₄), 1-penten-3-yne (C₅H₆), and pentadiene (C₅H₈), and/or cyclic molecules like

cyclopentadiene (C_5H_6), cyclopropylacetylene (C_5H_6), and cyclopentene (C_5H_8). Formation of aromatic compounds like phenylethyne (C_8H_6) and styrene (C_8H_8) is indicated by the peaks at mass numbers $m/z = 102-104$. Benzene and other ring components play a role in eg., Titan's atmosphere [28] [29] [30].

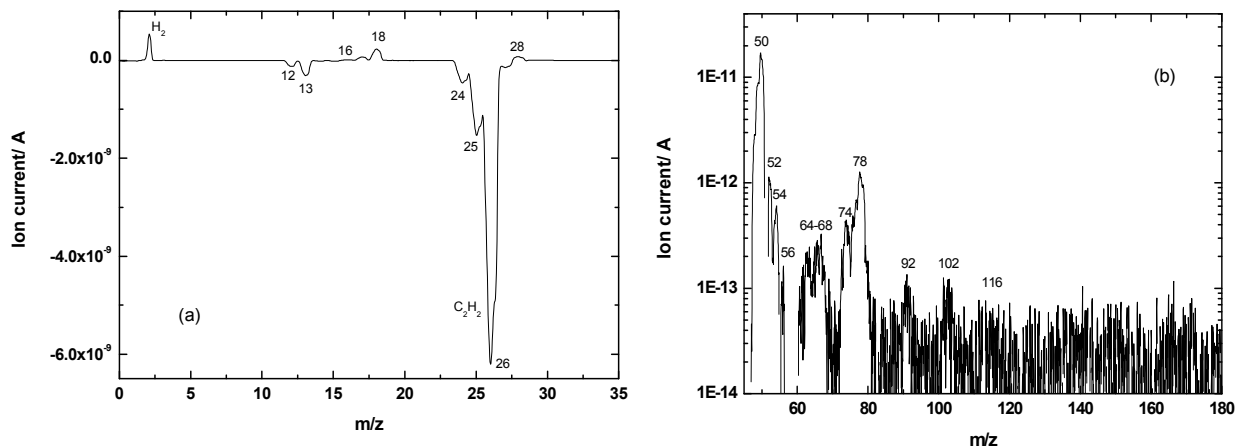


Figure 6.4 Difference mass spectrum with and without plasma in the mass range m/z up to 35 (a) and 45-180 (b) for a C_2H_2 /Ar gas mixture. Gas pressure 300 mbar, gas mixing ratio 1:2, plasma operation time 180 min. Note the different (linear and logarithmic) scales.

The FTIR spectrum of C_2H_2 is displayed in figure 6.5(a). It shows strong peaks at wavenumbers of 3290 cm^{-1} , 1320 cm^{-1} , and 730 cm^{-1} which are related to C-H stretching and C-H deformation vibrations of C_2H_2 [86]. After ignition of the plasma several new peaks appear in the spectrum as shown in figure 6.5(b). The pronounced peak at wavenumber 630 cm^{-1} and the small peak at wavenumber 1250 cm^{-1} are due to formation of biacetylene (butadiyne, C_4H_2) [135]. The small peak at 950 cm^{-1} indicates formation of C_2H_4 . Both molecules were also identified in the mass spectrum. CO formation by plasma-wall interaction is observed at 2150 cm^{-1} ($2045\text{ cm}^{-1} - 2240\text{ cm}^{-1}$). Aromatic compounds like benzene are not detected in the FTIR spectrum. According to the mass spectrum, production of aromatic molecules contributes less than 10^{-3} of the consumed C_2H_2 which is below the present FTIR detection limit.

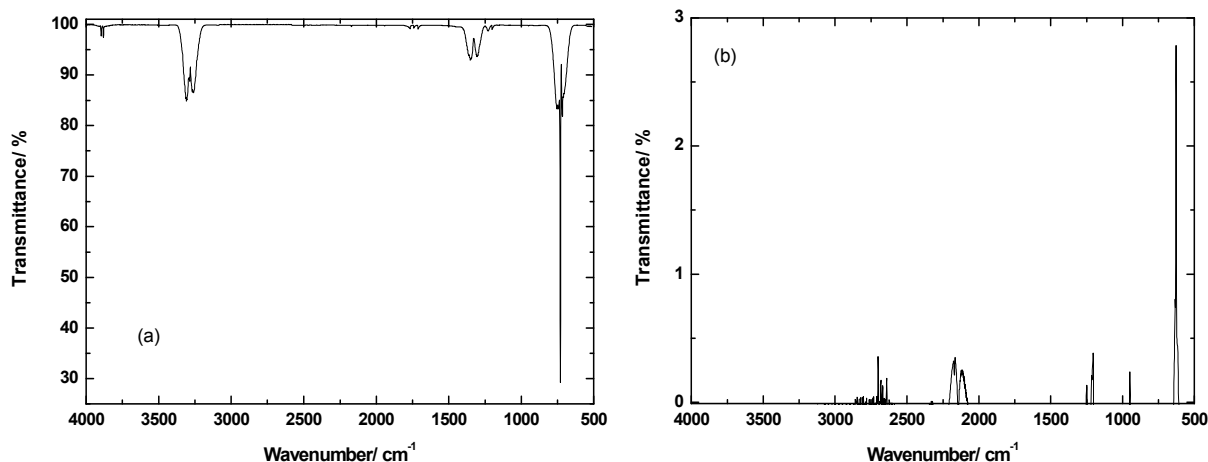


Figure 6.5 FTIR spectrum of C_2H_2/Ar gas mixture. (a) Without plasma, (b) Difference spectrum obtained by subtracting the spectrum after 180 mins with plasma on from the FTIR spectrum without plasma. Gas pressure 300 mbar, gas mixing ratio 1:2, cell pressure reduced to 50 mbar.

6.1.3 C_2H_4/Ar

Difference mass spectra from the C_2H_4/Ar gas mixture in the mass number ranges m/z up to 35 and 35 – 170 are displayed in the figure 6.6. The spectrum shows the expected consumption of about 60% of the initial ethylene (C_2H_4) gas. The (negative) peaks at $m/z = 12-14$ are related to the C, CH, and CH_2 fragments of the consumed C_2H_4 . The production of a significant amount of hydrogen which corresponds to about 23% of the consumed C_2H_4 is noted. Formation of CH_4 has been identified at mass numbers $m/z = 15-16$. Formation of a small amount of water (H_2O) is noted by the peaks at $m/z = 17$ and 18. We believe that the water results from the plasma interaction with oxygen-containing surfaces, e.g., the electrodes. A certain amount of the consumed C_2H_4 is used for the production of larger hydrocarbons. Hydrocarbon fragments with mass numbers up to $m/z \approx 140$ are observed. The spectrum shows several prominent groups which are separated by $\Delta m \approx 14$ corresponding to a CH_2 group. Evidently, one CH_2 radical is adding up in consecutive reactions leading to a periodic mass spectrum. The actual reaction pathways are more complicated, however, and may involve other radicals as well. Evidence for the formation of

aromatic compounds like benzene (C_6H_6), methyl-benzene or toluene (C_7H_8), and ethylbenzene (C_8H_{10}) is noted as side-peaks at $m/z = 78, 92$, and 106 , respectively. A similar mass spectrum was observed for a C_2H_4/N_2 gas mixture^[16]. The similarity seems to indicate that neither excited (metastable) argon atoms^[95] nor nitrogen radicals have a strong impact on hydrocarbon chemistry.

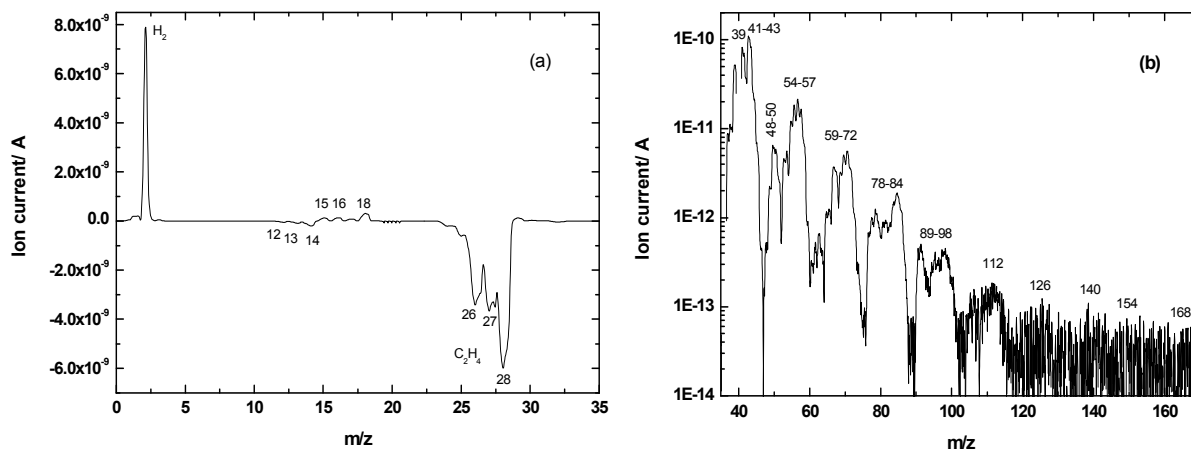


Figure 6.6 Difference mass spectrum with and without plasma in the range m/z up to 35 (a) and 35-170 (b) for a C_2H_4/Ar gas mixture. Note the different (linear and logarithmic scales), with gas ratio 1:2, pressure 300 mbar.

Figure 6.7(a) shows a FTIR spectrum of the C_2H_4/Ar gas mixture. Pronounced absorptions at wavenumbers 3106 cm^{-1} , 2989 cm^{-1} , 1887 cm^{-1} , 1444 cm^{-1} , and 949 cm^{-1} are attributed to C_2H_4 molecule^[90]. The difference spectrum displayed in figure 6.7(b) shows several additional peaks formed as a result of the plasma. Absorption due to methane (CH_4) is observed at wavenumbers 1306 cm^{-1} and in the $2900\text{ cm}^{-1} - 3000\text{ cm}^{-1}$ region. The later region is difficult to quantify since the bands of CH_4 and C_2H_6 partly overlap with C_2H_4 . Pronounced absorptions due to acetylene (C_2H_2) are detected at wavenumbers 730 cm^{-1} and 3300 cm^{-1} . Formation of biacetylene (C_4H_2)^[135], is observed at wavenumber 630 cm^{-1} . The tiny band at 2150 cm^{-1} is attributed to the formation of molecules with $C=O$ bonds (e.g., CH_2O , CH_3-CHO) presumably by reactions with oxygen-containing impurities from the chamber's electrodes and walls.

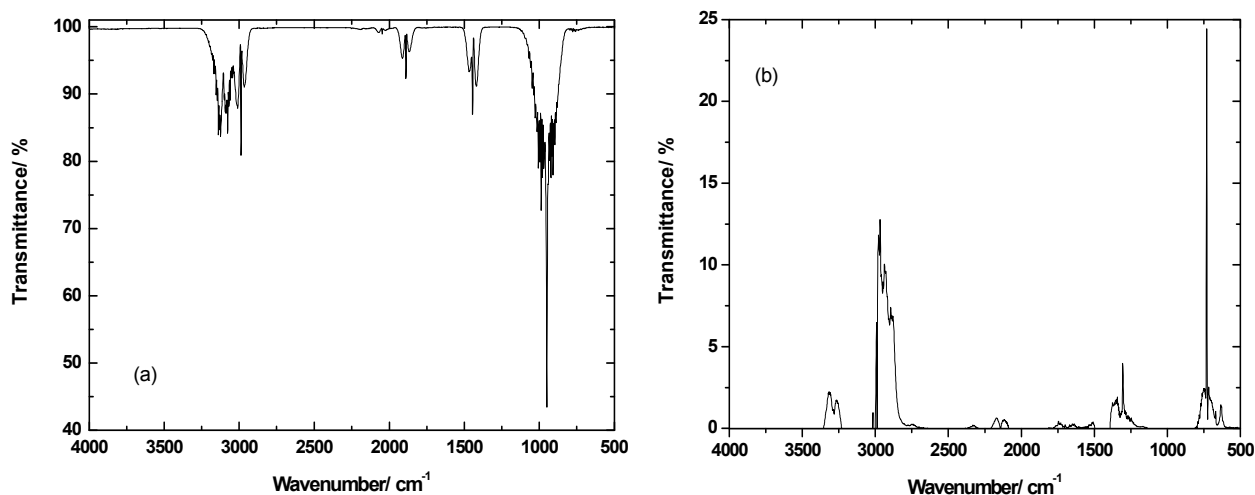


Figure 6.7 FTIR spectrum of C_2H_4/Ar gas mixture. (a) Without plasma, (b) Difference spectrum obtained by subtracting the spectrum after 180 mins with plasma and without plasma. Gas pressure 300 mbar, gas mixing ratio 1:2, cell pressure reduced to 50 mbar.

6.1.4 C_2H_6/Ar

Figure 6.8(a) displays the measured difference mass spectrum for mass numbers up to $m/z = 35$ on a linear scale obtained by subtracting the data without plasma from those obtained with plasma after 180 mins. The production of hydrogen (H_2) and methane (CH_4) and a significant consumption of ethane, the latter corroborated by the (negative) ethane peaks at $m/z = 25-30$, becomes evident. The most abundant fragment ion of ethane occurs at $m/z = 28$. In addition, production of larger hydrocarbons becomes evident from the mass spectrum in the range $m/z = 35-180$ which is displayed in figure 6.8(b) on a logarithmic scale. The mass spectrum is similar to the one from the C_2H_4/Ar gas mixture. The spectrum shows similar broad prominent peaks, each composed of several individual peaks that are attributed to C_nH_m molecules with n up to 12 and $m \approx 2n+2$. Again, the most prominent peaks, hence, approximately differ by $\Delta m \approx 14$ from each other. There is some evidence for the formation of aromatic compounds (benzene, toluene, ethylbenzene) which can be observed as side-

peaks at $m/z = 78, 92,$ and 106 . In comparison, it appears that these side-peaks are more pronounced for the C_2H_4 compared to the C_2H_6 gas mixture.

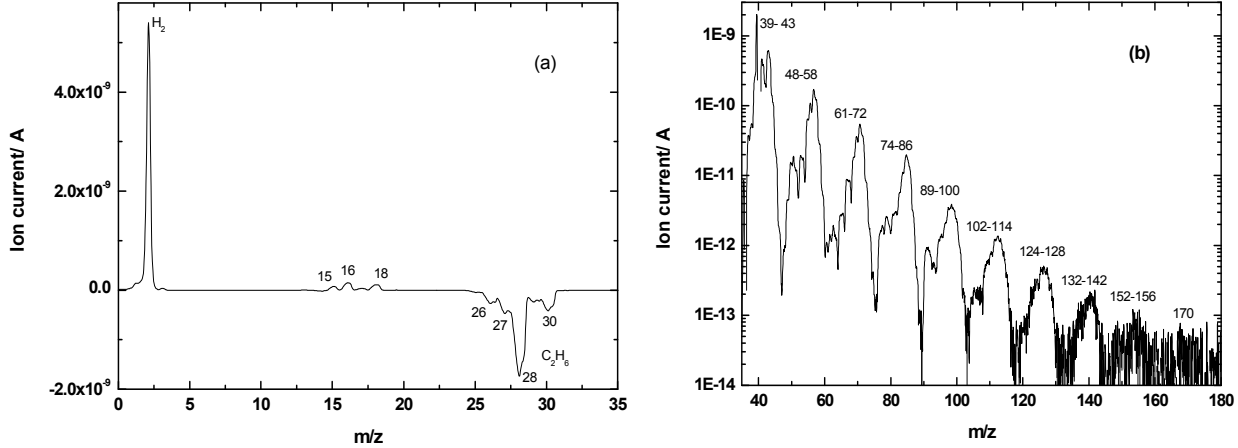


Figure 6.8 Difference mass spectra with and without plasma in the mass range m/z up to 35 (a) and 35-180 (b) for a C_2H_6/Ar gas mixture. Note the (linear and logarithmic scales), with gas ratio 1:2, pressure 300 mbar.

Figure 6.9 shows FTIR spectra of C_2H_6/Ar gas mixture. From the figure 6.9(a) the bands at wavenumbers 2900 cm^{-1} , 1470 cm^{-1} and 822 cm^{-1} are related to C-H stretching, deformation, and bending vibrations, respectively ^[90]. After Ignition of the plasma several new peaks appeared which are related to CH_4 (1306 cm^{-1}), C_2H_2 (732 cm^{-1} and 3300 cm^{-1}), and C_2H_4 (950 cm^{-1}).

Amount of gas consumed during 180 mins of plasma operation is summarized in table 1. C_2H_2 and C_2H_4 show the largest gas consumption of about 60% followed by CH_4 with 34% and C_2H_6 with about 19%. C_2H_2 and C_2H_4 thus have the highest decomposition rates of the investigated gases in a DBD plasma. The present result is in reasonable agreement with previous observation ^[116].

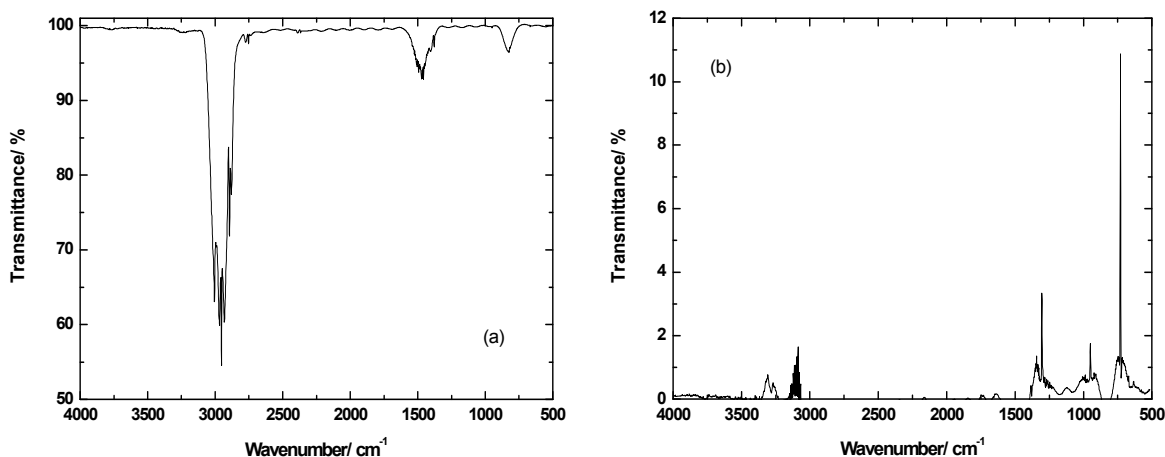


Figure 6.9 FTIR spectrum of C_2H_6/Ar gas mixture. (a) Without plasma, (b) Difference spectrum obtained by subtracting the spectrum after 180 mins with plasma and without plasma. Gas pressure 300 mbar, gas mixing ratio 1:2, cell pressure reduced to 50 mbar.

Apart from rather small amounts of H_2 and C_2H_4 only a few other gases are produced in the acetylene plasma. Presumably, acetylene quickly grows to large hydrogen-poor hydrocarbons outside of our detection range and/or is deposited as a film on the electrodes. Possible pathways are via C_4H_2 , C_4H_4 , C_6H_2 , and C_6H_6 as is evidenced by the observed peaks at mass numbers $m/z = 50, 52, 74$, and 78 (figure 6.4). Of these, C_4H_2 and C_6H_2 are chain molecules formed by polymerization of C_2H_2 , e.g., through chemical reactions involving C_2H radicals like ^{[117] [118]}



Chemical reactions studies during the pyrolysis of C_2H_2 indeed indicate that the corresponding reaction rates are rather large ^[79].

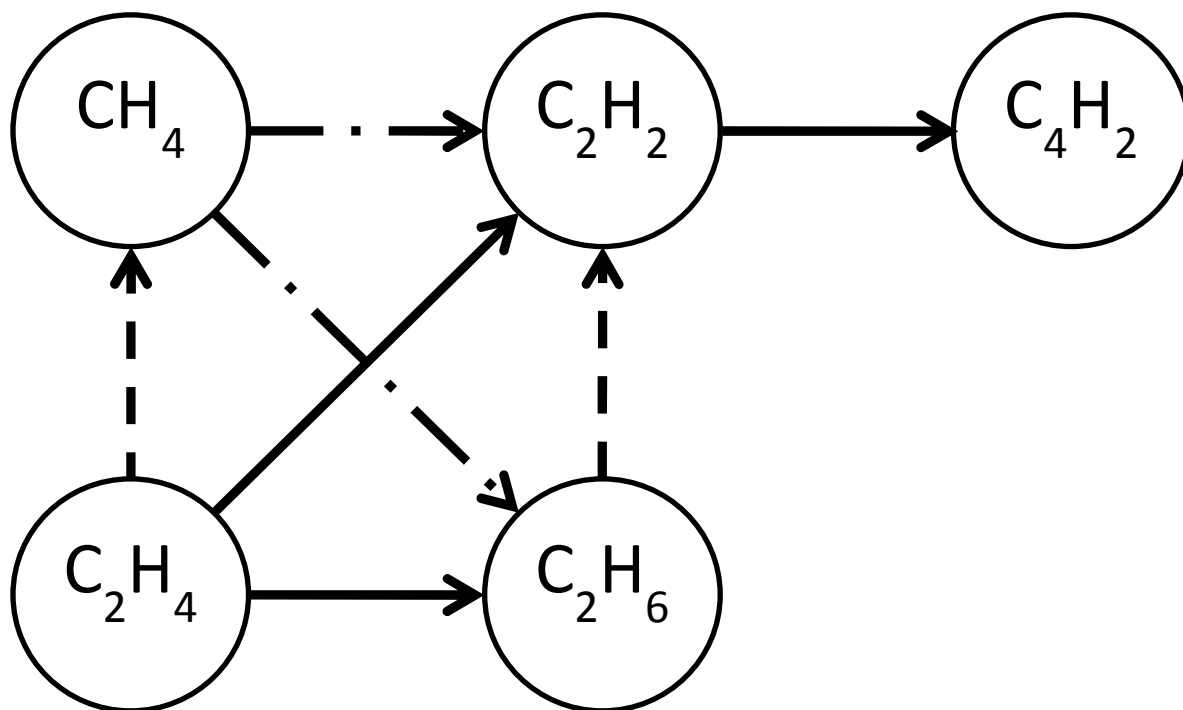


Figure 6.10 Reaction pathways among the CH_4 , C_2H_2 , C_2H_4 , C_2H_6 , and C_4H_2 . Arrows indicate the net balance of forward (e.g., $\text{CH}_4 \rightarrow \text{C}_2\text{H}_6$) and backward (e.g., $\text{CH}_4 \leftarrow \text{C}_2\text{H}_6$) pathways. Strong (solid lines), medium (dashed lines), and weak (dash-dot lines) pathways are indicated.

Large amounts of hydrogen molecules are produced by decomposition of CH_4 , C_2H_4 , and C_2H_6 . Typically, CH_4 and C_2H_6 produce about one hydrogen molecule per consumed CH_4 or C_2H_6 molecule. For C_2H_4 the corresponding number amounts to about 0.4 and is thus significantly smaller. Not surprisingly, the smallest amount of H_2 molecules is produced in the C_2H_2 gas mixture (about 0.05 per consumed C_2H_2 molecule).

C_2H_6 formation is the dominant process in the methane plasma. Taking into account that C_2H_6 contains twice as much carbon as CH_4 about 70% of the carbon is converted in this way. Much of the remaining gas (about 25%) is used for the production of (C_2H_2).

C_2H_2 and C_2H_6 formation are the dominant processes and of about equal importance in the C_2H_4 plasma; roughly 35% of the consumed C_2H_4 gases are produced in either way. C_2H_2

formation is the dominant process in the C_2H_6 plasma. Roughly 55% of the consumed C_2H_6 gas is used in this way. CH_4 and C_2H_4 formation contribute about 30% and 13%, respectively, to the C_2H_6 consumption.

The relative strength and the direction of the reaction pathways among the CH_4 , C_2H_2 , C_2H_4 , and C_2H_6 molecules are summarized in figure 6.10. Arrows indicate the net balance of forward (e.g., $CH_4 \rightarrow C_2H_6$) and backward (e.g., $CH_4 \leftarrow C_2H_6$) pathways. It follows that C_2H_4 quickly decomposes into C_2H_2 , C_2H_6 and CH_4 . C_2H_2 is thus predominately produced from C_2H_4 , moderately produced from C_2H_6 and weakly produced from CH_4 .

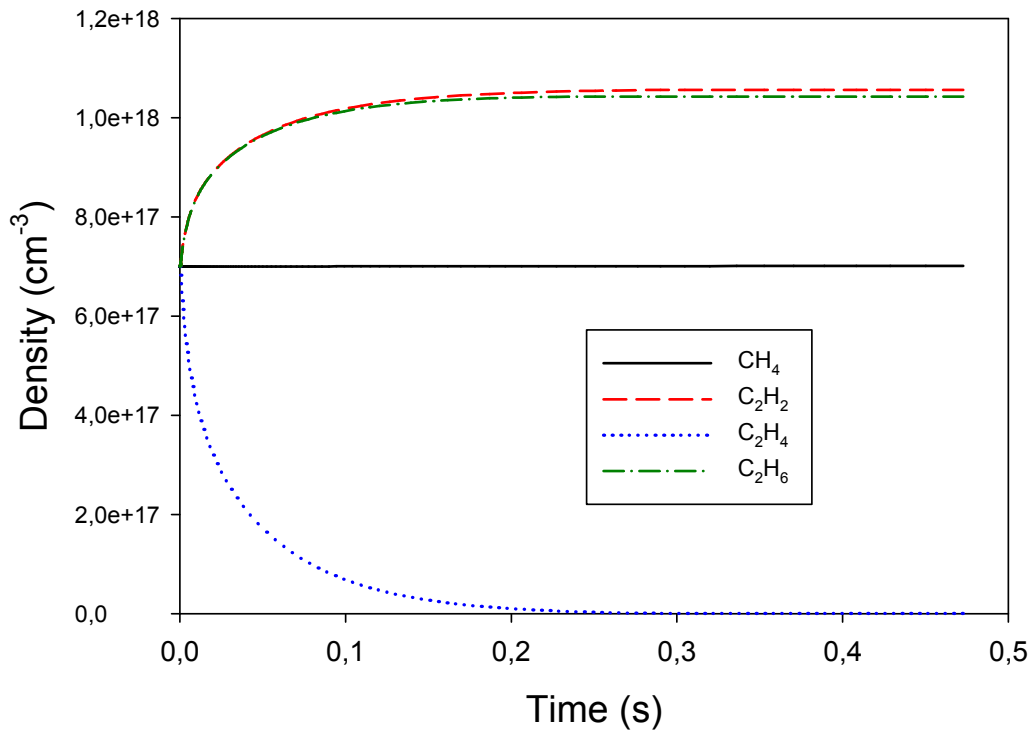


Figure 6.11 Simulation results for the temporal evolution of CH_4 , C_2H_2 , C_2H_4 and C_2H_6 molecules. Electron temperature 3 eV. Electron density 3 cm^{-3} .

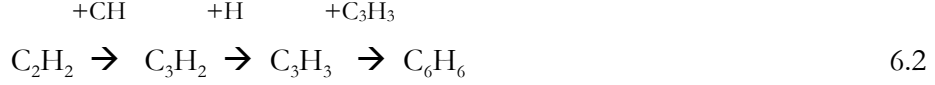
To calculate the densities of different hydrocarbons in the chamber we have employed zero-dimensional particle-balance model which is already reported ^[85]. The result obtained is in fair agreement with experimental data. The zero-dimensional particle-balance model assumes that the plasma is uniform, electrons and ions have a Maxwellian energy distribution, and

electron temperature and density, ion density and ion temperature are constant. The temporal behaviour of neutral and ion species densities is calculated from a system of particle balance equations. Neutral and ion densities are assumed to change due to volume chemical reactions. In the model we account for 174 volume reactions involving 14 neutrals and 13 charged species: C_2H_6 , C_2H_5 , C_2H_4 , C_2H_3 , C_2H_2 , C_2H , C_2 , CH_4 , CH_3 , CH_2 , CH , C , H_2 , H , and $C_2H_5^+$, $C_2H_4^+$, $C_2H_3^+$, $C_2H_2^+$, C_2H^+ , C_2^+ , CH_4^+ , CH_3^+ , CH_2^+ , CH^+ , C^+ , H_2^+ , H^+ . Simulation results for an initial CH_4 , C_2H_2 , C_2H_4 , and C_2H_6 gas mixture are shown in figure 6.11. Initial densities corresponding to a partial pressure of 25 mbar for each of the four molecules, electron temperature of 3 eV, and plasma (electron density of $1 \times 10^{10} / \text{cm}^3$) were chosen to simulate the experiment. The simulation confirms the predominant consumption of C_2H_4 (figure 6.11) which largely goes into the formation of C_2H_2 and, to a lesser extent, into the formation of C_2H_6 is produced while CH_4 remains largely constant.

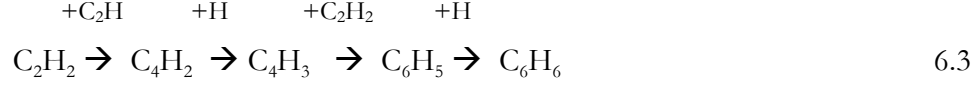
Due to small kinetic energy and mobility of molecules the time scale for chemical reactions to take place is much longer when compared to electron reaction times. We thus considered it justified to use time and space averaged values of the electron density. i.e., a mean electron density of $10^{12} / \text{m}^3$, in agreement with estimations based on the collected charge and an estimated electron transient time of 10 ns. For the electron temperature the value $T_e = 1 \text{ eV}$ consistent with the transient time estimate was used. As before this is only a crude approximation of the experimental conditions, as more detailed experimental measurements are yet lacking (Vladimir et al., work is in progress).

Evidence for the formation of aromatic compounds like benzene (C_6H_6), methyl-benzene or toluene (C_7H_8), and ethylbenzene (C_8H_{10}) is noted as peaks or side-peaks at $m/z = 78$, 92, and 106, respectively, in all mass spectra. Similar mass spectra were observed for C_2H_m/N_2 ($m = 2, 4, 6$) gas mixtures ^[16]. The similarity seems to indicate that neither excited (metastable) argon atoms ^[95] nor nitrogen radicals have a strong impact on hydrocarbon chemistry.

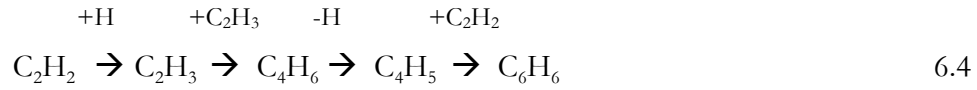
Several pathways for benzene formation via the C_2H_2 molecule have been proposed recently, e.g., ^[73]



Other pathways involving C_4H_2 , C_4H_3 , C_4H_5 , and C_4H_6 molecules were suggested by Wilson et al. [92],



And



However, no clear picture for benzene formation can be extracted from the present investigation.

Formation of higher order hydrocarbons is observed for all gas mixtures. About 0.6% of the consumed C_2H_2 gas is used in the formation of larger hydrocarbons, most notably C_4H_2 , C_4H_4 , C_6H_2 , and C_6H_6 . Apparently, C_2H_2 via reaction 6.1 quickly grows to much larger molecules including nano-particles and/or is deposited as a film. About 23% and 15% of the consumed CH_4 and C_2H_4 gases (8% and 9% of the initial gases), respectively, are converted to larger hydrocarbons. Similarly, about 15% of the consumed gas (3% of the initial gas) are converted during plasma operation in C_2H_6 . Apparently, plasma polymerization obeying a gross reaction scheme,



is a dominant process responsible for the periodic mass spectra from CH_4 , C_2H_4 , and C_2H_6 gas mixtures were the broad peaks differ by $\Delta m \approx 14$. The actual reaction schemes are more complicated, however, and may involve other radicals like CH , CH_3 , C_2H , C_2H_3 , etc., as well.

Table 6.1 Percentage gas production and consumption for CH₄/Ar and C₂H_m/Ar (m = 2, 4, 6) gas mixtures during 180 min of DBD plasma.

Plasma	% Production				
	H ₂	CH ₄	C ₂ H ₂	C ₂ H ₄	C ₂ H ₆
CH ₄	24	-34	4.5	0.4	13
C ₂ H ₂	3	-	-60	0.3	-
C ₂ H ₄	23	13	23	-60	23
C ₂ H ₆	17	11	10	2.4	-19

6.1.5 Time Dependency

The time dependent studies of H₂, and C₂H_m, (where, m= 2, 4, 6) is shown in the figure 6.12(a)(b)(c). Formation of hydrogen show a pronounced increase, while the C₂H_m (where, m= 2, 4, 6) peaks follow an approximately exponential decay. We note that consumption of C₂H_m (where, m= 2, 4, 6) molecules contributes to the formation of a hydrogen molecule roughly on a one-to-one basis. Decomposition of C₂H_m (where, m= 2, 4, 6) leading to the formation of hydrogen molecules, hence the dominant chemical reaction in the plasma. Furthermore, it appears that within experimental errors every consumed C₂H_m (where, m= 2, 4, 6) molecules contributes to the formation of an hydrogen molecule, i.e., a gross reaction scheme,

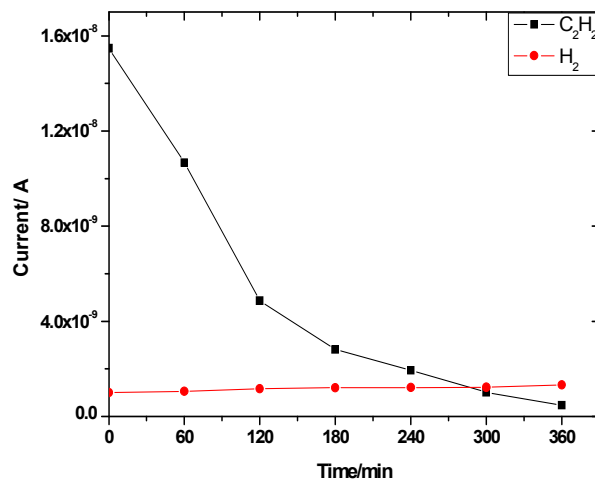


Figure 6.12 (a) Time dependent studies of H_2 , and C_2H_2 in C_2H_2/Ar plasma

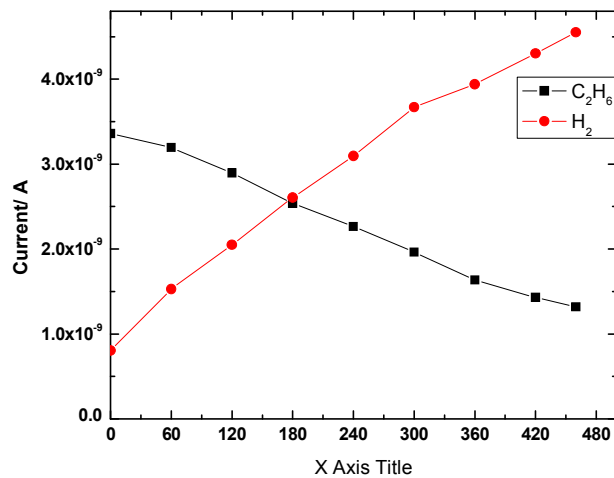
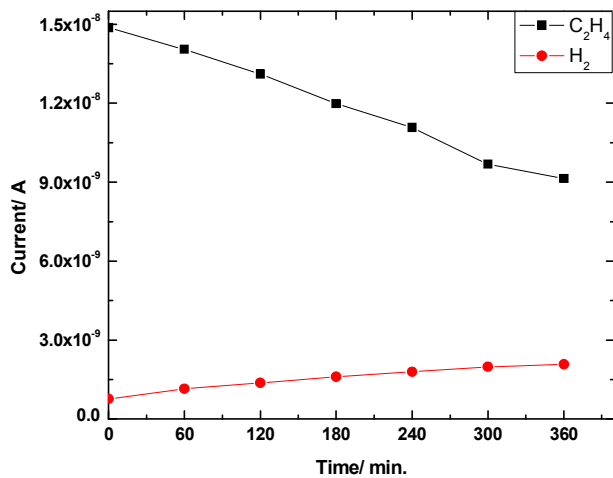


Figure 6.12(b) and 6.12(c) Time dependent studies of H_2 , and C_2H_4 in C_2H_4/Ar (b) and C_2H_6/Ar (c) plasma



seem to apply. In addition, a significant amount of the consumed C_2H_m (where, $m = 2, 4, 6$) is deposited as a thin film on the electrodes ^{[95] [96]}, most likely as amorphous C-H films.

The simple picture provided by reaction (ii) does not hold so well for formation of the small hydrocarbons which are formed with large probability. It has to be noted that the fragmentation pattern of C_2H_6 predominately produces an $m/z = 28$ peak making a proper assignment rather difficult. According to a widely accepted picture, C_nH_m formation takes place in sequential steps ^{[97] [98]}.

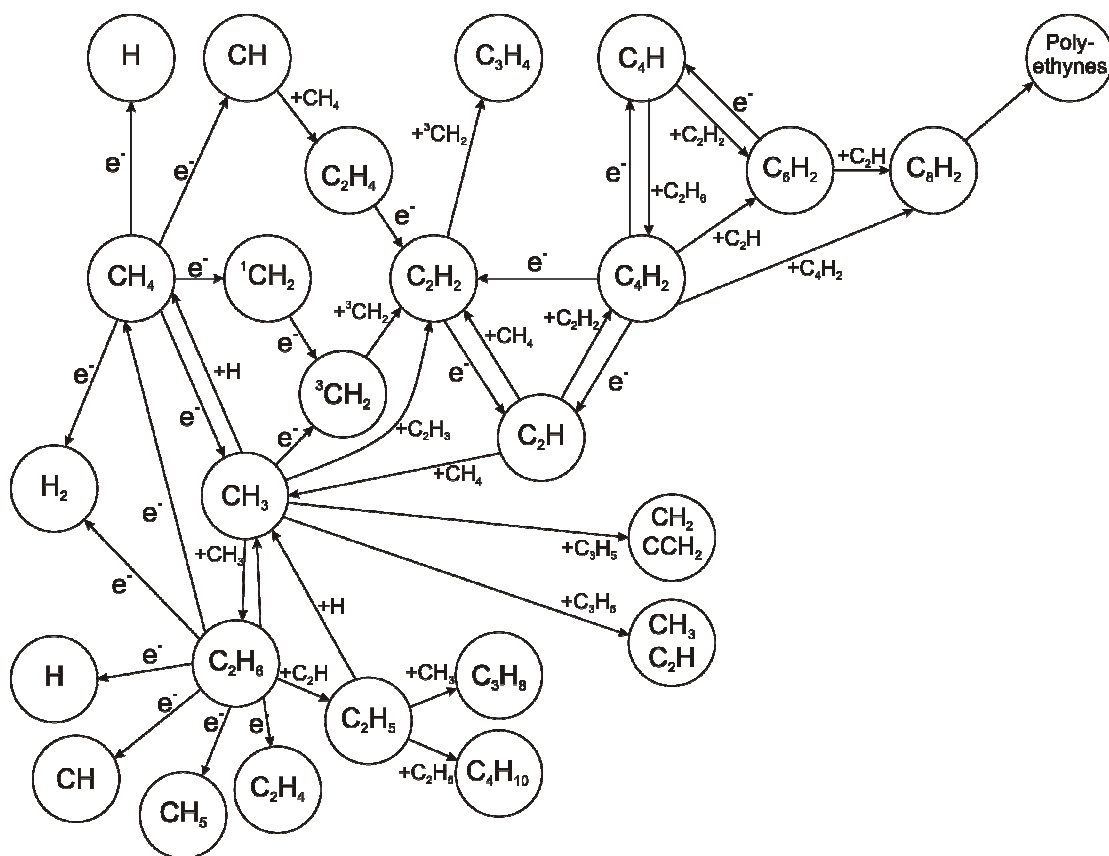


Figure 6.13 Schematic showing the Titan hydrocarbon chemistry (Ref: "Saturn" Arizona Press).

Schematic 6.13 shows the Titan hydrocarbon chemistry for simple molecule CH_4 . From the schematic one can see the possibility of breaking down of CH_4 into ways. As a result of dissociation CH_4 gas can produce radicals such as H_2 , H , CH_3 , CH_2 , and CH . These radicals can combine in various ways forming several higher order hydrocarbons till polyethynes. From the schematic one can see the formation of C_2H_2 can take place by five ways, so one can expect the abundant formation of C_2H_2 in the chamber. From the schematic we can also see the formation of smaller hydrocarbons like C_2H_4 and C_2H_6 . Again we have shown some possible dissociated radicals of C_2H_6 , out of these radicals we can see the formation of CH_4 as well.

6.2 Comparison of $\text{C}_2\text{H}_2/\text{Ar}$, $\text{C}_2\text{H}_4/\text{Ar}$ and $\text{C}_2\text{H}_6/\text{Ar}$ plasma with mass spectra and FTIR spectra

6.2.1 $\text{C}_2\text{H}_2/\text{C}_2\text{H}_4$ Plasma

The comparison of C_2H_2 and C_2H_4 plasma are shown in figure 6.14 and figure 6.16(a) both mass spectra and FTIR spectra. From the figure the following differences are noticed

- Formation of H_2 is slightly less see Table 6.1 in C_2H_2 plasma when compared to C_2H_4 plasma.
- Acetylene plasma is producing more dust so the formation of higher order peaks are relatively less when compared to C_2H_4 plasma
- Peak positions are shifted to larger mass numbers for C_2H_4 when compared to C_2H_2
- Figure 6.16(a) shows that the formation of alkanes (sp^3) is slightly less when compared to C_2H_4

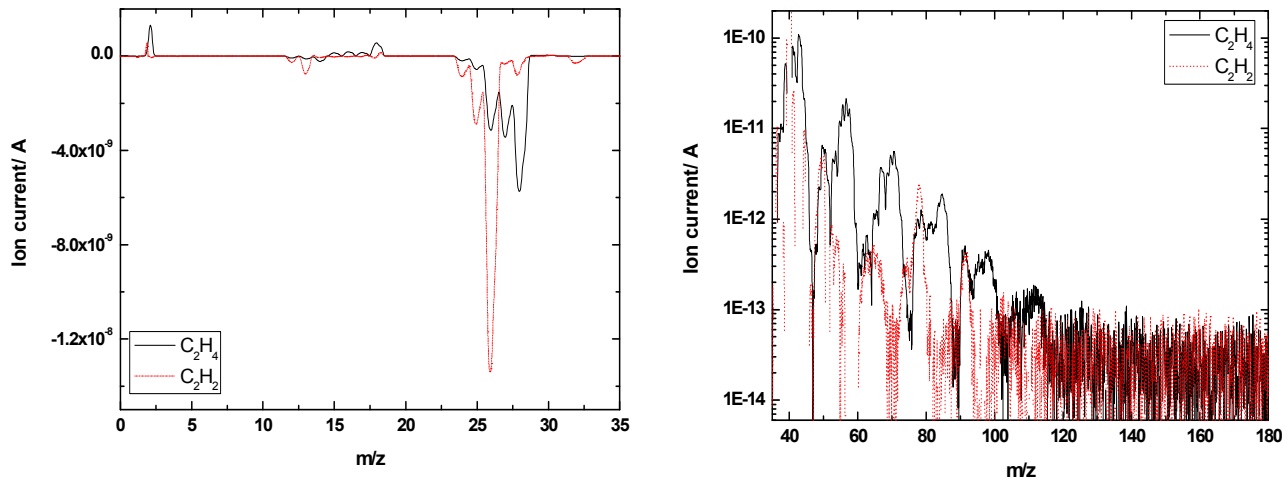


Figure 6.14 Comparison between difference mass spectrum of C_2H_2 and C_2H_4 plasma in the mass range m/z up to 35 & 35-180. Note the (linear and logarithmic scales), with gas ratio 1:2, pressure 300 mbar, and discharge power 2-5 W

6.2.2 C_2H_4/C_2H_6 Plasma

The comparison of C_2H_4 and C_2H_6 plasma is shown in figure 6.15 & figure 6.16 (b) both mass spectra and FTIR spectra. From the figure the following differences we found.

- From figure 6.15 (a) we can see the formation of H_2 is slightly less when compared to C_2H_6 plasma.
- Small shift in the peak positions at $m/z > 90$ between C_2H_4 and C_2H_6 plasma can noticed.
- Peaks which are appeared in the higher order m/z are splitted into multiple fragments in case of C_2H_4 plasma where as in case of C_2H_6 peaks are sharp.
- From figure 6.16 (b) we can see that the wavenumber around 2980 cm^{-1} indicates the formation of alkane group could be C_2H_6 .
- Formation of acetylene is more abundant in C_2H_4 plasma when compared to C_2H_6 plasma

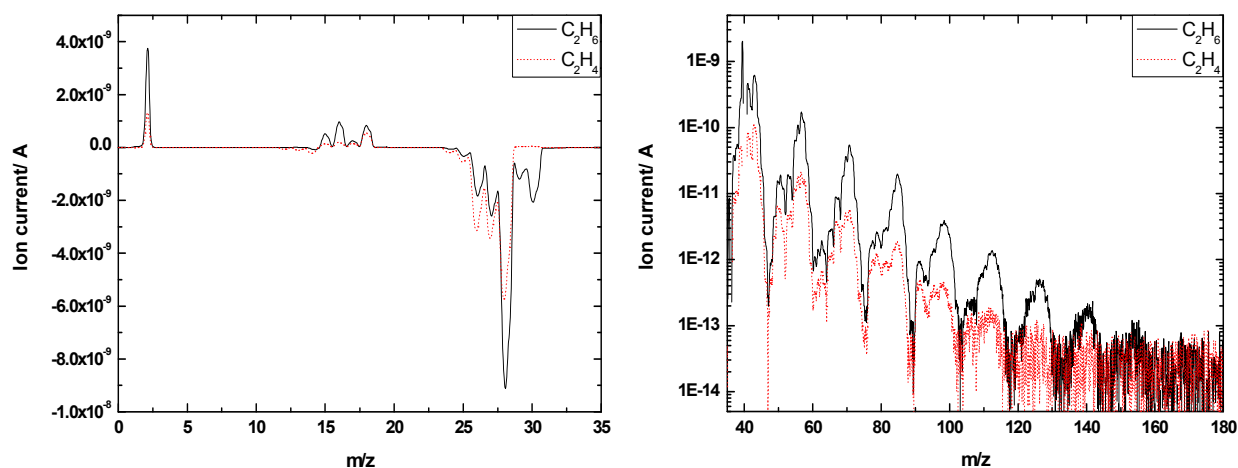


Figure 6.15 Comparison between difference mass spectrum of C_2H_4 and C_2H_6 plasma in the mass range m/z up to 35 & 35-180. Note the (linear and logarithmic scales), with gas ratio 1:2, pressure 300 mbar, and discharge power 2-5 W

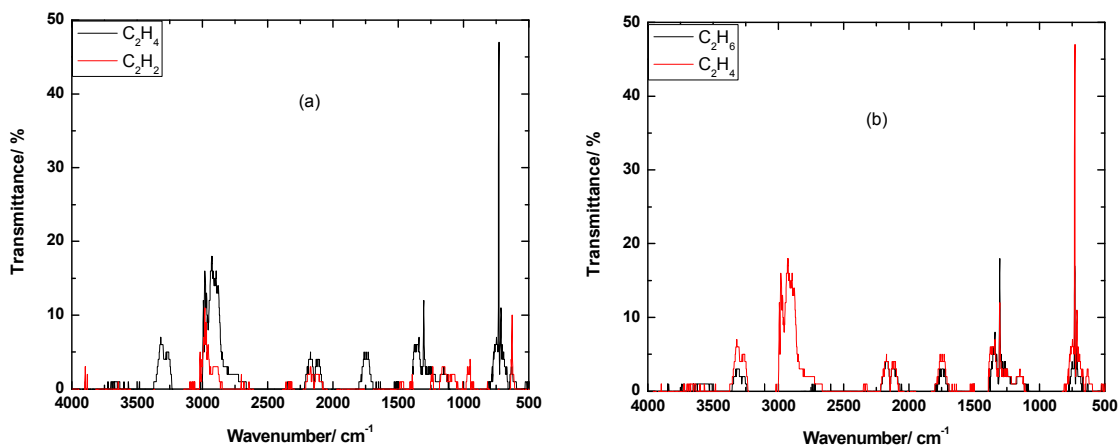


Figure 6.16 Comparison of difference FTIR spectrum of C_2H_4/C_2H_6 plasma and C_2H_2/C_2H_4 plasma, with gas ratio 1:2, pressure 300 mbar and discharge power 2-5 W

Chapter 7

Deposition and Characterization of Organic Polymer thin films using C_2H_m/N_2 ($m = 2, 4, 6$) gas mixtures by Dielectric Barrier Discharge

This chapter gives the deposition of amorphous CN_x thin films from C_2H_m/N_2 ($m = 2, 4, 6$) gas mixtures and their characterizations.

7.1 Preparation of Thin films

Two different kinds of substrates were used for the deposition experiments. One is an aluminium coated glass substrate with dimensions of 6 cm x 2 cm and Si (100) of dimensions 2 cm x 3 cm. The aluminium coating on the glass substrate was made by chemical vapor deposition (CVD) yielding a thickness of 190 nm.

The substrate can be placed on the glass electrode in the DBD chamber. The gas mixtures C_2H_m/N_2 ($m = 2, 4, 6$) and nitrogen gas mixtures can be fed by two different gas flow channels. For each experiment the gas ratio 1:2 has been taken. And the chamber pressure was maintained 300 mbar. All experiments were carried out with a frequency 5 kHz. And the power consumed for each experiment is 4 W.

7.2 Results and Discussion

In the following we discuss and compare the results obtained for a- $CN_x:H$ films obtained from C_2H_m/N_2 ($m = 2, 4, 6$) gas mixtures. The characterizations of the films have been done

from various spectroscopic techniques such as FT-IRRAS, X-ray Photoelectron Spectroscopy, and Spectroscopic ellipsometry (SE).

7.2.1 Fourier Transform Infrared Reflection Absorption Spectroscopy (FT-IRRAS)

The functional groups present on the surface of a-CN_x:H films deposited on aluminium coated glass substrate were determined by Fourier Transform Infrared Reflection Absorption Spectroscopy (BRUCKER, VERTEX 80V). Prior to the experiments, the sample compartment was evacuated to 2 mbar to reduce absorption of water vapor and CO₂. Spectra were recorded in the range 4000 to 500 cm⁻¹ with a spectral resolution of 0.7 cm⁻¹. Each spectrum was the average of 32 scans. A background spectrum was taken from each substrate prior to the deposition of CN_x films.

7.2.1.1 C₂H₂/N₂

Figure 7.1 shows FT-IRRAS spectrum for the CN_x film obtained from the C₂H₂/N₂ gas mixture at 300 mbar pressure with gas ratio 1:2. The CN_x film obtained from C₂H₂/N₂ plasma shows the N-H stretching vibrations at 3332 cm⁻¹ for amines ^{[23] [24] [99]}, and C-H stretching vibrations for highly unsaturated hydrocarbons, alkynes such as C₂H₂ or higher order alkynes chains. And at the same wavenumber O-H stretching vibrations for water has also been observed. Oxygen is considered as an impurity which comes while transferring the sample from DBD chamber to FTIR chamber. Wavenumber 2960 cm⁻¹ is related to C-H asymmetric stretching vibrations for CH₃ groups ^{[23][100]}. Wavenumber 2207 cm⁻¹ corresponds to C≡N stretching vibrations for nitriles and iso-nitriles ^{[99] [23] [100]}. Wavenumber 1945 cm⁻¹ is related to C≡C stretching vibrations for highly unsaturated alkynes chains ^[101]. A pronounced peak appearing at 1670 cm⁻¹ is related to C=C and C=N stretching vibrations ^{[23][100]} for alkenes like C₂H₄ or higher order alkenes chains. Deformation vibrations can be observed for the same molecules such as alkenes and CN-containing compounds at 1446 cm⁻¹ for C-H deformations and 1373 cm⁻¹ for C-N deformations, respectively. Wavenumbers 966 cm⁻¹ and 911 cm⁻¹ are related to C-H and N-H out-of-plane bending vibrations for C₂H₄ and amines

^[101]. Small bands appearing at 752 cm^{-1} and 710 cm^{-1} corresponds to C-H bending vibrations. Formation of aromatic compound (like Benzene) can be confirmed at wavenumber 636 cm^{-1} which is related to C-H bending vibrations for benzene.

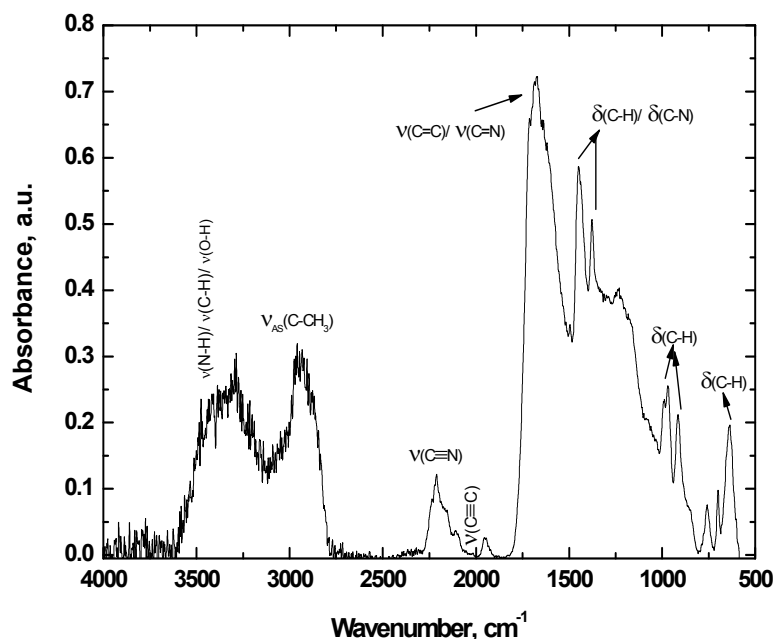


Figure 7.1 FTIR spectra of CN_x films obtained from $\text{C}_2\text{H}_2/\text{N}_2$ gas mixture, under 300 mbar pressure with gas ratio 1:2

7.2.1.2 $\text{C}_2\text{H}_4/\text{N}_2$

Figure 7.2 shows FT-IRRAS spectrum for the CN_x film obtained from the $\text{C}_2\text{H}_4/\text{N}_2$ gas mixture at 300 mbar pressure with gas ratio 1:2. In $\text{C}_2\text{H}_4/\text{N}_2$ thin film we observed almost same characteristic functional groups which were already been observed in the $\text{C}_2\text{H}_2/\text{N}_2$ thin film, only the difference in peak intensity and a very minute shift in the wavenumber. The CN_x film obtained from $\text{C}_2\text{H}_4/\text{N}_2$ plasma shows the N-H stretching vibrations at wavenumber 3332 cm^{-1} for amines ^{[23] [24] [99]}, and C-H stretching vibrations for highly unsaturated hydrocarbons, alkynes such as C_2H_2 or higher order alkynes chains. And at the

same wavenumber O-H stretching vibrations for water has also been observed. Wavenumbers 2946 cm^{-1} and 2870 cm^{-1} , corresponds to asymmetric and symmetric C-H stretching vibrations for CH_2 groups can be observed ^{[23][100]}. The bands appeared at wavenumbers 2235 cm^{-1} and 2194 cm^{-1} corresponds to $\text{C}\equiv\text{N}$ stretching vibrations for nitriles and iso-nitriles ^{[99] [23] [100]}. At wavenumbers 2014 cm^{-1} and 1960 cm^{-1} , $\text{C}\equiv\text{C}$ stretching vibrations for highly unsaturated alkynes ^[101] have been observed. At wavenumber 1642 cm^{-1} related to $\text{C}=\text{C}$ and $\text{C}=\text{N}$ stretching vibrations for alkenes and CN containing compounds. For the same molecules the bending vibrations can also be observed. Two well pronounced bands appeared at wavenumbers 1456 cm^{-1} and 1373 cm^{-1} corresponds to C-H and C-N bending vibrations ^[23], respectively. The bands formed at the wavenumber 966 cm^{-1} and 911 cm^{-1} are related to the C-H and N-H out-of-plane bending vibrations^[101]. At wavenumber 636 cm^{-1} corresponds C-H bending vibrations indicates the formation of aromatic compounds.

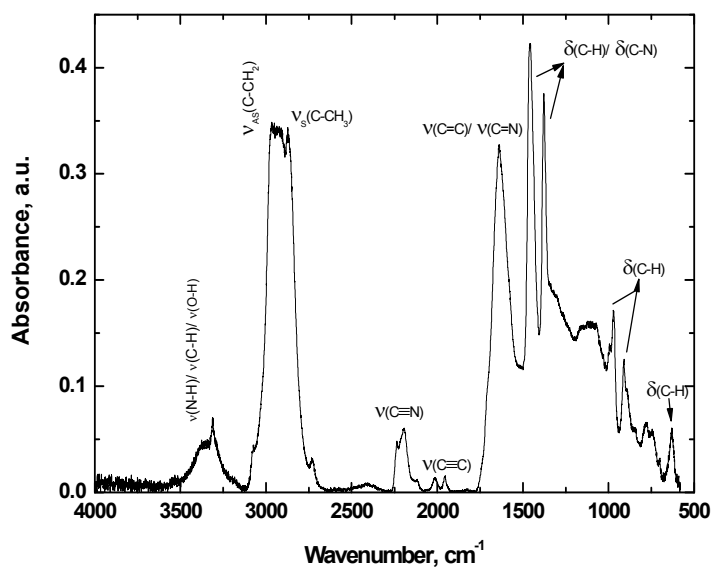


Figure 7.2 FTIR spectra of CN_x films obtained from $\text{C}_2\text{H}_4/\text{N}_2$ gas mixture, under 300 mbar pressure with gas ratio 1:2

7.2.1.3 C₂H₆/N₂

Figure 7.3 shows FT-IRRAS spectrum for the CN_x film obtained from the C₂H₆/N₂ gas mixture at 300 mbar pressure with gas ratio 1:2. The FT-IRRAS spectrum for C₂H₆/N₂ film looks almost similar to C₂H₄/N₂ with characteristic functional groups. As we observed in C₂H₂/N₂ and C₂H₄/N₂ films, C₂H₆/N₂ film also shows the characteristic functional group at wavenumber 3325 cm⁻¹ for N-H stretching vibrations for amines ^{[23] [24] [99]}, C-H stretching vibrations for highly unsaturated alkynes and O-H stretching vibrations for water. Wavenumbers 2960 cm⁻¹, 2928 cm⁻¹ and 2876 cm⁻¹ corresponds to C-H asymmetric

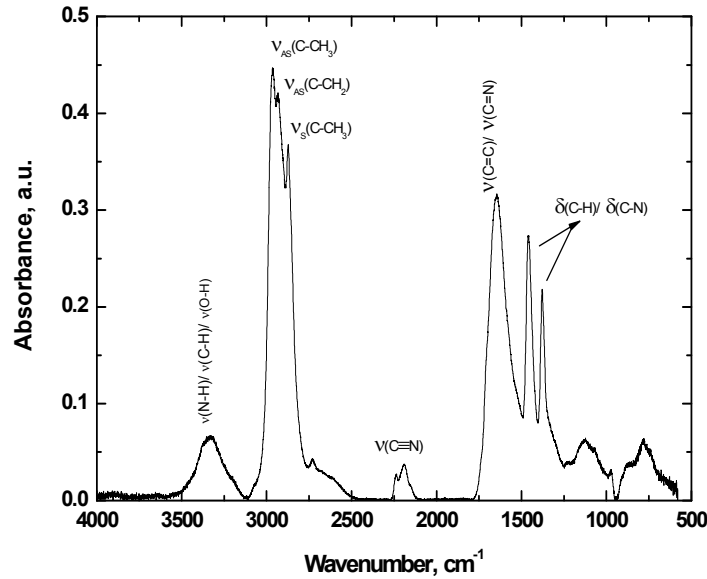


Figure 7.3 FTIR spectra of CN_x films obtained from C₂H₆/N₂ gas mixture, under 300 mbar pressure with gas ratio 1:2.

stretching vibrations for CH₃ groups, C-H asymmetric stretching vibrations for CH₂ groups and C-H symmetric stretching vibrations for CH₃ groups ^{[23][100]}, respectively. The bands appeared at wavenumbers 2235 cm⁻¹ and 2194 cm⁻¹ corresponds to C≡N stretching vibrations for nitriles and iso-nitriles ^{[99] [23] [100]}. A pronounced band appeared at 1642 cm⁻¹ is related to C=C and C=N stretching vibrations for alkenes and CN-containing compounds.

Wavenumbers 1456 cm^{-1} and 1373 cm^{-1} corresponds to C-H and C-N deformations^[101], respectively.

Table 7.1 Major assignments for FTIR absorption spectra for CN_x films obtained from $\text{C}_2\text{H}_m/\text{N}_2$ ($m = 2, 4, 6$) gas mixtures

Wavenumber/ cm^{-1}	Assignments
3332	$\sqrt{(\text{N-H})}$ / $\sqrt{(\text{C-H})}$ / $\sqrt{(\text{O-H})}$: Amines, Alkynes, H_2O
2960, 2876	$\sqrt{_{\text{as}}(\text{C-H})}$, $\sqrt{_{\text{s}}(\text{C-H})}$: CH_3 groups
2928, 2870	$\sqrt{_{\text{as}}(\text{C-H})}$, $\sqrt{_{\text{s}}(\text{C-H})}$: CH_2 groups
2235, 2194	$\sqrt{(\text{C}\equiv\text{N})}$: nitriles and Iso-nitriles
2014, 1960	$\sqrt{(\text{C}\equiv\text{C})}$: Alkynes
1642	$\sqrt{(\text{C}=\text{C})}$, $\sqrt{(\text{C}=\text{N})}$: Alkenes, CN-compounds
1456, 1373	$\delta(\text{C-H})$, $\delta(\text{C-N})$: Alkenes, amines
966, 911	$\delta(\text{C-H})$, $\delta(\text{N-H})$: Alkenes, Amines
739, 781	$\delta(\text{C-H})$, $\delta(\text{C-N})$: Alkynes, CN-compounds

$\sqrt{}$: stretching vibration, δ : Bending (scissoring) vibration or deformations,
s: symmetric, as: asymmetric

7.2.1.4 Comparison between $\text{C}_2\text{H}_m/\text{N}_2$ ($m = 2, 4, 6$) gas mixtures

Thin films obtained from all three gas mixtures showed almost same characteristics functional groups with different absorptions. The major differences observed are,

- The $\text{C}_2\text{H}_2/\text{N}_2$ plasma film was forming more dust in the chamber, as result of dust the film became thick with more dust on the surface, hence at wavenumber 3325 cm^{-1} appeared as blurred band, same reason holds for the next band which has been appeared at wavenumber 2960 cm^{-1} . But the intensity of absorption is more for 3325 cm^{-1} in $\text{C}_2\text{H}_2/\text{N}_2$ film. The intensity of absorption for 2960 cm^{-1} band is less when compared to $\text{C}_2\text{H}_4/\text{N}_2$ and $\text{C}_2\text{H}_6/\text{N}_2$ plasma because of the difference in thickness of the film.

- $\text{C}\equiv\text{C}$ band is completely absent in $\text{C}_2\text{H}_6/\text{N}_2$ film, but it is intense in $\text{C}_2\text{H}_2/\text{N}_2$ plasma. The band intensity decreases in $\text{C}_2\text{H}_4/\text{N}_2$ film.
- similarly, for all other bands the intensity of absorption is more in $\text{C}_2\text{H}_2/\text{N}_2$ film when compared to $\text{C}_2\text{H}_4/\text{N}_2$ and $\text{C}_2\text{H}_6/\text{N}_2$ film. And it is observed that few bands are totally absent in $\text{C}_2\text{H}_6/\text{N}_2$ film.

7.2.2 X-ray Photoelectron Spectroscopy (XPS)

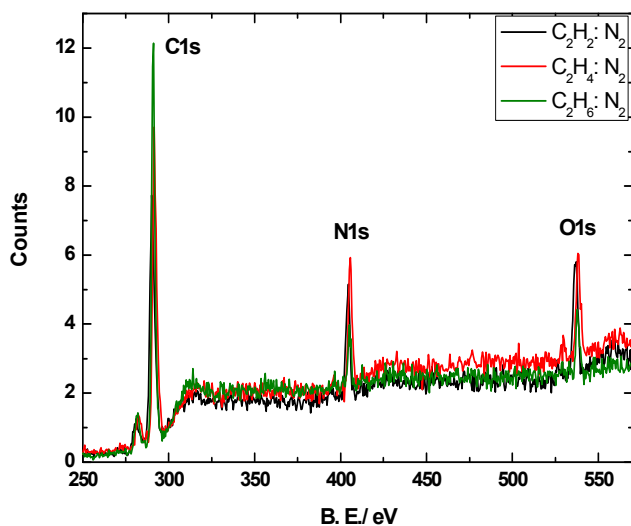


Figure 7.4 Typical XPS overview spectrum for CN_x film obtained from $\text{C}_2\text{H}_m/\text{N}_2$ ($m = 2, 4, 6$) gas mixtures, under 300 mbar pressure with gas ratio 1:2.

The surface chemical compositions of the CN_x film deposited on Si (100) substrate have been investigated by X-ray Photoelectron Spectroscopy on a VG Microtech (CLAM2:Multi-technique 100 mm hemispherical electron analyzer) X-ray photoelectron spectroscope, using Mg $\text{K}\alpha$ radiation (photo energy 1253 eV) as the excitation source and the binding energy (BE) of Au (Au 4f7/2: 84.00 eV) as the reference. The XPS spectra were collected in constant analyzer energy mode, pass energy of 23.5 eV, 0.125 eV/ step, and at a chamber pressure of 10^{-8} mbar.

Figure 7.4 shows a typical XPS overview spectrum of a-CN_x:H film deposited on the substrate Si (100) using gas mixtures C₂H_m/N₂ (m = 2, 4, 6), under 300 mbar pressure with a gas ratio of 1:2. The overview spectrum of the a-CN_x:H films obtained from gas mixtures C₂H_m/N₂ (m = 2, 4, 6) are displayed in the binding energy range 200 eV to 600 eV, which shows the C-1s, N-1s, and O-1s at binding energies of 285 eV, 400 eV and 531.8 eV, respectively ^{[24] [99]}. The experimentally observed spectrum shows a chemical shift 6 eV that is caused by an anomalous behavior of the surface charge distribution, this has been calibrated. From the figure 7.4 we can observe that the intensity of the N1s peak is larger in the a-CN_x:H film obtained from C₂H₄/N₂ plasma. The C1s and N1s XPS peaks are comparatively broadened and become asymmetric in a-CN_x:H film obtained from C₂H₄/N₂ plasma. These effects are a clear indication that nitrogen is involved in chemical bonds with carbon in different chemical states, e.g., C-C or C-N bonds. A certain image of the possible chemical bonds between nitrogen and carbon can be deduced from a deconvolution of the individual C-1s and N-1s lines into Gaussian line shapes. The best Gaussian fits to the XPS lines resulted in four different peaks for the C-1s line and three peaks for the N-1s line. In order to minimize interference between the peaks during de-convolution, all spectra have been fitted with equal line widths (full-width-at-half-maximum, FWHM) of the involved individual peak, thereby reducing the number of free parameter and yielding a more stable result.

Typical C-1s and N-1s XPS spectra are displayed in Figure 7.5, 7.6, 7.7, for a-CN_x:H film obtained from C₂H_m/N₂ (m = 2, 4, 6) gas mixture. The C-1s spectrum exhibits peaks at 284.2 eV (C1), 285.1 eV (C2), 286.7 eV (C3), and 288.3 eV (C4), which have been attributed to C=C, C=N, C-N or C≡N, and C-O bonds, respectively for the film obtained from C₂H₂/N₂ gas mixture.

Similarly, the de-convoluted N-1s spectrum shows three peaks at 398.1 eV (N1), 399.3 eV (N2), and 400.00 eV (N3) which have been assigned to C-N or C≡N, C=N, and N-O bonds ^{[24] [99]}, respectively. The N-sp³ C and N-sp C peaks have been assigned within the range 398.5 eV to 399.12 eV and 400.0 eV to 400.7 eV, respectively. Due to this strong interference of the energetic positions it is difficult to distinguish between C-N and C≡N spectral lines in N-1s XPS analysis ^{[24] [99]}.

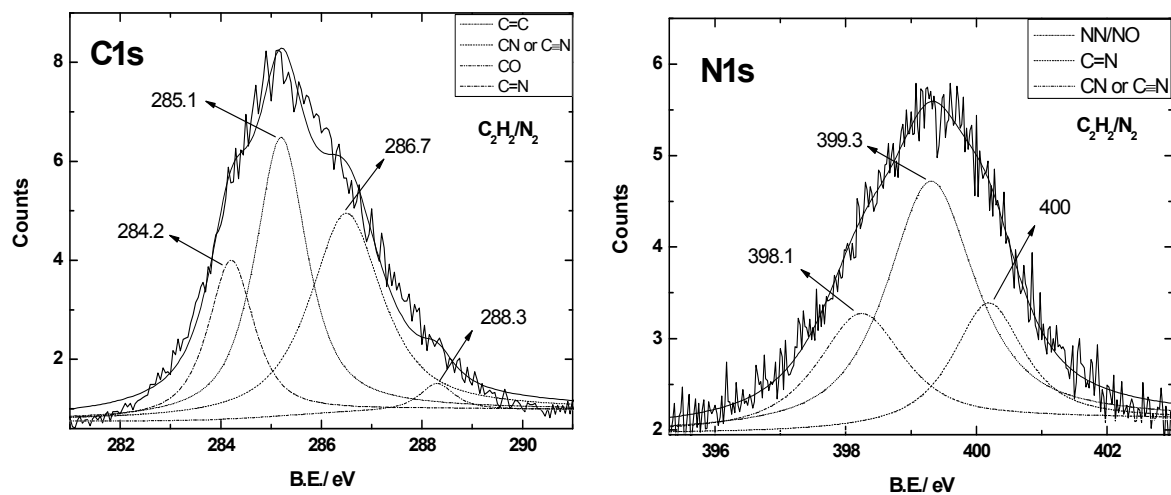


Figure 7.5 XPS spectrum for C1s and N1s for CN_x film obtained from gas mixture $\text{C}_2\text{H}_2/\text{N}_2$, under 300 mbar pressure, with gas ratio 1:2.

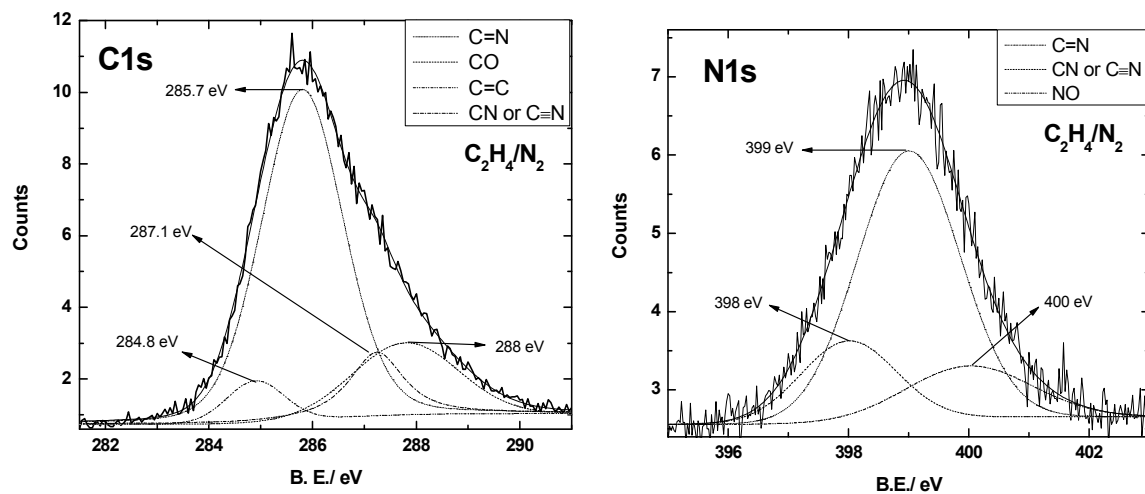


Figure 7.6 XPS spectrum for C1s and N1s for CN_x film obtained from gas mixture $\text{C}_2\text{H}_4/\text{N}_2$, under 300 mbar pressure, with gas ratio 1:2.

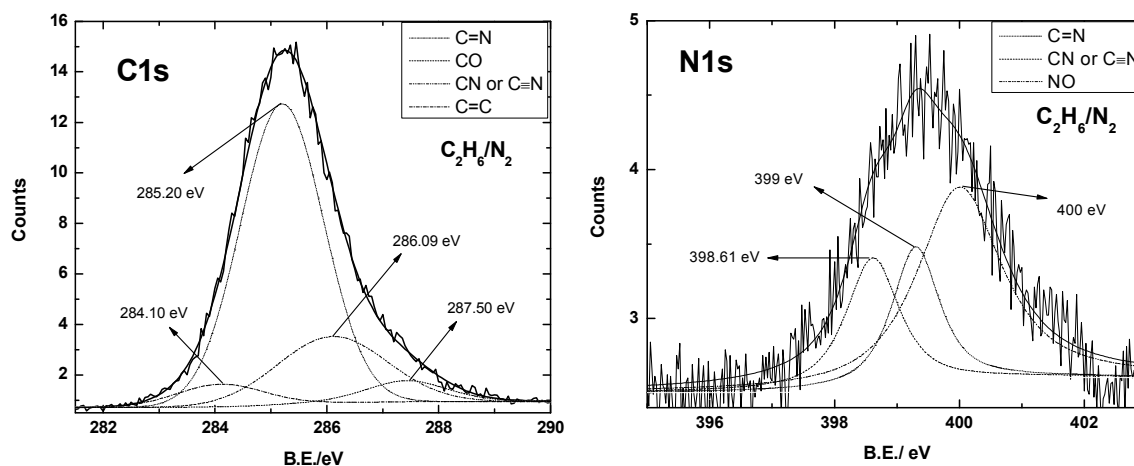


Figure 7.7 XPS spectrum for C1s and N1s for CN_x film obtained from gas mixture C₂H₆/N₂, under 300 mbar pressure with gas ratio 1:2.

The C(1-4) and N(1-3) peaks can also be observed from the films obtained from C₂H₄/N₂ and C₂H₆/N₂ gas mixtures, with a very minute shift in binding energy, this could be due to the different quantity of nitrogen incorporation into the films obtained with different gas mixtures. The N/C ratio for the film obtained from C₂H₂/N₂ gas mixture was found to be 0.27, while the film obtained from C₂H₄/N₂ gas mixture was 0.25 and the film obtained from C₂H₆/N₂ was 0.12

7.2.3 Spectroscopic Ellipsometry (SE)

Spectroscopic ellipsometry investigations were carried out with a phase modulated ellipsometer Jobin-Yvon UVISSEL (HORIBA Jobin-Yvon Inc., Edison, USA). The investigated wavelength region was 380 - 830 nm with energy step of less than 0.5 nm. The experiments were carried out under incidence angle of 70° resulted from Brewster's angle of Si (100) wafer substrate.

Spectroscopic ellipsometry measurements were performed on the deposited CN_x polymer films. To derive optical constants and layer thickness the following calculation procedure has

been performed. For an ellipsometric modeling it is critical to correctly parameterize the complex dielectric functions of an analyzed layer. Introductory parameterization of optical indices of each layers is necessary to calculate the ellipsometric angles Δ and Ψ . Deposited layer structure was assumed as a four phase model in all investigated cases: silicon substrate - amorphous hydrogenated carbon-nitride layer - surface roughness - ambient. Layer roughness was applied using Bruggeman effective medium approximation ^[102] considered as a 50% mixture of hydrogenated carbon-nitride layer and void. The optical indices of Si (100) wafer over covered by a 2.2 nm thick SiO₂ native oxygen layer were obtained from the database ^[103].

The dispersion of the optical properties of CN_x layer was described by the Tauc-Lorentz oscillator (TL) model. Proposed dispersion model was recently used for amorphous semiconductors by Gioti et al and Logothetidis et al ^{[104][105]}. TL model was also applied for amorphous carbonous layers deposited by RF magnetron sputtering ^[104]. Moreover, TL model is in wide-spread usage for description of dispersion of the optical properties of a-C, a-C:H ^[106] and CN_x layers deposited by DBD discharge ^[107]. This model is the combination of the Tauc joint density of states ^[108] and the quantum mechanical Lorentz oscillator model ^[109]. TL model fits to the dielectric functions of amorphous material class, which exhibit a peculiarity due to the presence of two separated contribution of inter-band electronic transition related to sp² and sp³ bonded carbon ^[110]. The appropriate parameters of the TL model were applied for the analyzed layer considering different chemical composition, which is derived from the plasma composition.

Applied optical model was fitted to the experimental data using the Levenberg-Marquardt nonlinear least-squares algorithm. The fitting measure mean square error (MSE) was used for verification of the ability of the applied model to fit the experimental data. As the fitting measure the mean square error (MSE) was utilized ^[111], which is given by:

$$MSE = \frac{1}{2N - M} \sum_{i=1}^N \left[\left(\frac{\Psi_i^{\text{mod}} - \Psi_i^{\text{exp}}}{\sigma_{\Psi,i}^{\text{exp}}} \right)^2 + \left(\frac{\Delta_i^{\text{mod}} - \Delta_i^{\text{exp}}}{\sigma_{\Delta,i}^{\text{exp}}} \right)^2 \right] \quad (1)$$

In Eq. (1) Δ_i^{exp} , Δ_i^{mod} , Ψ_i^{exp} , Ψ_i^{mod} and σ_i represent the investigated, calculated, and standard deviations at data set i , while N is the number of measurement points and M is the

number of fitted parameters. Effective fitting allows a quantitative description of tholins optical constant and thickness of the deposited samples.

The fitting procedure described above gives accurate values of film thicknesses as well as variation of the refractive index and extinction coefficient versus wavelength. Spectral variations of n and k of C_2H_4/N_2 and C_2H_6/N_2 films with thicknesses are presented in Figure 7.8. The averaged thickness from four points on the sample is presented and the thickness for C_2H_4/N_2 film is found to be 60 nm and while for C_2H_6/N_2 it is 150 nm. Moreover, each ellipsometric scan integrate thickness from the light spot radius of 1 mm. Optical constants look like quantities related by Kramers-Kronig relations ^[111]. It means that n achieves an inflection point at a wavelength where k exhibits a maximum. Refractive indices increase from low to high wavelengths. Maximum of extinction coefficient of C_2H_6/N_2 film (0.65) is positioned at 450 nm. It is higher than the highest k value of C_2H_4/N_2 film (0.55). Moreover, maximum of k value in C_2H_6/N_2 sample is shifted by about 50 nm toward the higher wavelengths. The inflection points in the n graphs are not evident. They must be located around the wavelengths, where the k maximum is located. The thickness of the C_2H_6/N_2 sample is twice as larger as the C_2H_4/N_2 film. It was measured in not exactly same points on the samples. Since the films are made using DBD plasma, samples have a non-uniform thickness ^[107]. Moreover, difference comes also from lower activity of C_2H_6 precursor in layer nucleation concerned with higher level of saturation of the carbon bonds in this hydrocarbon molecule. Type of hydrocarbon used influence also on nitrogen activation and incorporation to the layer. The XPS measurements shows that the intensity for nitrogen peak (N1s) is higher in C_2H_4 sample compared to C_2H_6 one. As the nitrogen content in the film increases, the refractive index shifts toward lower values (see Figure 7.8). Moreover, the low values of the refractive index reflect the relatively localized structure of electronic charge distributions. Higher reduction of n by nitrogen incorporation may change also polarization of the bonds.

Spectral variation of extinction coefficient exhibits smaller values for C_2H_4 samples compared to C_2H_6 films. Bonding with higher amount of nitrogen decrease amount of sp^3 phase and increase absorption. The extinction coefficient slowly decreases from around 0.1 to almost zero as wavelength increases from 400 up to 800 nm. This fact goes from previously mentioned anomalous dispersion related to Kramers-Kronig material behaviour.

For C_2H_2/N_2 film it was difficult to analyze ellipsometry since it had lot of dust on the surface.

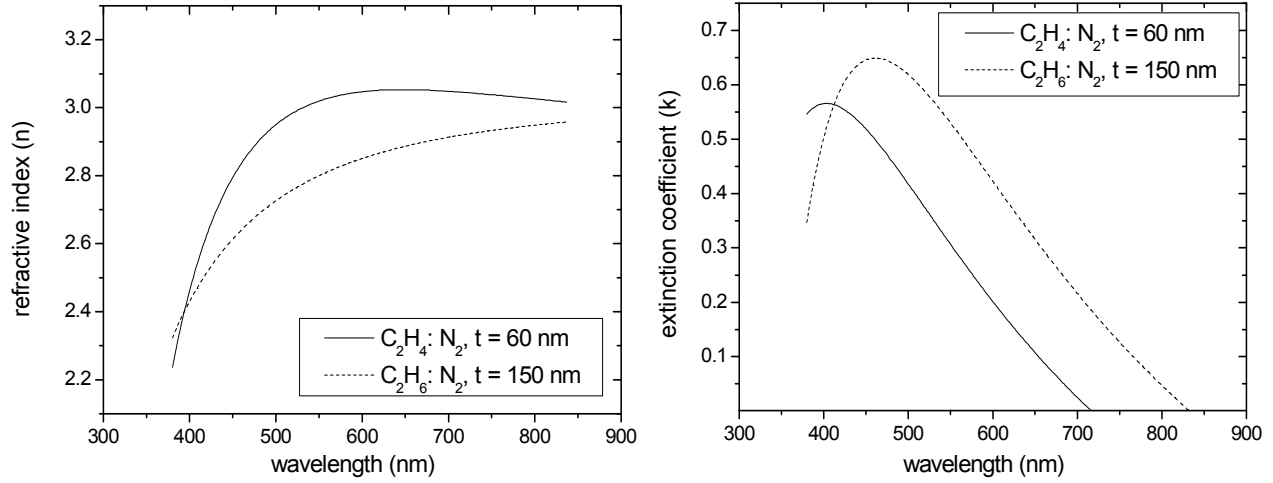
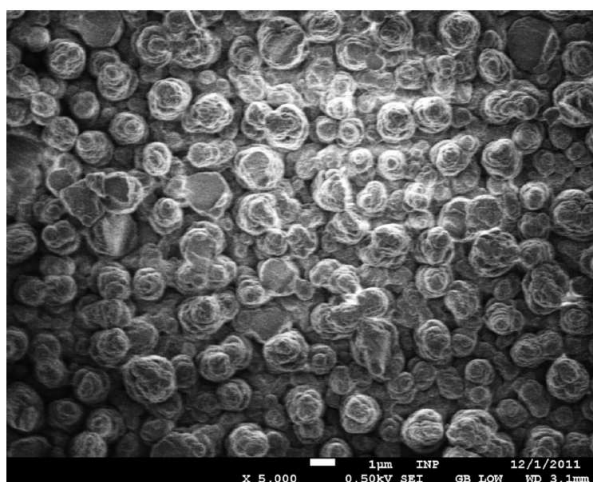


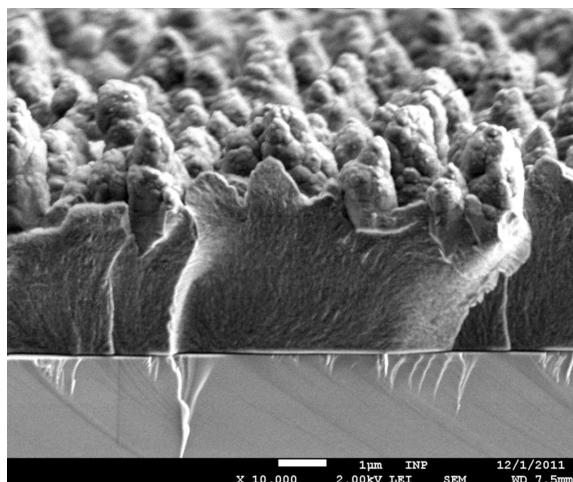
Figure 7.8 Ellipsometric analysis of CN_x film obtained from two different gas mixtures C_2H_6/N_2 (dotted line) and C_2H_4/N_2 (solid line), under 300 mbar pressure with gas ratio 1:2.

7.2.4 Scanning Electron Microscopy

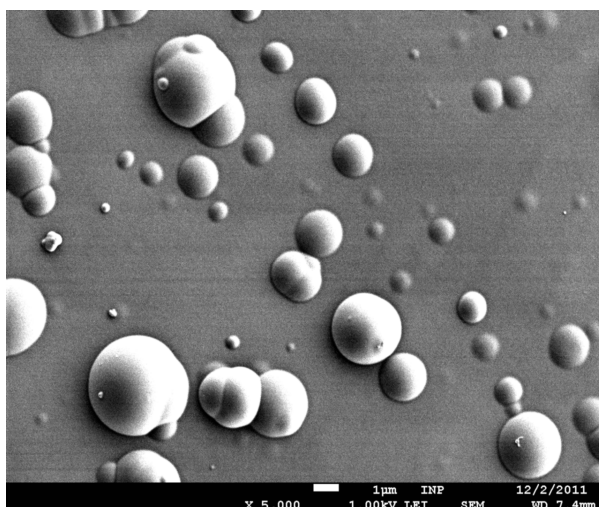
The morphological structure of thin films has been analyzed with a field emission scanning electron microscope (JEOL JSM-7500Fa) employing a field-emission electron gun, a semi-in lens conical objective and a secondary electron in-lens detector. It allows for high-resolution and high-quality image observation of a specimen at a maximum specified resolution of 1.0 nm. In the present study, scanning electron microscopy (SEM) of the dielectric samples has been performed in the gentle beam mode with accelerating voltages in the range of 0.5 and 2 kV, magnifications ranging from 70 000 to 100 000 at working distance between 5 and 3 mm, and without an additional metal coating prior to the SEM analysis.



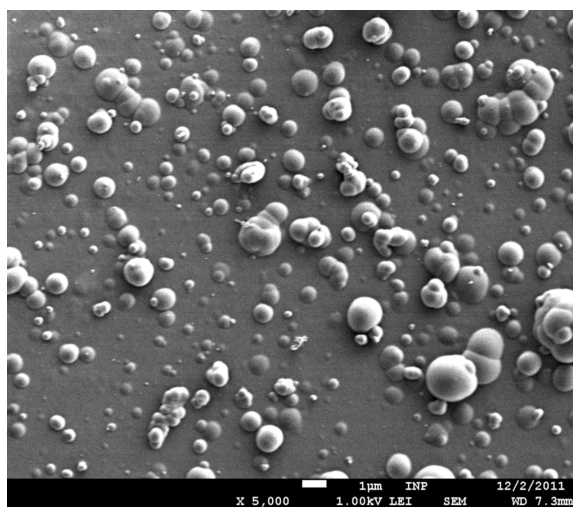
(a)



(b)



(a)



(b)

Figure 7.9 Scanning electron microscope images depicting surface morphology for $a\text{-CN}_x\text{:H}$ films deposited using $\text{C}_2\text{H}_m/\text{N}_2$ ($m = 2, 4, 6$) gas mixtures, on Si (100) substrate at 300 mbar pressure with gas ratio 1:2. (a) $\text{C}_2\text{H}_2/\text{N}_2$ film, (b) $\text{C}_2\text{H}_2/\text{N}_2$ film (cross-section view), (c) $\text{C}_2\text{H}_4/\text{N}_2$ film, and (d) $\text{C}_2\text{H}_6/\text{N}_2$ film.

The surface morphology for the deposited $a\text{-CN}_x\text{:H}$ films have been derived from scanning electron microscopy. Figure 7.9 (a) and 7.9 (b) shows the SEM image for the CN_x film

obtained from C_2H_2/N_2 gas mixture. The film was deposited under pressure 300 mbar with gas ratio 1:2. From figure 7.9 (a) and 7.9 (b) (cross-sectional view), the surface of the CN_x film looked like a cauli flower structure. Figure 7.9 (c) and 7.9 (b) shows the SEM image for the CN_x film obtained from C_2H_4/N_2 and C_2H_6/N_2 gas mixtures under the same experimental conditions which has been used for C_2H_2/N_2 film. From the morphology of C_2H_4/N_2 and C_2H_6/N_2 films we can see the formation of globule like structure for both the films. The globule size is comparatively larger in C_2H_4/N_2 film when compared to C_2H_6/N_2 film. And the globules are densely formed in C_2H_6/N_2 film. Because of the difference in chemical growth structures have been occurred in all these three films, hence the films look different in their surface morphology.

7.2.5 Deposition Rate

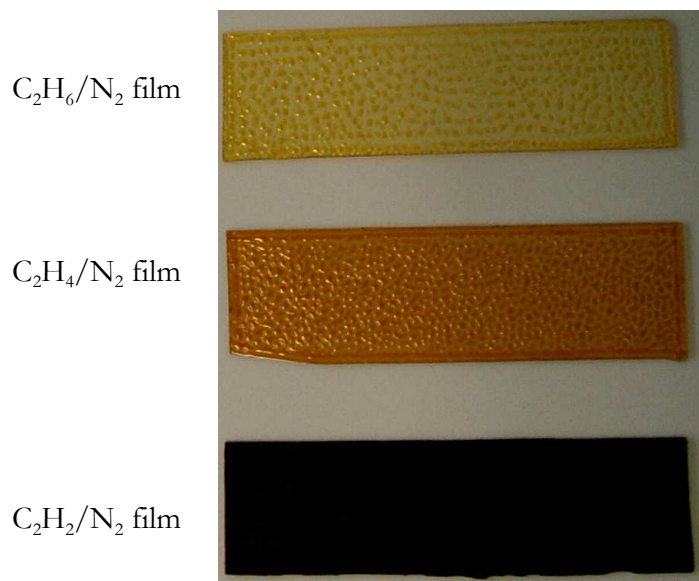


Figure 7.10 a- $CN_x:H$ film deposited using gas mixtures C_2H_m/N_2 ($m = 2, 4, 6$) on glass substrate under 300 mbar pressure with gas ratio 1:2

Deposited films are displayed in figure 7.10. The films show a brown or yellow color which varies from deep dark brown to light yellow for films from C_2H_2 and C_2H_6 gas mixtures, respectively. C_2H_4/N_2 and C_2H_6/N_2 films were sticky in nature. The thickness of the films is

of the order of several 10 μm for 5 hours deposition. Films are not uniform and show small structures which are almost regularly distributed and separated by 1-2 mm from each other.

Deposition rates were estimated from the additional mass deposited on the glass substrates which were weighed with a microbalance before and after deposition. Typical deposition rates are in the range 0.1-0.4 $\mu\text{g}/(\text{sec cm}^2)$ (Table 7.2). Assuming a film density of 2 g/cm^3 this corresponds to about 0.5-2 nm/s.

Gas mixture	Deposition Rate ($\mu\text{g cm}^{-2} \text{s}^{-1}$)
$\text{C}_2\text{H}_6:\text{N}_2$	0.125
$\text{C}_2\text{H}_4:\text{N}_2$	0.245
$\text{C}_2\text{H}_2:\text{N}_2$	0.43

Table 7.2 shows the deposition rate for different gas mixtures

Chapter 8

Deposition and Characterization of Diamond Like Carbon (DLC) films using C_2H_m/Ar ($m = 2, 4, 6$) gas mixtures by Dielectric Barrier Discharge

This chapter explains the deposition of DLC films using gas mixtures C_2H_m/Ar ($m = 2, 4, 6$) and their characterizations.

8.1 Preparation of Thin films

Two different kinds of substrates were used for the deposition experiments. One is aluminium coated glass substrate which has dimensions 6 cm x 2 cm and Si (100) of dimensions 2 cm x 3 cm. The aluminium coating on the glass substrate was made by Chemical Vapor Deposition (CVD) yielding a thickness of 190 nm.

The substrate can be placed on the glass electrode in the DBD chamber. The gas mixtures C_2H_m ($m = 2, 4, 6$) and argon can be fed by two different gas flow channels. For each experiment the gas ratio 1:2 has been taken. And the chamber pressure was maintained 300 mbar. All experiments were carried out with a frequency 5 kHz. And the power consumed for each experiment is 4 W.

8.2 Results and Discussion

Characterization of the films has been done by FT-IRRAS, X-ray Photo Electron Spectroscopy (XPS) and ellipsometry.

8.2.1 Fourier Transform Infrared Reflection Absorption Spectroscopy (FT-IRRAS)

The chemical compositions of DLC films deposited on aluminium coated glass substrate were determined by Fourier Transform Infrared Reflection Absorption Spectroscopy (BRUCKER, VERTEX 80V). Prior to the experiments, the sample compartment was evacuated to 2 mbar to reduce absorption of water vapor and CO₂. Spectra were recorded in the range 4000 to 500 cm⁻¹ with a spectral resolution of 0.7 cm⁻¹. Each spectrum was the average of 20 scans. A background spectrum was taken from each substrate prior to the deposition of DLC films.

Figures 1a, 1b, and 1c show FTIR spectra of DLC films deposited on an aluminium coated glass substrate by using C₂H_m/Ar (m = 2, 4, 6) gas mixtures at 300 mbar gas pressure with a gas ratio 1:2.

8.2.1.1 C₂H₂/Ar

Figure 8.1 shows FT-IRRAS spectrum for the a-C:H film obtained from the gas mixture C₂H₂/Ar gas mixture at 300 mbar pressure with gas ratio 1:2. The a-C:H film obtained from C₂H₂/Ar plasma shows the C-H stretching vibrations for highly unsaturated hydrocarbons, alkynes such as C₂H₂ or higher order alkyne chains at wavenumber 3312 cm⁻¹. At the same wavenumber we can also observe the O-H stretching vibrations for H₂O has also been observed^[112]. The wavenumber 2960 cm⁻¹ is related to C-H asymmetric stretching vibrations for CH₃ groups have been observed^{[112] [113] [114] [115]}. The wavenumbers 2223 cm⁻¹ – 2105 cm⁻¹ corresponds to C≡C stretching vibrations for alkynes^[113]. A well pronounced band can be observed at a wavenumber 1708 cm⁻¹ which corresponds to C=C stretching vibrations for alkenes^[112]. The wavenumbers 1443 cm⁻¹, 1235 cm⁻¹^{[112] [115]} and 967 cm⁻¹ (out-of-plane C-H deformation) corresponds to bending vibrations for alkenes such as C₂H₄/ higher chain alkene or aromatic compounds^[89].

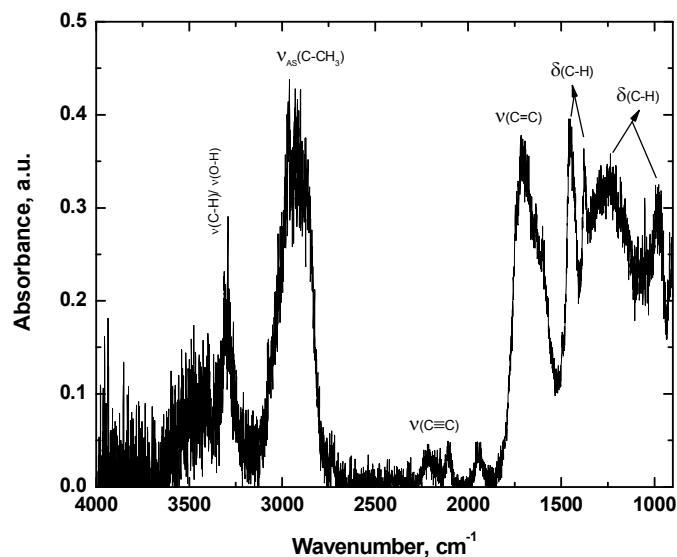


Figure 8.1 FTIR spectra of DLC films obtained from C_2H_2/Ar gas mixture, under 300 mbar pressure with gas ratio 1:2

8.2.1.2 C_2H_4/Ar

Figure 8.2 shows the FT-IRRAS spectrum for a-C:H film obtained from the C_2H_4/Ar gas mixture at 300 mbar pressure with gas ratio 1:2. The spectrum obtained for C_2H_4/Ar films looks rich in functional groups which are deposited on the surface. The intensity of the bands are high when compared to the film obtained from C_2H_2/Ar gas mixture. The broad band at 3390 cm^{-1} is related to O-H stretching vibrations for the H_2O , which is considered as an impurity formed while transferring the sample from DBD chamber to FT-IRRAS sample compartment. Around 3300 cm^{-1} wavenumber we can observe the C-H stretching vibrations for alkynes such as C_2H_2 or higher order alkyne molecules ^[112]. Wavenumbers 2953 cm^{-1} and 2864 cm^{-1} , corresponds to asymmetric and symmetric C-H stretching vibrations for CH_3 groups can be observed ^{[112] [113] [114] [115]}. The broad band appeared in the region 2718 cm^{-1} – 2642 cm^{-1} is related again to the O-H stretching vibrations. The wavenumber 2300 cm^{-1} – 2019 cm^{-1} is related to $C\equiv C$ stretching vibrations for alkynes ^[113]. At wavenumber 1704 cm^{-1} $C=C$ stretching vibrations can be observed for alkene molecules such as C_2H_4 or higher

order alkene chains ^[112]. The deformation vibrations for alkenes can be observed at the wavenumbers 1463 cm⁻¹ ^[112] ^[115] and 960 cm⁻¹ ^[89]. The deformation vibrations for saturated alkanes can be observed at wavenumbers 1381 cm⁻¹ and 1022 cm⁻¹ ^[89]. The bands formed on the C₂H₄/Ar film have high intensity of absorption when compared to C₂H₂/Ar film due to the difference in thickness.

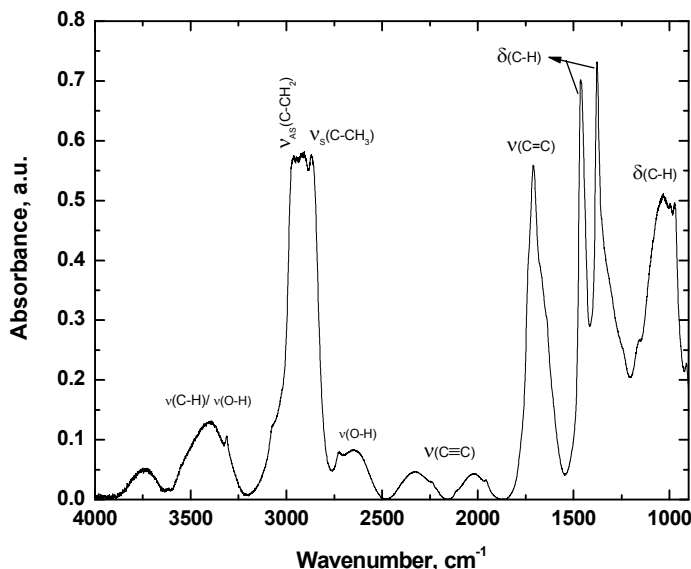


Figure 8.2 FTIR spectra of DLC films obtained from C₂H₄/Ar gas mixture, under 300 mbar pressure with gas ratio 1:2

8.2.1.3 C₂H₆/Ar

Figure 8.3 shows FT-IRRAS spectrum for the DLC film obtained from the C₂H₆/Ar gas mixture at 300 mbar pressure with gas ratio 1:2. The FT-IRRAS spectrum obtained for the film obtained from C₂H₆/Ar gas mixture have comparatively less functional groups on the film surface with less intensity of absorption. The broad band in the region 3400 cm⁻¹ – 3100 cm⁻¹ is related to O-H stretching vibrations for H₂O. At the same wavenumber region we can also find the C-H stretching vibrations for alkynes such as C₂H₂ or higher order alkyne chains ^[112]. The wavenumbers 2956 cm⁻¹, 2923 cm⁻¹, and 2870 cm⁻¹, are related to C-H

asymmetric stretching vibrations for CH_3 groups, C-H asymmetric stretching vibrations for CH_2 groups and C-H symmetric stretching vibrations for CH_3 groups ^{[112] [113] [114] [115]}, respectively. A well pronounced band at the wavenumber 1651 cm^{-1} corresponds to C=C stretching vibrations for alkenes ^[112]. Deformation vibrations for alkenes and saturated alkanes can be found at the wavenumbers 1456 cm^{-1} and 1381 cm^{-1} ^{[112] [115] [89]}, respectively. Again the deformation vibrations for saturated alkanes and highly unsaturated alkynes can be found at the wavenumber, 1123 cm^{-1} ^[89]. When compared to the films obtained from $\text{C}_2\text{H}_2/\text{Ar}$ and $\text{C}_2\text{H}_4/\text{Ar}$ gas mixtures, $\text{C}_2\text{H}_6/\text{Ar}$ gas mixture's film have less functional groups with less intensity of absorption.

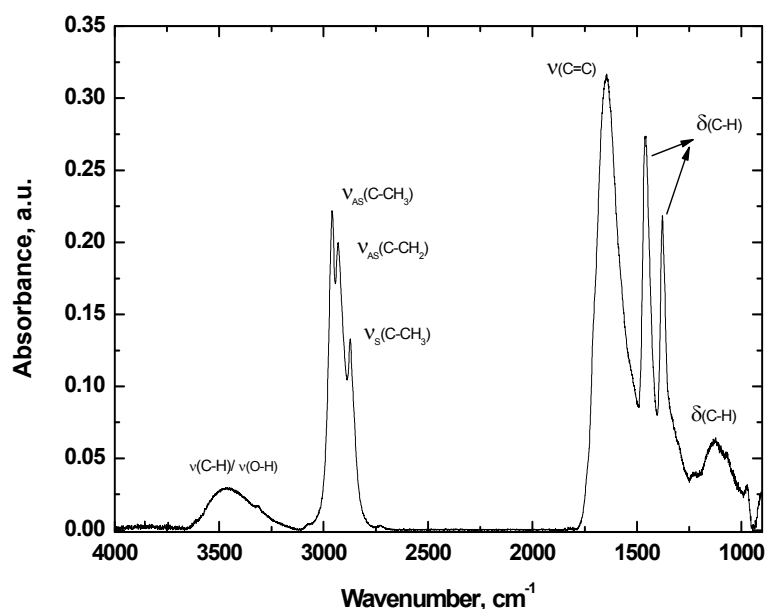


Figure 8.3 FTIR spectra of DLC films obtained from $\text{C}_2\text{H}_6/\text{Ar}$ gas mixture, under 300 mbar pressure with gas ratio 1:2

Table 8.1 Major assignments for FTIR absorption spectra for DLC films obtained from C_2H_6/Ar ($m = 2, 4, 6$) gas mixtures

Wavenumber/ cm^{-1}	Assignments
3100 - 3732	$\nu(C-H)/\nu(O-H)$: Alkynes, H_2O
2960, 2876	$\nu_{as}(C-H), \nu_s(C-H)$: CH_3 groups
2953, 2864	$\nu_{as}(C-H), \nu_s(C-H)$: CH_2 groups
2100,	$\nu(C\equiv C)$: Alkynes
1960	$\nu(C=C)$: Alkenes (cyclic molecules)
1642	$\nu(C=C)$: Alkenes
1463, 1381	$\delta(C-H), \delta(C-H)$: Alkenes, alkanes
940	$\delta(C-H)$: Alkenes
781	$\delta(C-H)$: Alkynes

ν : stretching vibration, δ : Bending (scissoring) vibration or deformations,
s: symmetric, as: asymmetric

8.2.1.4 Comparison between C_2H_m/Ar ($m = 2, 4, 6$) gas mixtures

Thin films obtained from all three gas mixtures showed almost same characteristics functional groups with different intensity of absorptions. The major differences observed are,

- The C_2H_2/Ar plasma film was forming more dust in the chamber, as result of dust the film became thick with more dust on the surface. The functional groups present on the surface were almost same except a very small shift in the wavenumber with different intensity of absorption when compared to the films obtained from C_2H_4/Ar and C_2H_6/Ar gas mixtures.
- $C\equiv C$ stretching vibrations absorption band is completely invisible in the films obtained from C_2H_6/Ar gas mixture, whereas this band is visible in the films obtained from C_2H_2/Ar and C_2H_4/Ar gas mixtures.

- The film obtained from C_2H_4/Ar gas mixture looked rich in functional groups present on the surface with high intensity of absorption. The film showed more water of hydration for example at the wavenumber 3732 cm^{-1} and the broad band appeared in the region 2718 cm^{-1} - 2642 cm^{-1} is related to O-H stretching vibrations.

8.2.2 X-ray Photoelectron Spectroscopy (XPS)

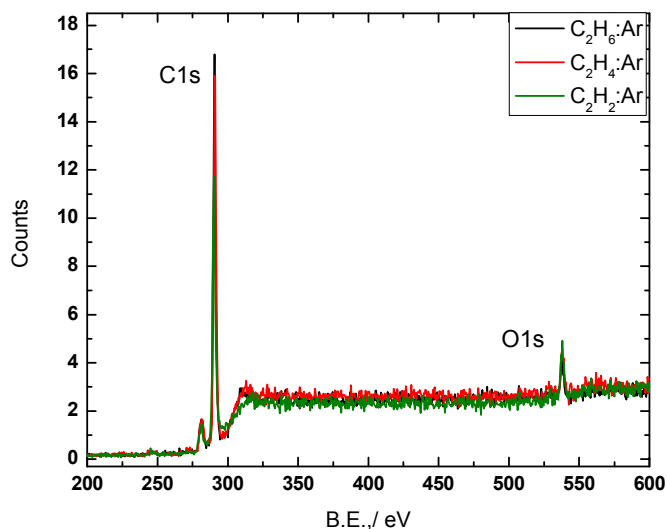


Figure 8.4 Typical XPS overview spectrum for DLC film obtained from C_2H_m/Ar ($m = 2, 4, 6$) gas mixtures, under 300 mbar pressure with gas ratio 1:2

The surface chemical compositions of the DLC film deposited on Si (100) substrate have been investigated by X-ray Photoelectron Spectroscopy on a VG Microtech (CLAM2:Multi-technique 100 mm hemispherical electron analyzer) X-ray photoelectron spectroscope, using Mg $K\alpha$ radiation (photo energy 1253 eV) as the excitation source and the binding energy (BE) of Au (Au $4f_{7/2}$: 84.00 eV) as the reference. The XPS spectra were collected in constant analyzer energy mode, pass energy of 23.5 eV, 0.125 eV/ step, and at a chamber pressure of 10^{-8} mbar. Figure 8.4 shows the typical C1s peak for a-C:H film which has been appeared at binding energy 285 eV for all three gas mixtures. For the a-C:H film obtained from all different gases shows the C1s peak at the same value of binding energy except the difference on the surface composition of carbon and oxygen, oxygen is an impurity occurred

while transferring a-C:H film from DBD chamber to XPS chamber. The oxygen impurity is found more on the a-C:H film obtained from C_2H_2/Ar plasma, while for film obtained from C_2H_m/Ar ($m = 4$ and 6) is less but more carbon content has been observed on the surface [119] [120] [121].

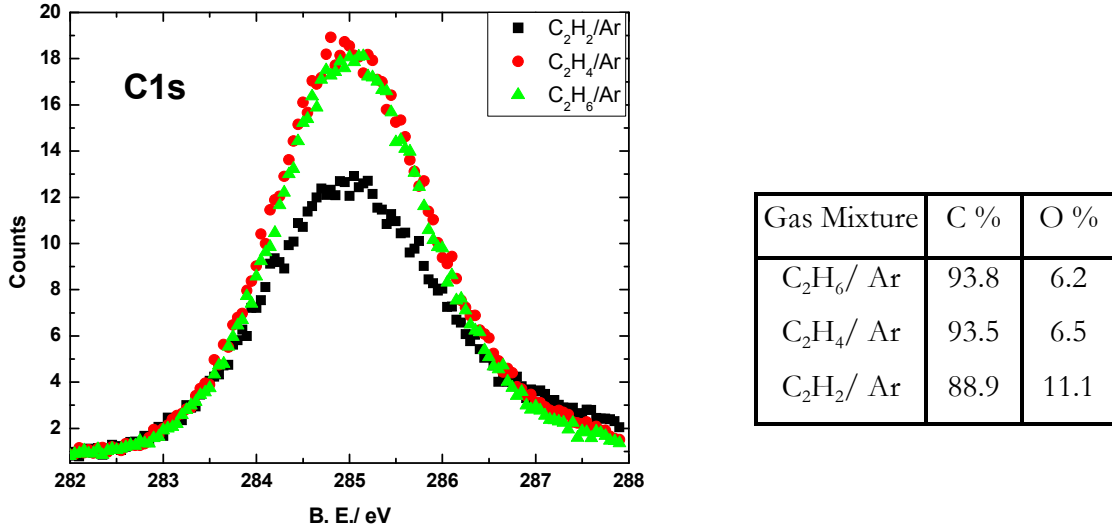


Figure 8.5 XPS spectrum for C1s for DLC film obtained from gas mixture C_2H_m/Ar ($m = 2, 4, 6$), under 300 mbar pressure with gas ratio 1:2.

8.2.3 Spectroscopic Ellipsometry (SE)

Spectroscopic ellipsometry investigations were carried out with a phase modulated ellipsometer Jobin-Yvon UVISSEL (HORIBA Jobin-Yvon Inc., Edison, USA). The investigated wavelength region was 380 - 830 nm with energy step of less than 0.5 nm. The experiments were carried out under incidence angle of 70° resulted from Brewster's angle of Si (100) wafer substrate.

To derive optical constants and layer thickness the following calculation procedure has been performed. Deposited layer structure was assumed as a four phase model in all investigated cases: silicon substrate - amorphous hydrogenated carbon (a:C-H) layer - surface roughness - ambient. Layer roughness was applied using Bruggeman effective medium approximation^[102] considered as a 50% mixture of hydrogenated carbon (a:C-H) layer and void. The optical

indices of Si (100) wafer over covered by a 2.2 nm thick SiO₂ native oxygen layer were obtained from the database ^[103]. The dispersion of the optical properties of DLC layer was described by the Tauc-Lorentz oscillator (TL) model. We used recently proposed dispersion model for amorphous semiconductors by Gioti et al and Logothetidis et al ^{[104] [105]}. The appropriate parameters of the TL model were applied for the analyzed layer considering different chemical composition, which is derived from the plasma composition.

Spectroscopic measurements were performed on the deposited a:C-H polymer films. Ellipsometric modelings have to be performed to obtain optical constants and layer thickness. For an ellipsometric modeling it is critical to correctly parameterize the complex dielectric functions of an analyzed layer. Introductory parameterization of optical indices of each layer is necessary to calculate the ellipsometric angles Δ and Ψ . In this study the four-phase structure model of each sample was proposed. Applied optical model was fitted to the experimental data using the Levenberg-Marquardt nonlinear least-squares algorithm. The fitting measure mean square error (MSE) was used for verification of the ability of the applied model to fit the experimental data. As the fitting measure the mean square error (MSE) was utilized ^[111], which is given by:

$$MSE = \frac{1}{2N - M} \sum_{i=1}^N \left[\left(\frac{\Psi_i^{\text{mod}} - \Psi_i^{\text{exp}}}{\sigma_{\Psi,i}^{\text{exp}}} \right)^2 + \left(\frac{\Delta_i^{\text{mod}} - \Delta_i^{\text{exp}}}{\sigma_{\Delta,i}^{\text{exp}}} \right)^2 \right] \quad (1)$$

In Eq. (1) Δ_i^{exp} , Δ_i^{mod} , Ψ_i^{exp} , Ψ_i^{mod} and σ_i represent the investigated, calculated, and standard deviations at data set i , while N is the number of measurement points and M is the number of fitted parameters. Effective fitting allows a quantitative description of DLC film's optical constant and thickness of the deposited samples.

The main point of ellipsometric investigation was to extract parameters of DLC layer from assigned four-phase model. For this purposes authors applied two different models of dispersion of the optical constants. Tauc-Lorentz oscillator (TL) model has to be applied to simulate samples deposited in higher hydrocarbons like C₂H₄ and C₂H₆. Therefore, this plasma mixture creates amorphous carbonous samples. TL model was applied for amorphous carbonous layers deposited by RF magnetron sputtering ^[104]. Moreover, TL model is in wide-spread usage for description of dispersion of the optical properties of a-C,

a-C:H^[106] and CN_x layers deposited by DBD discharge^[107]. This model is the combination of the Tauc joint density of states^[108] and the quantum mechanical Lorentz oscillator model^[109]. TL model fits to the dielectric functions of amorphous material class, which exhibit a peculiarity due to the presence of two separated contribution of inter-band electronic transition related to sp² and sp³ bonded carbon^[110].

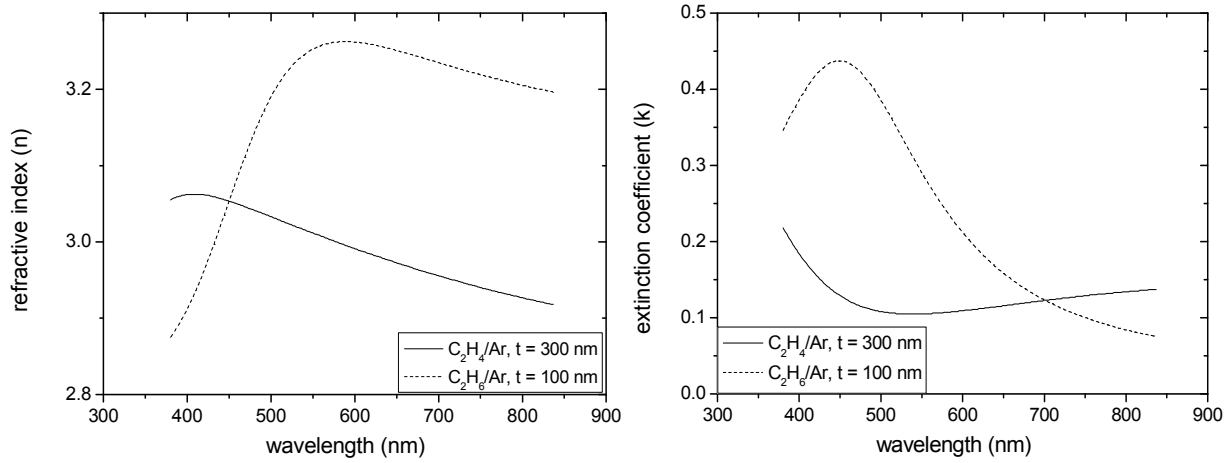


Figure 8.6 Ellipsometric analysis of DLC film obtained from two different gas mixtures C₂H₆/Ar (dotted line) and C₂H₄/Ar (solid line), under 300 mbar pressure with gas ratio 1:2.

The fitting procedure described above gives accurate values of film thicknesses as well as variation of the refractive index and extinction coefficient versus wavelength. Spectral variations of n and k of C₂H₄/N₂ and C₂H₆/N₂ films are presented in Figure 8.6. They look like quantities related by Kramers-Kronig relations^[111]. It means that n achieves an inflection point at a wavelength where k exhibits a maximum. Refractive indices increase from low to high wavelengths. Maximum of extinction coefficient of C₂H₆/Ar film (0.65) is positioned at 450 nm. It is higher than the highest k value of C₂H₄/Ar film (0.15). Moreover, maximum of k value in C₂H₆/Ar sample is shifted by about 50 nm toward the higher wavelengths. The inflection points in the n graphs are not evident. They must be located around the wavelengths, where the k maximum is located. The thickness of the C₂H₄/Ar sample is thrice as larger as the C₂H₆/Ar film. It was measured in not exactly same points on the

samples. Since the films are made using DBD plasma, samples have a non-uniform thickness^[107]. Moreover, difference comes also from lower activity of C_2H_6 precursor in layer nucleation concerned with higher level of saturation of the carbon bonds in this hydrocarbon molecule. The low values of the refractive index reflect the relatively localized structure of electronic charge distributions. Higher reduction of n may also change polarization of the bonds.

Spectral variation of extinction coefficient exhibits smaller values for C_2H_4 samples compared to C_2H_6 films. Bonding with higher amount of nitrogen decrease amount of sp^3 phase and increase absorption. The extinction coefficient slowly decreases from around 0.1 to almost zero as wavelength increases from 400 up to 800 nm. This fact goes from previously mentioned anomalous dispersion related to Kramers-Kronig material behavior. For C_2H_2/N_2 film it was difficult to analyze ellipsometry since it had lot of dust on the surface.

8.2.4 Deposition Rate

Deposited films are displayed in figure 8.7. The films show a brown or yellow color which varies from dark brown to light yellow for films from C_2H_2 and C_2H_6 gas mixtures, respectively. C_2H_4/Ar and C_2H_6/Ar films were sticky in nature.

Deposition rates were estimated from the additional mass deposited on the glass substrates which were weighed with a microbalance before and after deposition. Typical deposition rates are in the range 0.05 - 0.3 $\mu g / (sec\ cm^2)$ (Table 8.2).

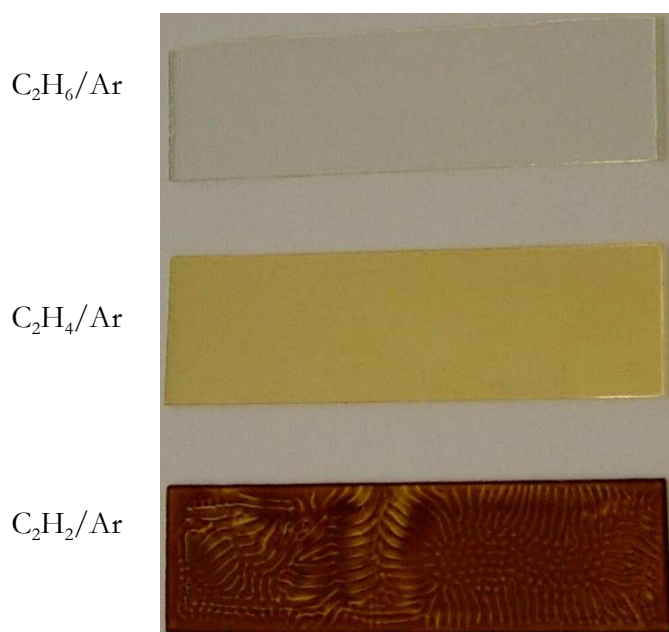


Figure 8.7 a-C:H film deposited using gas mixtures C_2H_m/Ar ($m = 2, 4, 6$) on glass substrate under 300 mbar pressure with gas ratio 1:2

Table 8.2 shows the deposition rate for different gas mixtures

Gas mixture	Deposition Rate ($\mu\text{g cm}^{-2} \text{s}^{-1}$)
$C_2H_6: Ar$	0.08
$C_2H_4: Ar$	0.18
$C_2H_2: Ar$	0.28

Chapter 9

9.1 Conclusion

This thesis deals with synthesis and deposition of plasma polymers in a DBD at atmospheric pressure. Which assist to understand the chemical reactions involved in the formation of tholins, which are found in Titan atmosphere.

In addition DBDs have attracted much interest in recent years because of their wide applications. These are the simplest technique to study the gas chemistry and for the deposition of thin films. For our study we have used CH_4/N_2 , $\text{C}_2\text{H}_m/\text{N}_2$ ($m = 2, 4, 6$) and CH_4/Ar , $\text{C}_2\text{H}_m/\text{Ar}$ ($m = 2, 4, 6$) gas mixtures at atmospheric pressure of 300 mbar with gas ratio 1:2. Plasma diagnostics were carried out using mass spectrometry and FTIR spectroscopy.

Mass spectrometry diagnostics reveals the plasma chemical reactions of $\text{C}_2\text{H}_m/\text{N}_2$ ($m = 2, 4, 6$) gas mixtures leads to the formation of hydrogen, higher order hydrocarbons including aromatic compounds and nitrogen containing organic compounds at atmospheric pressure of 300 mbar with gas ratio 1:2. Significant differences between the different gas mixtures were noted. In $\text{C}_2\text{H}_2/\text{N}_2$ the dominant reaction of the formed C_2H radical leads to the formation of the hydrogen-poor molecules C_4H_2 and C_6H_2 . Formation of nitrogen containing compounds was noticed to be less. About 15% of the consumed C_2H_4 and C_2H_6 were converted into larger hydrocarbons, compared to about 1% of the consumed C_2H_2 .

FTIR spectroscopy reveals the formation of smaller hydrocarbons found in Titan atmosphere^{[127] [128] [129]} and also the components for tholin formation, such as CH_4 , C_2H_2 , C_2H_4 , C_2H_6 , C_4H_2 and nitrogen containing compounds such as HCN , NH_3 from CH_4/N_2 and $\text{C}_2\text{H}_m/\text{N}_2$ ($m = 2, 4, 6$) gas mixtures. Formation of acetylene and HCN was noticed to be abundant. Percentage formation and consumption of gases have been reported.

Mass spectrometry for $\text{C}_2\text{H}_m/\text{Ar}$ ($m = 2, 4, 6$) gas mixtures shows the production of hydrogen and higher order hydrocarbons including the aromatic compounds. Significant differences between the different gas mixtures were noted. In $\text{C}_2\text{H}_2/\text{Ar}$ the dominant reaction of the formed C_2H radical leads to the formation of the hydrogen-poor molecules

C_4H_2 and C_6H_2 . The production of hydrogen, and higher order hydrocarbons is noticed to be less when compared to C_2H_4/Ar and C_2H_6/Ar gas mixtures. This is due to the reason that acetylene plasma was producing more dust in the chamber, as a result of dust; chemical reactions have been resisted.

FTIR spectroscopy for CH_4/Ar and C_2H_m/Ar ($m = 2, 4, 6$) reveals the formation of smaller hydrocarbons which are found in titan atmosphere such as CH_4 , C_2H_2 , C_2H_4 , C_2H_6 , C_4H_2 molecules. Significant differences between all these gas mixtures were observed. Percentage formation and consumption of gases are calculated.

Thin films deposited on Si(100) and aluminium coated glass substrate using C_2H_m/N_2 ($m = 2, 4, 6$) and C_2H_m/Ar ($m = 2, 4, 6$) gas mixtures have been studied by DBD at atmospheric pressure, with 1:2 gas ratio. The diagnostics for the films were performed using FT-IRRA spectroscopy, XPS, and spectroscopic ellipsometry. Surface morphology were derived from scanning electron microscopy.

Thin films obtained from C_2H_m/N_2 ($m = 2, 4, 6$) gas mixture had almost same functional groups except the intensity of the individual bands. Several functional groups such as saturated alkanes, unsaturated alkenes and highly unsaturated alkynes, NH_2 , $C-N$, $C=N$, and $C\equiv N$ etc., were observed. XPS analysis shows that the N/C ratio for thin films obtained from C_2H_2/N_2 gas mixture is 0.27 and the film obtained from C_2H_4/N_2 gas mixture is 0.25. While the film obtained from C_2H_6/N_2 gas mixture shows 0.12. The amount of nitrogen in the films varies as the hydrocarbon varies from C_2H_2 to C_2H_4 to C_2H_6 . The N/C ratio was more on the surface for the films obtained from C_2H_2/N_2 and C_2H_4/N_2 gas mixtures. Spectroscopic ellipsometric analysis shows that the thin films obtained from C_2H_4/N_2 gas mixture have thickness 60 nm and the maximum refractive index is found to be 3.0 and the film obtained from C_2H_6/N_2 gas mixture shows the thickness of 150 nm with maximum refractive index 2.8. Scanning electron microscopy shows that the thin film obtained from C_2H_2/N_2 gas mixture shows cauli flower structure, and the formation of globule structure was observed in C_2H_4/N_2 and C_2H_6/N_2 films. The diameter of the globule increases in C_2H_6/N_2 film to C_2H_4/N_2 film. This is due to the different growth structures which have been occurred in the film formation for all three gas mixtures. Typical deposition rates are in the range 0.1-0.4 $\mu g/(\text{sec cm}^2)$. Assuming a film density of 2 g/cm^3 this corresponds to about 0.5-2 nm/s.

DLC thin films were deposited on Si (100) and aluminium coated glass substrate using C_2H_m/Ar ($m = 2, 4, 6$) gas mixtures by DBD at atmospheric pressure, with 1:2 gas ratio. FT-IRRAS shows that the films obtained from C_2H_2/Ar gas mixture has high intensity of absorption for several functional group compared to the films obtained from other gas mixtures because of the difference in thickness of the film. The sp^3 bonding is observed to be larger in C_2H_2/Ar film which is one of the criteria that DLC film would have. The types of functional groups observed from all three films were almost same except the intensity of the individual bands. Thin films obtained from C_2H_2/Ar and C_2H_4/Ar gas mixtures exhibited comparatively larger functional groups on the surface of the films when compared to C_2H_6/Ar film. And XPS analysis shows that the typical peak for C1s at binding energy of 285 eV for all the films obtained from C_2H_m/Ar ($m = 2, 4, 6$) gas mixtures. Spectroscopic ellipsometric analysis shows that the thin films obtained from C_2H_4/Ar gas mixture has thickness 300 nm and the refractive index was found to be 3.0, while the film obtained from C_2H_6/Ar gas mixture shows the thickness 100 nm with refractive index 3.2. Typical deposition rates are in the range 0.05-0.3 $\mu g/ (sec\ cm^2)$.

Bibliography

- [1] J. A. Bittencourt, "Fundamentals of plasma physics" third edition.
- [2] Wikipedia: [http://en.wikipedia.org/wiki/Plasma_\(physics\)](http://en.wikipedia.org/wiki/Plasma_(physics))
- [3] Gomez, E., Rani, D.A., Cheeseman, C.R., Deegan, D., Wise, M., Boccaccini, A.R. (2009). "Thermal plasma technology for the treatment of wastes: A critical review". Journal of Hazardous Materials 161 (2–3): 614–626.
- [4] National Research Council (1991). Plasma Processing of Materials: Scientific Opportunities and Technological Challenges. National Academies Press. ISBN 0309045975.
- [5] Nemchinsky, V.A., Severance, W.S. (2006). "What we know and what we do not know about plasma arc cutting". J. Phys. D: Appl. Phys. 39 (22): R423–R438.
- [6] Hippler, R., Kersten, H., Schmidt, M., Schoenbach, K.M., ed. (2008). "Plasma Sources". Low Temperature Plasmas: Fundamentals, Technologies, and Techniques (2 ed.). Wiley-VCH. ISBN 3527406735.
- [7] Peretich, M.A., O'Brien, W.F., Schetz, J.A. (2007). Plasma torch power control for scramjet application. Virginia Space Grant Consortium. Retrieved 12 April 2010.
- [8] R. Castell, E. J. Iglesias, and J. Ruiz-Camacho, Brazilian Journal of Physics, vol. 34, no. 4B, December, 2004
- [9] Dr. David P. Stern. "The Fluorescent Lamp: A plasma you can use.". Retrieved 2010-05-19.

- [10] Sobolewski, M.A.; Langan & Felker, J.G. & B.S. (1997). Electrical optimization of plasma - enhanced chemical vapor deposition chamber cleaning plasmas. 16. J. Vac. Sci. Technol. B. pp. 173-182.
- [11] J. Park et al. (2001). "Discharge phenomena of an atmospheric pressure radio-frequency capacitive plasma source". Journal of Applied Physics 89 (1): 20. Bibcode2001JAP, 89, 20P. doi: 10.1063/1.1323753
- [12] U. Kogelschatz, B. Eliasson and W. Egli; "Dielectric-Barrier Discharges. Principle and Applications" J. Phys. IV France Volume 07, Number C4, October 1997, Pages C4-47- C4-66
- [13] B. Eliasson and U. Kogelschatz "Non equilibrium volume plasma chemical processing" IEEE Transactions Plasma Science. Vol. 19, Issue 6, 1063-1077 (1991)
- [14] J. Amouroux, D. Morvan, S. Cavadias, Ph. Adam, M. F. Gonnord, K. Coulibaly, A. Vincent, S. Morel, F. Daou, S. Ognier, P. Rousseau, and L. Martin, "Pollution Control and Depollution Processes by Plasma Techniques" Technical Physics, Vol. 50, No. 5, 2005, pp. 603–612.
- [15] G. Prieto, Y. Iitsuka, H. Yamauchi, A. Mizuno, O. Prieto, and C. R. Gay, "Urea in Water-in-Oil Emulsions for Ammonia Production" International Journal of Plasma Environmental Science and Technology Vol.3, No.1, MARCH 2009.
- [16] H.C. Thejaswini, Abhijit Majumdar, Tin Maung Tun, and Rainer Hippler, "Plasma chemical reactions in C_2H_2/N_2 , C_2H_4/N_2 , and C_2H_6/N_2 gas mixtures of a laboratory dielectric barrier discharge" Advances in Space Research, 48 (2011) 857- 861
- [17] Ghasi Ram Dey, Tomi Nath Das, "Gas-phase and On-surface Chemical Reduction of CO_2 to HCHO and CO under Dielectric Barrier Discharge" Plasma Chem Plasma Process (2006) 26:495–505

- [18] J. Vrajova, L. Chalupova, J. Cech, F. Krcma, and P. Stahel, “Paper sterilization by atmospheric pressure DBD discharge” *Chem. Listy* 102, s1445–s1449 (2008)
- [19] Hiroyuki Eto, Yoshihito Ono, Akihisa Ogino, and Masaaki Nagatsu, “Sterilization of Tubular Medical Instruments Using Wire-type Dielectric Barrier Discharge” *J. Plasma Fusion Res. SERIES*, Vol. 8 (2009)
- [20] Hiroyuki Eto, Yoshihito Ono, Akihisa Ogino, and Masaaki Nagatsu, “Low-Temperature Internal Sterilization of Medical Plastic Tubes Using a Linear Dielectric Barrier Discharge
- [21] Hilmar Esrom, Robert Seebock, Marlene Charbonnier, and Maurice Romand, “Surface activation of polyimide with dielectric barrier discharge for electroless metal deposition” *Surface and Coatings Technology* 125 (2000) 19–24
- [22] I. Radu, M. Reiche, M. Zoberbier, M. Gabriel, and U. Gosele, “Low-temperature wafer bonding via DBD surface activation” *Electrochemical Society Proceedings* Volume 2005-06
- [23] Ulrike Martens, H. C. Thejaswini, Abhijit Majumdar, and Rainer Hippler, “Deposition of Amorphous Hydrogenated Carbon Nitride Films with a Dielectric Barrier Discharge” *Plasma Processes and Polymers*, 2012, DOI: 10.1002/ppap.201100185
- [24] Abhijit Majumdar, Jan Schäfer, Puneet Mishra, Debabrata Ghose, Jürgen Meichsner, and, Rainer Hippler, “Chemical composition and bond structure of carbon-nitride films deposited by CH₄/N₂ dielectric barrier discharge” *Surface & Coatings Technology* 201 (2007) 6437–6444
- [25] Mounir Laroussi, “Nonthermal decontamination of biological media by atmospheric pressure plasmas: review, analysis, and prospects” *IEEE Transactions on plasma science*, Vol. 30, 2002, 1409-1415

- [26] Wikipedia [http://en.wikipedia.org/wiki/Titan_\(moon\)](http://en.wikipedia.org/wiki/Titan_(moon))
- [27] Wikipedia <http://en.wikipedia.org/wiki/Cassini%E2%80%93Huygens>
- [28] Sagan, C., Khare, B.N. Tholins: organic chemistry of interstellar grains and gas. *Nature* 277, 102, 1979
- [29] Cui, J., Yelle, R.V., Vuittonb, V., Waite Jr., J.H., Kasprzakd, W.T., Gell, D.A., Niemannd, H.B., Muller-Wodarg, I.C.F., Borggren, N., Fletcher, G.G., Patrick, E.L., Raaen, E., Magee, B.A. Analysis of Titans neutral upper atmosphere from cassini ion neutral mass spectrometer measurements. *Icarus* 200, 581615, 2009
- [30] Bishun. N. Khare, and Carl Sagan, Amino acids derived from titan tholins, *Icarus*, 68, 176-184, 1986
- [31] Ralph Delmdahl and Steffen Weissmantel Guenter Reisse, Diamond Like Carbon films, *Advanced materials and processes*, April 2010, 23-25
- [32] Ali Erdemir and Christophe Donnet, Tribology of diamond-like carbon films: recent progress and future prospects, *J. Phys. D: Appl. Phys.* 39 (2006) R311–R327
- [33] A. Y. Liu, M. L. Cohen: *Science*: 245, 841 (1989)
- [34] A. Y. Liu, M. L. Cohen, *Phys. Rev. B* 41(15) (1990) 10727
- [35] M. L. Cohen, *Phys. Rev. B* 32, 7988 (1985)
- [36] Yafei Zhang, Zhonghua Zhou, Hulin Li, *Appl. Phys. Lett.* 68, 634, (1996)
- [37] Sanjay Mathur, Jessica Altmayer and Hao Shen, *Z. Anorg. Chem.* 2004, 630, 2042 – 2048

- [38] Yibin Li, Sam Zhang, Y. Liu, T. P. Chen, Thirumany Sritharan and Cong Xu,
Journal of Nanoscience and Nanotechnology Vol. 9, 1-5, 2009
- [39] Yi Wang, E. Y. Jiang, H. L. Bai, and P. Wu, Journal of Vacuum Science and
Technology A, 17, 3308 (1999)
- [40] W. Dawei, F. Dejun, G. Huaixi, Z. Zhilong, M. Xianquan, and F. Xiangjun, Phys.
Rev. B 56, 4949 (1997).
- [41] M. Ricci, M. Trinquedecoste, F. Auguste, R. Canet, P. Delhaes, C. Guimon, G.
Pfister-Guillouzo, B. Nysten, and J. P. Issi, J. Mater. Res. 8, 480 (1993).
- [42] P. Merel, M. Chaker, M. Tabbal, M. Moisan, Appl. Phys. Lett. 71 (1997) 3814.
- [43] Y. Aoi, K. Ono, E. Kamijo, J. Appl. Phys. 86 (1999) 2318.
- [44] J. T. Dawley, P. G. Clem, M. P. Siegal and D. L. Overmyer, J. Mater. Res., Vol 16,
(2001) 13
- [45] Liu Huwei and Fu Ruonong, Journal of Analytical and Applied Pyrolysis, 14 (1988)
163 - 169
- [46] Vishnu S, Nadkarni and Shriniwas D, Samant, Radiation Measurements, Vol. 27,
No. 3, pp. 505 - 510 (1997)
- [47] Ramon Gomez Aguilar, Jaime Ortiz Lopez, Lat. Am. J. Phys. Educ. Vol. 5, No. 2
(2011)
- [48] C. W. Ong, X. -A. Zhao, Y. C. Tsang, C. L. Choy, P. W. Chan, Thin Solid Films 280
(1996) 1
- [49] Y. H. Cheng, X. L. Qiao, J. G. Chen, Y. P. Wu, C. S. Xie, Y. Q. Wang, et al.,

Diamond Relat. Mater. 11(2002) 1511

[50] Hand book of Organic spectroscopy by William Kemp, Third edition

[51] <http://www.scienceaid.co.uk/chemistry/fundamental/particles.html>

[52] Dr. Alison E. Ashcroft, "An introduction to mass spectrometry"

<http://www.astbury.leeds.ac.uk/facil/MStut/mstutorial.htm>

[53] http://en.wikipedia.org/wiki/Quadrupole_mass_analyzer

[54] Mass spectrometry resource, University of Bristol, School of Chemistry

[55] FTIR Spectroscopy by Jorge. E. Perez and Richard T. Meyer,

http://www.irgas.com/ftir_spectroscopy.html

[56] Online edition for students of organic chemistry lab courses at the University of Colorado, Boulder, Dept of Chem and Biochem. (2002)

[57] Inna Kurganskaya, Andreas Luttge, Andrew R. Barron, "The application of VSI (Vertical Scanning Interferometry) to the study of crystal surface processes", Chemistry of electronic materials.

[58] <http://www.newport.com/Introduction-to-FT-IR-Spectroscopy/405840/1033/content>

[59] Wikipedia:

en.wikipedia.org/wiki/Fourier_transform_infrared_spectroscopy#Applications

[60] John F. Moulder, William F. Stickle, Peter E. Sobol and Kenneth D. Bomben, "Handbook of X-ray Photoelectron Spectroscopy.

- [61] <http://www.chem.queensu.ca/people/faculty/horton/images/figure2.png>
- [62] wikipedia.org/wiki/X-ray_photoelectron_spectroscopy
- [63] K. Vedam, "Spectroscopic ellipsometry: a historical overview", *Thin Solid films*, 313-314 (1998) 1-9
- [64] Christian Bernhard and Todd Holden,
"www.academic.brooklyn.cuny.edu/physics/holden/ellipsometry.htm"
- [65] Aspnes D.E. (1985). The Accurate Determination of Optical Properties by Ellipsometry. In: Palik E.D. (ed.) *Handbook of Optical Constants of Solids*, pp. 89-112. Academic Press, Orlando.
- [66] Reimer, L. (1998) *Scanning electron microscopy: physics of image formation and microanalysis*. Springer, 527 p.
- [67] Goldstein, J. (2003) *Scanning electron microscopy and x-ray microanalysis*. Kluwer Academic/ Plenum Publishers, 689 p.
- [68] Susan Swapp, "Geochemical Instrumentation and analysis: Scanning Electron Microscopy" University of Wyoming.
- [69] http://www.wikipedia.org/wiki/Scanning_electron_microscope
- [70] Wagner, H.-E., Brandenburg, R., Kozlov, K.V., Sonnenfeld, A., Michel, P., Behnke, J.F. *Vacuum* 71, 417, 2003
- [71] Boufendi, L., Bouchoule, A. Particle nucleation and growth in a low pressure argon-silane discharge. *Plasma Sources Sci. Technol.* 3, 262, 1994
- [72] Boufendi, L., Hermann, J., Bouchoule, A., Dubreuil, B., Stoffels, E., Stoffels, W.W.,

de Giorgi, M.L. Study of initial dust formation in an Ar-SiH₄ discharge by laser induced particle explosive evaporation. J. Appl. Phys. 76, 148, 1994

- [73] Wong, A.-S., Yung, Y.L., Friedson, A.J. Geophys. Res. Lett. 30, 1447, 2003
- [74] Kunde, V.G., Aikin, A.C., Hanel, R.A., Jennings, D.E., Maguire, W.C., Samuelson, R.E. C₄H₂, HC₃N and C₂N₂ in Titans atmosphere. Nature 292, 686, 1981
- [75] Winter, J., Berndt, J., Hong, S.-H., Kovacevic, E., Stefanovic, I, Stepanovic, O. Dust formation in Ar/CH₄ and Ar/C₂H₂ plasmas. Plasma Sources Sci. Technol. 18, 034010, 2009
- [76] Do, H.T., Thieme, G., Frohlich, M., Kersten, H., Hippler, R. Ion molecule and dust particle formation in Ar/CH₄, Ar/C₂H₂ and Ar/C₃H₆ radio-frequency plasmas. Contrib. Plasma Phys. 45, 378, 2005
- [77] Do, H.T., Sushkov, V., Hippler, R. Tunable diode laser absorption spectroscopy of argon metastable atoms in Ar/C₂H₂ dusty plasmas. New. J. Phys. 11, 033020, 2009
- [78] Mao, M., Benedikt, J., Consoli, A., Bogaerts, A. J. Phys. D: Appl. Phys. 41, 225201, 2008
- [79] Norinaga, K., Deutschmann, O. Detailed kinetic modeling of gas-phase reactions in the chemical vapour deposition of carbon from light hydrocarbons. Ind. Eng. Chem. Res. 46, 3547, 2007
- [80] Majumdar, A., Kumar Singh, R., Palm, G.J., Hippler, R. J. Appl. Phys. 106, 084701, 2009
- [81] Sarra-Bournet, C., Gherardi, N., Gle'nat, H., Laroche, G., Massines, F. Effect of C₂H₄/N₂ ratio in an atmospheric pressure dielectric barrier discharge on the plasma

deposition of hydrogenated amorphous carbon-nitride films (a-C:N:H). Plasma Chem. Plasma Process 30, 213, 2010

- [82] Raulin, F., B, Accaoui., A, Razaghi., M, Dang-Nhu., A, Coustenis and D, Gautier., Infrared spectra of gaseous organics: Applications to atmosphere of Titan II. Infrared intensities and frequencies of C₄ alkanenitriles and benzene. Spectrochimica Acta, Vol. 46A, No. 5, pp. 671-683, 1990
- [83] Ch. Hollenstein., Plasmas and Polymers, Vol. 3, No. 4, 1998
- [84] Rosa Di Mundo, Fabio Palumbo, Francesco Fracassi, Riccardo d' Agostino., Plasma Process and Polymers 2009, 6, 506-511
- [85] Majumdar, A, Behnke J F, Hippler R, Matyash K, Schneider R, J. Phys. Chem (2005)
- [86] Linstorm and W. G. Mallard., NIST FTIR Spec Data Center, S. E. Stein, director, Mass Spectra and IR spectra (COBLENTZ SOCIETY) in Nist Chemistry WebBook, NIST Standard Reference database Number 69, Eds. P. J., National Institute of Standards and Technology, Gaithersburg MD, 20899, <http://webbook.nist.gov> (retrieved July 30, 2009)
- [87] Patrice Raynaud, Bernard Despax, Yvan Segui and Hubert Caquineau., Plasma Process and Polymers 2005, 2, 45-52
- [88] Gerard Deleris and Cyril Petibois., Vibrational Spectroscopy 2003, 32, 129-136
- [89] A handbook of organic chemistry by William Kemp, Third edition
- [90] Linstorm and W. G. Mallard., NIST Mass Spec Data Center, S. E. Stein, director, Mass Spectra and IR spectra (COBLENTZ SOCIETY) in Nist Chemistry WebBook, NIST Standard Reference database Number 69, Eds. P. J., National Institute of

Standards and Technology, Gaithersburg MD, 20899, <http://webbook.nist.gov>
(retrieved July 30, 2009)

- [91] Deschenaux Ch, A Affolter, D Magni, Ch Hollenstein and P Fayet
J. Phys. D: Appl. Phys. 32 (1999) 1876-1886
- [92] Wilson, E, H. Atreya and S, K., Journal of Geophysical Research, Vol. 108, 2003,
NO. E2, 801-810
- [93] Stein, S. E. NIST mass spec data center, in: Linstrom, P.J., Mallard, W.G. (Eds.),
Mass Spectra in NIST Chemistry WebBook, NIST Standard Reference Database
Number 69, National Institute of Standards and Technology, Gaithersburg MD,
20899. Available from: <http://webbook.nist.gov> (retrieved 15.07.2010)
- [94] Colthup N B, Daly L H and Wiberley S E 1990 Introduction to Infrared and Raman
Spectroscopy (Boston: Academic)
- [95] Riccardi, C, Barni R, Fontanesi M, Tosi P, Czech. J. Phys. 50/S3, 389 (2000)
- [96] Aumaille, K, Vallee C, Granier A, Goullet A, Gaboriau F and Turban G 2000 Thin
solids Films 359 188(2000)
- [97] Basner R, Foest R, Schmit M, Hempel F, Becker K, Proc. XXIII ICPIG (Toulouse,
France, July 17-22, 1997), Vol IV, p. 196 (1997); Basner R, Foest R, Schmit M,
Hempel F, Becker K, Gaseous Dielectric, Vol VIII, Christophotou L G, James D R,
Eds., New York: Plenum, p. 161(1998)
- [98] Lafleur, A, L., J. J. Gagel, J. P. Longwell, and P. A. Monchamp, Mikrochim. Acta
(Wien) I, 35-38 (1988)
- [99] A. Majumdar, Karsten Schroder and Rainer Hippler, Journal of applied physics, 104,
074702, (2008)

- [100] Jinmo Kim, Donggeun Jung, Yongsup Park, Yongki Kim, Dae Won Moon, Tae Geol Lee, *Applied Surface Science* 253 (2007) 4112 – 4118
- [101] S. B. Munteanu, C. Vasile, *Journal of Optoelectronics and Advanced Materials* Vol. 7, No. 6, December 2005, p. 3135 - 3148
- [102] G. E. Jellison and F. A. Modine, “Parameterization of the optical functions of amorphous materials in the interband region,” *Applied Physics Letters*, vol. 69, no. 3, pp. 371-373, Jul. 1996
- [103] K. Rages and J. B. Pollack, “Titan aerosols: Optical properties and vertical distribution,” *Icarus*, vol. 41, no. 1, pp. 119-130, Jan. 1980
- [104] B. N. Khare et al., “Production and Optical Constants of Ice Tholin from Charged Particle Irradiation of (1:6) C₂H₆/H₂O at 77 K,” *Icarus*, vol. 103, no. 2, pp. 290-300, Jun. 1993
- [105] B. N. Khare, C. Sagan, E. T. Arakawa, F. Suits, T. A. Callcott, and M. W. Williams, “Optical constants of organic tholins produced in a simulated Titanian atmosphere: From soft x-ray to microwave frequencies,” *Icarus*, vol. 60, no. 1, pp. 127-137, Oct. 1984
- [106] P. Coll et al., “Experimental laboratory simulation of Titan’s atmosphere: aerosols and gas phase,” *Planetary and Space Science*, vol. 47, no. 10-11, pp. 1331-1340, October
- [107] M. Christopher P., “Elemental composition, solubility, and optical properties of Titan’s organic haze,” *Planetary and Space Science*, vol. 44, no. 8, pp. 741-747, Aug. 1996
- [108] S. I. Ramirez, P. Coll, A. da Silva, R. Navarro-González, J. Lafait, and F. Raulin, “Complex Refractive Index of Titan’s Aerosol Analogues in the 200–900 nm

- Domain,” *Icarus*, vol. 156, no. 2, pp. 515-529, Apr. 2002
- [109] D. Bruggeman, “The calculation of various physical constants of heterogeneous substances. I. The dielectric constants and conductivities of mixtures composed of isotropic substances,” *Annalen der Physik*, vol. 24, no. 7, pp. 636-64, 1935
- [110] Christian Sarra-Bournet, Nicolas Gherardi, Herve’ Gle’nat, Gae’tan Laroche, Francoise Massines, *Plasma Process and Polymers* 2010, 30, 213 - 239
- [111] B. N. Khare, C. Sagan, W. R. Thompson, E. T. Arakawa, C. Meisse, and P. S. Tuminello, “Optical properties of poly-HCN and their astronomical applications,” *Canadian Journal of Chemistry*, vol. 72, pp. 678-694, Mar. 1994
- [112] J. Ristein, R. T. Stief, L. Ley and W. Beyer, “A comparative analysis of a-C:H by infrared spectroscopy and mass selected thermal effusion”, *J. Appl. Phys.*, Vol. 84, No. 7, October 1998
- [113] R. J. Lade, D. J. Munns, S. E. Johnson, P. W. May, K. N. Rosser, M. N. R. Ashfold, “Investigation of hydrogenated amorphous carbon (a-C:H) films produced by ArF (193 nm) laser ablation of poly (methyl methacrylate)”, *Diamond and related materials*, 7 (1998) 699-703
- [114] Young-Ho Son, Woo-Chul Jung and Jae-In Jeong, “FTIR Characteristics of hydrogenated amorphous carbon films prepared by ECR-PECVD”, *Journal of the Korean Physical Society*, Vol. 39, No. 4, October 2001, pp. 713-717
- [115] A. C. Ferrari, S. E. Rodil and J. Robertson, “Interpretation of infrared and Raman spectra of amorphous carbon nitrides”, *Physical Review B* 67, 155306 (2003)
- [116] A. Indarto, N. Coowanitwong, J.-W. Choi, H. Lee, H.K. Song, *Fuel Proc. Technol.* 89, 214-219 (2008)

- [117] J.O.P. Pedersen, B.J. Opansky, S.R. Leone, J. Phys. Chem. 97, 6822-6829 (1993)
- [118] T. Kovács, M.A. Blitz, P.W. Seakins, J. Phys. Chem. A 114, 4735-4741 (2010)
- [119] J. Filik, P.W. May, S.R.J. Pearce, R.K. Wild, K.R. Hallam, Diamond and Related Materials 12 (2003) 974-978
- [120] R.M. Dey, M. Pandey, D. Bhattacharyya, D.S. Patil, and S. K. Kulkarni, Bull. Mater. Sci., Vol. 30, No.6, December 2007, pp. 541-546
- [121] Liuhe Li, Haiquan Zhang, Yanhua Zhang, Paul K. Chu, Xiubo Tian, Lifang Xia, Xinxin Ma, Materials Science and Engineering B94 (2002) 95 /101
- [122] Catherine D. Neish, Arpad Somogyi, and Mark A. Smith, Astrobiology, Volume 10, Number 3, 2010 © Mary Ann Liebert, Inc. DOI: 10.1089=ast.2009.0402
- [123] Cabane M. and Chassefiere E. (1995), Planet. Space Sci. 43:47-65
- [124] Somogyi A, Oh C Smith, M.A. and Lunine, J.I, (2005) J. Am. Soc. Mass Spectrom, 16:850-859
- [125] Morgan L. Cable, Sarah M. Hörst, Robert Hodyss, Patricia M. Beauchamp, Mark A. Smith, and Peter A. Willis, dx.doi.org/10.1021/cr200221x/ Chem. Rev. 2012, 112, 1882-1909
- [126] Thomas Gautier, Nathalie Carrasco, Arnaud Buch, Cyril Szopa, Ella Sciamma-O'Brien, Guy Cernogora, Icarus, Volume 213, Issue 2, June 2011, Pages 625-635
- [127] Hiroshi Imanaka and Mark A. Smith, PNAS, July 13, 2010, vol. 107, no. 28, 12423 - 12428
- [128] M Mao, A Bogaerts, Journal of Physics D: Applied Physics 43, 20 (2010) 205201

- [129] Hiroshi Imanaka, B. N. Khare, Jamie E. Elsila, Emma L. O. Bakes, Christopher P. McKay, Dale P. Cruikshank, Seiji Sugita, Takafumi Matsui and Richard N. Zare, *Icarus* 168 (2004) 344 – 366
- [130] I C F Mueller-Wodarg, D.F. Strobel, J. I. Moses, J. H. Waite, J. Crovisier, R. V. Yelle, S. W. Bougher, R. G. Roble, *Space Sci Rev* (2008) 139, 191 – 234
- [131] J. Hunter Waite, Jr., et al., *Science* 308, 982 (2005)
- [132] Arthur G. Suits, *J. Phys. Chem. A*, Vol. 113, No. 42, 2009
- [133] J. C. Legrand, A. M. Diamy, R. Hrach, V. Hrachova, *Vacuum* 50, 491-5 (1998)
- [134] J. C. Legrand, A. M. Diamy, R. Hrach, V. Hrachova, *Vacuum* 52, 27- 32 (1999)
- [135] M. Khelifi, P. Paillous, C. Delpech, M. Nishio, P. Bruston, F. Raulin, *J. Mol. Spectrosc.* 174, 116 (1995)
- [136] H. Imanaka, M.A. Smith, *PNAS* 107, 12423 (2010)
- [137] H. Kiyooka, O. Matsumoto, Reaction scheme of ammonia synthesis in ECR Plasmas, *Plasma chemistry and Plasma Processing* 16, 547 (1996)
- [138] M. Touvelle, J. L. Munoz Licea, M. Venugopalan, *Plasma Chemistry and Plasma Processing* 7, 101 (1987)
- [139] H. Uyama, O. Matsumoto, *Plasma Chemistry and Plasma Processing* 9, 13 (1989)
- [140] J.-P.H. van Helden, *The Generation of Molecules through Plasma Surface Interactions*, Proefschrift, Technische Universiteit Eindhoven (2006)

List of figures

1.1 Simple circuit showing plasma generation ^[2] and Plasma generated under barrier discharge ^[8]	2
1.2 Flow chart shows the classification of discharge.....	4
1.3 Schematic of the different configurations of DBD ^[12]	6
2.1 Schematic of the typical mass spectrometer ^[51]	11
2.2 Schematic of the quadrupole mass filter ^[54]	13
2.3 Stretching and bending vibrational modes for H ₂ O ^[56]	15
2.4 Stretching and bending vibrational modes for CO ₂ ^[56]	15
2.5 Schematic representation of the Michelson interferometry set-up ^[57]	16
2.6 Schematic diagram of X-ray Photoelectron Spectroscopy ^[61]	18
2.7 A typical experimental setup of an ellipsometry ^[64]	20
2.8 Schematic diagram of the SEM experimental set-up ^[69]	23
3.1 Schematic of the DBD experimental setup.....	26
3.2 Three dimensional picture of the electrodes.....	28
4.1 Mass spectra obtained from a C ₂ H ₄ /N ₂ gas mixture without plasma (a) and	

after 360 min with the plasma on (b).....	29
4.2 Difference mass spectrum with and without plasma in the mass range m/z=35-180 for a C ₂ H ₂ /N ₂ gas mixture.....	31
4.3 Difference mass spectrum with and without plasma in the mass range m/z=35-180 for a C ₂ H ₄ /N ₂ gas mixture.....	32
4.4 Difference mass spectrum with and without plasma in the mass range m/z = 35-180 for a C ₂ H ₆ /N ₂ gas mixture.....	33
4.5 Comparison of C ₂ H ₂ /N ₂ and C ₂ H ₄ /N ₂ mass spectra with plasma in the mass range m/z up to 35-180.....	35
4.6 Comparison of C ₂ H ₄ /N ₂ and C ₂ H ₆ /N ₂ mass spectra with plasma in the mass range m/z up to 180.....	35
4.7 Time dependent production and consumption of C ₂ H _m /N ₂ (m = 2, 4, 6) gas mixtures..	36
5.1 FTIR spectrum of CH ₄ /N ₂ gas mixture, with gas ratio 1:2, 300 mbar pressure (a) with and without plasma (b) Difference spectra obtained after the subtraction with 180 mins plasma and without plasma.....	38
5.2 FTIR spectrum of C ₂ H ₂ /N ₂ gas mixture, with gas ratio 1:2, 300 mbar pressure (a) without plasma (b) Difference spectra obtained after the subtraction with 180 mins plasma and without plasma.....	40
5.3 FTIR spectrum of C ₂ H ₄ /N ₂ gas mixture, with gas ratio 1:2, 300 mbar pressure (a) without plasma (b) Difference spectra obtained after the subtraction with 180 mins plasma and without plasma.....	41
5.4 FTIR spectrum of C ₂ H ₆ /N ₂ gas mixture, with gas ratio 1:2, 300 mbar pressure	

(a) without plasma (b) Difference spectra obtained after the subtraction with 180 mins plasma and without plasma.....	42
5.5 Reaction pathways among the hydrocarbons and HCN.....	46
6.1 Mass spectra obtained from C ₂ H ₄ /Ar gas mixture (a) without plasma and (b) after 420min with plasma on.....	49
6.2 FTIR spectrum of C ₂ H ₄ /Ar without plasma & with 180 mins plasma on under the 300 mbar pressure and ratio is 1:2.....	50
6.3 FTIR spectrum of CH ₄ /Ar gas mixture, with gas ratio 1:2, 300 mbar pressure (a) without plasma (b) Difference spectra obtained after the subtraction of with 180 mins plasma and without plasma.....	51
6.4 Difference mass spectrum with and without plasma in the mass range m/z up to 35 and 45-145 for a C ₂ H ₂ /Ar gas mixture. Note the different (linear and logarithmic) scales.....	53
6.5 FTIR spectrum of C ₂ H ₂ /Ar gas mixture, with gas ratio 1:2, 300 mbar pressure (a) without plasma (b) Difference spectra obtained after the subtraction of with 180 mins plasma and without plasma.....	54
6.6 Difference mass spectrum with and without plasma in the range m/z up to 35 and 35-170 for a C ₂ H ₄ /Ar gas mixture. Note the different (linear and logarithmic scales).....	55
6.7 FTIR spectrum of C ₂ H ₄ /Ar gas mixture, with gas ratio 1:2, 300 mbar pressure (a) without plasma (b) Difference spectra obtained after the subtraction of with 180 mins plasma and without plasma.....	56
6.8 Difference mass spectrum with and without plasma in the mass range m/z	

up to 35 and 35-180 for a C_2H_6/Ar gas mixture.....	57
6.9 FTIR spectrum of C_2H_6/Ar gas mixture, with gas ratio 1:2, 300 mbar pressure (a) without plasma (b) Difference spectra obtained after the subtraction of with 180 mins plasma and without plasma.....	58
6.10 Reaction pathways among hydrocarbons.....	59
6.11 Simulation results for the temporal evolution of hydrocarbons.....	60
6.12 Time dependent studies of H_2 , C_2H_m (where, $m= 2, 4, 6$) and higher order hydrocarbons in C_2H_2/ Ar , C_2H_4/ Ar and C_2H_6/ Ar plasma.....	64
6.13 Schematic showing the Titan hydrocarbon chemistry (Ref: “Saturn” by Arizona Press).....	65
6.14 Comparison between difference mass spectrum of C_2H_2 and C_2H_4 plasma in the mass range m/z up to 35 & 35-180.....	67
6.15 Comparison between difference mass spectrum of C_2H_4 and C_2H_6 plasma in the mass range m/z up to 35 & 35-180.....	68
6.16 Comparison of difference FTIR spectrum of C_2H_4/C_2H_6 plasma and C_2H_2/C_2H_4 plasma.....	68
7.1 FTIR spectra of CN_x films obtained from C_2H_2/N_2 gas mixture, under 300 mbar pressure with gas ratio 1:2.....	71
7.2 FTIR spectra of CN_x films obtained from C_2H_4/N_2 gas mixture, under 300 mbar pressure with gas ratio 1:2.....	72
7.3 FTIR spectra of CN_x films obtained from C_2H_6/N_2 gas mixture, under 300 mbar	

pressure with gas ratio 1:2.....	73
7.4 Typical XPS overview spectrum for CN_x film obtained from $\text{C}_2\text{H}_m/\text{N}_2$ ($m = 2, 4, 6$) gas mixtures, under 300 mbar pressure with gas ratio 1:2.....	75
7.5 XPS spectrum for C1s and N1s for CN_x film obtained from gas mixture $\text{C}_2\text{H}_2/\text{N}_2$, under 300 mbar pressure, with gas ratio 1:2.....	77
7.6 XPS spectrum for C1s and N1s for CN_x film obtained from gas mixture $\text{C}_2\text{H}_4/\text{N}_2$, under 300 mbar pressure, with gas ratio 1:2.....	77
7.7 XPS spectrum for C1s and N1s for CN_x film obtained from gas mixture $\text{C}_2\text{H}_6/\text{N}_2$, under 300 mbar pressure with gas ratio 1:2.....	78
7.8 Ellipsometric analysis of CN_x film obtained from two different gas mixtures $\text{C}_2\text{H}_6/\text{N}_2$ (black line) and $\text{C}_2\text{H}_4/\text{N}_2$ (red line), under 300 mbar pressure with gas ratio 1:2.....	81
7.9 SEM of $\text{C}_2\text{H}_m/\text{N}_2$ film deposited on Si(100) at 300 mbar pressure, gas ratio 1:2.....	82
7.10 a- CN_x :H film deposited using gas mixtures $\text{C}_2\text{H}_m/\text{N}_2$ ($m = 2, 4, 6$) on glass substrate under 300 mbar pressure with gas ratio 1:2.....	83
8.1 FTIR spectra of DLC films obtained from $\text{C}_2\text{H}_2/\text{Ar}$ gas mixture, under 300 mbar pressure with gas ratio 1:2.....	87
8.2 FTIR spectra of DLC films obtained from $\text{C}_2\text{H}_4/\text{Ar}$ gas mixture, under 300 mbar pressure with gas ratio 1:2.....	88
8.3 FTIR spectra of DLC films obtained from $\text{C}_2\text{H}_6/\text{Ar}$ gas mixture, under 300 mbar pressure with gas ratio 1:2.....	89

8.4 Typical XPS overview spectrum for DLC film obtained from C_2H_m/Ar ($m = 2, 4, 6$) gas mixtures, under 300 mbar pressure with gas ratio 1:2.....	91
8.5 XPS spectrum for C1s for DLC film obtained from gas mixture C_2H_m/Ar ($m = 2, 4, 6$), under 300 mbar pressure with gas ratio 1:2.....	92
8.6 Ellipsometric analysis of DLC film obtained from two different gas mixtures C_2H_6/Ar (black line) and C_2H_4/Ar (dotted line), under 300 mbar pressure with gas ratio 1:2.....	94
8.7 a-C:H film deposited using gas mixtures C_2H_m/Ar ($m = 2, 4, 6$) on glass substrate under 300 mbar pressure with gas ratio 1:2.....	96

List of Tables

1.1 Typical conditions for barrier discharges are given below. ^[13]	6
5.1 Percentage production and percentage consumption of gases for CH ₄ /N ₂ and C ₂ H _m /N ₂ (m = 2, 4, 6) plasma.....	46
5.2 Major plasma content assignments for plasma FTIR spectra absorption bands.....	47
6.1 Percentage gas production and consumption for CH ₄ /Ar and C ₂ H _m /Ar (m = 2, 4, 6) gas mixtures during 180 min of DBD plasma.....	63
7.1 Major assignments for FTIR absorption spectra for CN _x films obtained from C ₂ H _m /N ₂ (m = 2, 4, 6) gas mixtures.....	74
7.2 Deposition rate for C ₂ H _m /N ₂ (m = 2, 4, 6) gas mixtures.....	84
8.1 Major assignments for FTIR absorption spectra for DLC films obtained from C ₂ H ₆ /Ar (m = 2, 4, 6) gas mixtures.....	90
8.2 Deposition rate for C ₂ H _m /Ar (m = 2, 4, 6) gas mixtures.....	96

Abbreviation

APBD:	Atmospheric Pressure Barrier Discharge
DBD:	Dielectric Barrier Discharge
CCP:	Capacitively Coupled Plasma
ICP:	Inductively Coupled Plasma
RF:	Radio Frequency
VD:	Volume Discharge
SD:	Surface Discharge
ESA:	European Space Agency
NASA:	National Aeronautics and Space Administration
UV:	Ultra-Violet
MS:	Mass Spectrometry
QMS:	Quadrupole Mass Spectrometer
CVD:	Chemical Vapor Deposition
PVD:	Physical Vapor Deposition
PLD:	Pulsed Laser Deposition
PECVD:	Plasma Enhanced Chemical Vapor Deposition
FTIR:	Fourier Transform Infrared Spectroscopy
FTIRRAS:	Fourier Transform InfraRed Reflection Absorption Spectroscopy
XPS:	X-ray Photo electron Spectroscopy
SE:	Spectroscopic Ellipsometry
SEM:	Scanning (Secondary) Electron Microscopy
CCD:	Charge Couple Device
BE:	Binding Energy
CN:	Carbon Nitride
DLC:	Diamond Like Carbon
NIST:	National Institute of Standards and Technology

Declaration

Here by I declare that this work has so far neither been submitted to the Faculty of Mathematics and Natural Sciences at the Ernst-Moritz-Arndt-University of Greifswald nor to another scientific institution for the purpose of the degree of doctorate.

Furthermore I declare that I have written this work by myself and that I have not used any other resources, other than mentioned earlier in this work.

Hiermit erkläre ich, dass diese Arbeit bisher von mir weder an der Mathematisch Naturwissenschaftlichen Fakultät der Ernst-Moritz-Arndt-Universität Greifswald noch einer anderen wissenschaftlichen Einrichtung zum Zwecke der Promotion eingereicht wurde.

Ferner erkläre ich, dass ich diese Arbeit selbständig verfasst und keine anderen als die darin angegebenen Hilfsmittel und und Hilfen benutzt und keine Textabschnitte eines Dritten ohne Kennzeichnung übernommen habe.

Greifswald

Date 30. Jul. 2012

Signature

List of Publications

1. C N Tharamani, **H C Thejaswini**, and S Sampath., Synthesis of size-controlled Bi particles by electrochemical deposition. Bull. Mater. Sci., Vol. 31, No. 3, June 2008, pp. 207 – 212
2. G K Ramesha, **H C Thejaswini**, Jyothsna Rikie and S Sampath., Direct Electrochemistry of Cytochrome-C, Hemoglobin and Myoglobin using Layer- By- Layer assembly of Nanostructures. Manuscript prepared.
3. **H C Thejaswini**, A Majumdar, Tin M Tun and Rainer Hippler, Plasma chemical reactions in C_2H_6/N_2 , C_2H_4/N_2 and C_2H_2/N_2 gas mixtures of a laboratory Dielectric Barrier Discharge. Advances in Space Research, Vol. 48 (2011) pp 857-861.
4. U. Martens, **H C Thejaswini**, A Majumdar and Rainer Hippler, Deposition of Amorphous Carbon Nitride films with a Dielectric Barrier Discharge. Plasma Process and Polymers, 5 MAR 2012, pp 1-5.
5. **H C Thejaswini**, R. Bogdanowicz, V. Danilov, J. Schäfer, J. Meichsner and Rainer Hippler, Deposition and characterization of Organic thin films prepared under Atmospheric Pressure Dielectric Barrier Discharge. Manuscript prepared. Submitted to Plasma Process and Polymers
6. **H C Thejaswini**, U. Martens and Rainer Hippler., Comparative plasma chemical reaction studies of C_2H_2/Ar , C_2H_4/Ar and C_2H_6/Ar gas mixtures in an atmospheric pressure Dielectric Barrier Discharge. Ready to submit
7. **H C Thejaswini** and Rainer Hippler., FTIR plasma phase analysis of C_2H_m/N_2 (where, $m = 2, 4, 6$), CH_4/N_2 and CH_4/Ar gas mixtures in a Dielectric Barrier Discharge. Ready to submit
8. **H C Thejaswini** and Rainer Hippler., Deposition of Diamond like carbon films by Atmospheric Pressure Dielectric Barrier Discharge. Ready to submit

Presentations and Conference Proceedings

1. "Plasma Chemical Reactions of hydrocarbons in a Dielectric Barrier Discharge"
Talk given in IMPRS Program. In October, 2009
2. "Plasma Chemical Reactions of C_2H_m/N_2 and C_2H_m/Ar (Where, $m= 2, 4, 6$) gas mixtures in a Dielectric Barrier Discharge" Talk given in IMPRS Program. In October, 2010
3. "Comparitive plasma chemical reactions of C_2H_m/N_2 and C_2H_m/Ar (Where, $m= 2, 4, 6$) gas mixtures in a Dielectric Barrier Discharge" Talk given in HEPP Program. In December, 2011
4. G K Ramesha, **H C Thejaswini**, Jyothsna Rikie and S Sampath., "Direct Electrochemistry of Cytochrome- C, Hemoglobin and Myoglobin using Layer- By- Layer assembly of Nanostructures" In: Proceedings 10th CRSI National Symposium in Chemistry, 1-3 February 2008 held at Indian Institute of Science, Bangalore, INDIA
5. Ye Zhu, **H C Thejaswini** and Yoon-Bo Shim., "A multi-label strategy based on carbon nanotube amplification for immunodetection" In: Proceedings of 3rd BK-21, International Symposium and workshop on materials Chemistry, 19 and 20th of Oct 2008 held at Haeundae Grand Hotel, Busan.
6. **H C Thejaswini**, A Majumdar, Tin M Tun and Rainer Hippler., Plasma chemical reactions of hydrocarbons in an atmospheric pressure dielectric barrier discharge. In: Proceedings of Deutsche Physikalische Gesellschaft Conference, March 8-12, 2010, Hannover, Germany. P 19.10
7. R Hippler, **H C Thejaswini**, A Majumdar, Plasma chemical reactions of hydrocarbons in an atmospheric pressure dielectric barrier discharge. In: Proceedings of 38th scientific assembly of the Committee on Space Research, July 18-25, 2010, Bremen, Germany.
8. **H.C. Thejaswini**, U. Martins, R. Bogdanowicz, A. Majumdar & Rainer Hippler.,

Deposition of functional films by atmospheric Pressure Discharge. Poster presented in SFB - TR24 workshop, September 26-28, 2011, Potsdam, Germany.

9. **H.C. Thejaswini**, R. Bogdanowicz & Rainer Hippler., Deposition of organic polymer films by Atmospheric Pressure Dielectric Barrier Discharge. Poster presented in HEPP Program, October 26-28, 2011, Garching, Germany.

Curriculum Vitae

ADDRESS H C Thejaswini

130, Geshwister-Scholl-Strasse 11c, Greifswald 17491, Germany.

Email: thejuhc@gmail.com or thejaswini@physik.uni-greifswald.de

Ph: 004917662370799

EDUCATION

Ph. D.	Ernst-Moritz-Arndt University, Greifswald, Germany Major: Plasma Physics	April' 2009 - Present
M. Sc.	Bangalore University, Bangalore, India. Major: Physical Chemistry	Aug' 2003 - May' 2005
B. Sc.	Sri Siddaganga College for Women, Tumkur, Bangalore University, India Major: Chemistry, Mathematics, Physics	June' 2000 - July' 2003

RESEARCH EXPERIENCE

- Ph.D. Student

April' 2009 - Present

Ernst-Moritz-Arndt University Greifswald, Greifswald, Germany

Advisor: Prof. Rainer Hippler

Project: "Synthesis & Deposition of Organic Polymers in an
Atmospheric Pressure Dielectric Barrier Discharge"

- Synthesis of higher order Hydrocarbons and Nitrogen containing compounds using gas mixtures C_2H_m/Ar and C_2H_m/N_2 (Where, $m = 2, 4, 6$) in an Atmospheric Pressure Dielectric Barrier Discharge (ADBD). Plasma diagnostics were carried out using Mass spectroscopy and FTIR spectroscopy.

- Deposition of Carbon-Nitrogen films on Si (100) substrate using gas mixtures C_2H_m/N_2 (Where, $m = 2, 4, 6$) in an Atmospheric Pressure Dielectric Barrier Discharge (ADBD). Characterization of the surface were carried out using various spectroscopic techniques such as XPS, FTIR, Ellipsometry, Profilometry, and SEM.

- Deposition of Diamond Like Carbon (DLC) films on Si (100) substrate using gas mixtures C_2H_m/Ar (Where, $m = 2, 4, 6$) in an Atmospheric Pressure Dielectric Barrier Discharge (ADBD). Characterization of the surface were carried out using various spectroscopic techniques such as XPS, FTIR, Raman Spectroscopy, Ellipsometry, Profilometry, and SEM.

- Project Assistant

Aug' 2008 - Dec' 2008

Institute of Bio - Physio Sensors Technology

Pusan National University, South Korea.

Advisor: Prof. Yoon Bo Shim

Project: “Simultaneous detection of Hemoglobin and Glycated hemoglobin using Conducting polymer via Amino Phenyl Boronic acid interaction”.

- Project Assistant

June' 2006 - July' 2008

Department of Inorganic & Physical Chemistry

Indian Institute of Science, Bangalore, INDIA

Advisor: Prof. S. Sampath

Project: I had been the part of the research work carried out in Interfacial & Surface Chemistry laboratory, that focuses on the solid-liquid and solid-solid interfaces

involving modified surfaces and new materials.

Exfoliated Graphite (EG) and Exfoliated Graphite Oxide (EGO) Inorganic Materials:
Preparation and application studies of Exfoliated Graphite and Exfoliated Graphite Oxide as an adsorbent and electrode material for heme protein study (Adsorbate materials used are Di-Methyl Sulphide-DMS, Lead-Pb, and Dyes. Heme proteins used: Hemoglobin, Glycated Hemoglobin, Myoglobin and Cytochrome-C)

Preparation of Organic thin films by Self Assembled Monolayers (SAM) and Langmuir-Blodgett (LB) films.

Synthesis and characterization of nanoparticles prepared by citrate method and electrochemical method.

AWARDS

Brain-Korea 21 Scholarship 2008

Max-Planck Scholarship 2009

AFFILIATIONS

Member for International Max-Planck Research School for Bounded Plasma (IMPRS)

Member for International Helmholtz Graduate School for Plasma Physics (HEPP)

COMPUTER SKILLS

Operating systems: windows XP, windows 97/98, windows vista

Microsoft applications: Microsoft PowerPoint, Word, Excel

Scientific applications: Origin, Corel draw, ISIS draw

INSTRUMENT HANDLING

- Electrochemical Techniques such as CV, DPV, Impedence, LSV

- Fourier Transform Infrared Spectroscopy (FTIR)
- Ultra Violet - visible Spectroscopy (UV - vis)
- Langmuir - Blodgett (LB)
- Electrochemical Quartz Crystal Microbalance (EQCM)
- Dielectric Barrier Discharge
- Mass spectroscopy (MS)
- X- ray Photo electron Spectroscopy (XPS)

PERSONAL DETAILS

Date of Birth: 21.09.1982
Sex: Female
Marital Status: Married
Nationality: Indian
Languages known: English, Kannada, Hindi